University of Texas at El Paso
DigitalCommons@UTEP

Open Access Theses & Dissertations

2018-01-01

Characterization And Geochemistry Of Carbonate Caprock Associated With The Gypsum Valley Salt Wall, Paradox Basin, Colorado: Implications For Understanding Lateral Caprock Emplacement

Piper Lee Poe
University of Texas at El Paso, piperlpoe@gmail.com

Follow this and additional works at: https://digitalcommons.utep.edu/open_etd

 Part of the Geology Commons

Recommended Citation
Poe, Piper Lee, "Characterization And Geochemistry Of Carbonate Caprock Associated With The Gypsum Valley Salt Wall, Paradox Basin, Colorado: Implications For Understanding Lateral Caprock Emplacement" (2018). *Open Access Theses & Dissertations*. 148.
https://digitalcommons.utep.edu/open_etd/148

This is brought to you for free and open access by DigitalCommons@UTEP. It has been accepted for inclusion in Open Access Theses & Dissertations by an authorized administrator of DigitalCommons@UTEP. For more information, please contact lweber@utep.edu.

CHARACTERIZATION AND GEOCHEMISTRY OF CARBONATE CAPROCK ASSOCIATED WITH THE GYPSUM VALLEY SALT WALL, PARADOX BASIN, COLORADO: IMPLICATIONS FOR UNDERSTANDING LATERAL CAPROCK EMPLACEMENT

PIPER LEE POE
Master's Program in Geological Sciences

APPROVED:

_____
Katherine A. Giles, Ph.D., Chair

_____
Benjamin Brunner, Ph. D.

_____
Eric E. Hiatt, Ph.D.

_____
Charles Amber, Ph.D.
Dean of the Graduate School

Copyright ©

by

Piper Poe

2018

Dedication

To Dr. Eric Hiatt, who unknowingly put me on the road to find my passion for science.

CHARACTERIZATION AND GEOCHEMISTRY OF CARBONATE CAPROCK ASSOCIATED WITH THE GYPSUM VALLEY SALT WALL, PARADOX BASIN, COLORADO: IMPLICATIONS FOR UNDERSTANDING LATERAL CAPROCK EMPLACEMENT

by

PIPER LEE POE, B.S. Geology

THESIS

Presented to the Faculty of the Graduate School of

The University of Texas at El Paso

in Partial Fulfillment

of the Requirements

for the Degree of

MASTER OF SCIENCE

Department of Geological Sciences
THE UNIVERSITY OF TEXAS AT EL PASO
December 2018

Acknowledgements

This work would not have been accomplished without my advisor, Dr. Kate Giles. I thank her for her constant inspiration and enthusiasm, and the countless opportunities she provided me throughout this process. Her persistent confidence in my work and my abilities have allowed me to go farther than I thought possible. The love and excitement she has for geology is incredibly contagious and makes working with her an absolute pleasure.

The financial support from the sponsors of the Institute of Tectonic Studies Salt-Sediment Research Consortium at the University of Texas at El Paso provided the tools to complete this study. Current sponsors include ExxonMobil, Hess, BP, BHP-Billiton, Repsol, Total, Chevron, and Conoco Phillips. Additional funding from the Geological Society of America Research Grants, Geological Society of America Travel Grants, American Association of Petroleum Geologists Grants-In-Aid, American Association of Petroleum Geologists-Southwest Section, and the University of Texas at El Paso Dodson Research Grant provided funds for multiple geochemical analyses, to complete fieldwork in Colorado and to travel to the Dead Sea, Israel to present my research at the Penrose Conference.

The creation of this thesis would not have been possible without those who contributed their knowledge and expertise, including Dr. Ben Brunner, Dr. Eric Hiatt, Dr. Richard Langford, Evey Gannaway, Carl Fiduk, Dr. Mark Rowan, Dr. Chris Jackson, and Dr. Frank Peel. I thank Rachelle Kernen for the guidance, advise and the opportunities she provided throughout this process, and for trusting me to be a part of her work. I also want to thank my trusty field assistant and best friend, Rafael Delfin, for the great times and moral support that immensely contributed to the writing of this thesis. Finally, a special thanks to Nila Matsler for her great organization and refreshing conversation.

Abstract

On the northeastern side of Gypsum Valley salt wall in the Paradox Basin of Colorado, discontinuous exposures of layered gypsum and carbonate rocks were previously mapped as the contact between diapiric Paradox Formation and marine limestone of the Pennsylvanian Honaker Trail Formation. Utilizing new and existing mapping, petrographic and isotopic geochemical analyses, this study reinterprets this zone to represent lateral gypsum and carbonate caprock that formed in the Triassic during passive rise of the Gypsum Valley salt wall. Gypsum Valley lateral carbonate caprock can be distinguished from Pennsylvanian and Permian depositional carbonate strata exposed elsewhere on the salt wall by the recognition of caprock distinctive fabrics (i.e. massive, porphyritic, layered and brecciated), the lack of fossils or sedimentary structures, the lack of depositional interfingering with the adjacent outboard Triassic Chinle Formation stratigraphy, and its carbon isotopic signature (< –6 ‰) that reflects the contribution of isotopically light carbon from the oxidation of hydrocarbons during caprock formation. Additionally, the preliminary results from the lateral carbonate caprock produced a U-Pb age of 211 ±16Ma, which is consistent with the upper Triassic age suggested by the association with the Chinle Formation. The orientation of the lateral caprock layering parallels that of the adjacent halokinetically drape-folded Chinle strata, which contains fluvial channel conglomerate-bearing, caprock-derived clasts. This confirms that the carbonate caprock had already formed in the Triassic in a crestal position on top of the Gypsum Valley salt wall during Chinle deposition and was subsequently rotated by halokinetic drape folding to its flanking position during continued passive diapirism.

In addition to the reinterpretation of the studied gypsum and carbonate units as lateral caprock, the term “capstone” was introduced when discussing a particular caprock lithology, as a distinction from the term “caprock” that is generally used in reference to the entire rock body. A

capstone classification is proposed based on the recognition of four distinct megascopic fabric types: 1) massive: consisting of a homogeneous mineralogy and texture; 2) porphyritic: comprising two distinct crystal sizes; 3) layered: subdivisions based on layer size that includes: microlaminated (1-3mm), laminated (3-10mm), and banded (>10mm); and 4) brecciated: these units are subdivided based on the degree of separation between brecciated capstone fragments, which may be close, loose, or spatially independent and subdivided into crackle breccia, mosaic breccia, and disorganized breccia, respectively. Paragenetic relationships indicate micritic dolomite to be the original carbonate capstone fabric formed during the Triassic. Thus, the additional capstone fabrics and mineralogies exposed today signify the diagenetic alteration of the original dolomite capstone, likely by multiple fluid flow events. Therefore, it is possible to use the evolution of capstone fabrics as an archive of fluid flow at the salt-sediment interface.

Table of Contents

Acknowledgements v

Abstract vi

Table of Contents viii

List of Tables xi

List of Figures xii

Chapter 1: Introduction 1
- 1.1. Caprock Formation 1
- 1.2. Lateral Caprock 4
- 1.3. Significance 10
- 1.4. Research Objectives 11
- 1.5. Geologic Setting 12
- 1.6. Methods 16

Chapter 2: Fabric Classification of the Gypsum and Carbonate Caprock at the Gypsum Valley Salt Wall 22
- 2.1. Massive Capstone 23
  - 2.1.1. Massive dolomite capstone 23
  - 2.1.2. Massive Calcite Capstone 25
  - 2.1.3. Massive Gypsum Capstone 25
- 2.2. Porphyritic Capstone 25
  - 2.2.1. Porphyritic silica-dolomite capstone 28
  - 2.2.2. Porphyritic silica-calcite capstone 28
  - 2.2.3. Porphyritic calcite capstone 28
  - 2.2.4. Porphyritic gypsum capstone 32
- 2.3. Layered Capstone 32
  - 2.3.1. Microlaminated Capstone 34
    - 2.3.1.1. Microlaminated Dolomite Capstone 34
    - 2.3.1.2. Microlaminated Calcite Capstone 34
    - 2.3.1.3. Microlaminated Gypsum Capstone 37
  - 2.3.2. Laminated Capstone 37
    - 2.3.2.1. Laminated Calcite Capstone 37
    - 2.3.2.2. Laminated Dolomite Capstone 40

2.3.2.3. Laminated Silica-Dolomite Capstone 40
2.3.3. Banded Capstone 43
2.3.3.1. Banded Calcite-Dolomite Capstone 43
2.3.3.2. Banded Calcite Capstone 43
2.4. Brecciated Capstone 46
2.4.1. Crackle Breccia Capstone 46
2.4.1.1. Crackle Breccia Dolomite Capstone 46
2.4.2. Mosaic Breccia Capstone 48
2.4.2.1. Mosaic Breccia Dolomite Capstone 48
2.4.2.2. Mosaic Breccia Gypsum-Dolomite Capstone 48
2.4.3. Disorganized Breccia Capstone 51
2.4.3.1. Disorganized Breccia Dolomite Capstone 51
2.4.3.2. Disorganized Breccia Calcite Capstone 53
Chapter 3: Distribution of Capstone Fabrics Along the Gypsum Valley Salt Wall 55
3.1. The Nubbin 55
3.2. Box Canyon – Bridge Canyon 58
3.2.1. Box Canyon 58
3.2.1. Bridge Canyon 58
3.3. Mary Jane Draw 61
3.4. Carbonate Caprock Clasts 63
Chapter 4: Geochemical Observations of Gypsum Valley Carbonate Caprock 65
4.1. $\delta^{18}O$ versus $\delta^{13}C$ Cross-Plot: Carbonate Capstone Fabrics 65
4.2. $\delta^{18}O$ versus $\delta^{13}C$ Cross-Plot: Carbonate Capstone Petrographic Observations 69
4.3. Carbon and Oxygen Isotopic Signature of Carbonate Clasts Found within the Chinle Formation 70
4.4. U-Pb Age Dating of Carbonate Capstones 72
Chapter 5: Discussion 75
5.1. Interpretation of Capstone Fabrics 75
5.1.1. Massive Capstone 75
5.1.2. Porphyritic Capstone 75
5.1.3. Layered Capstone 76
5.1.4. Brecciated Capstone 77

5.2. Paragenesis of Capstone Fabrics....78
5.2.1. Paragenetic Relationships within Caprock....78
5.2.2. Controls on the Spatial Distribution of Capstone Fabrics....80
5.3. Geochemical Signature of Carbonate Capstone....82
5.3.1. Isotopically Low Carbon Signature of Carbonate Capstone....82
5.3.2. Diagenetic Overprinting of Complex Carbonate Capstone Fabrics....85
5.3.3. Geographic Distribution of Geochemical Signatures along the Gypsum Valley Salt Wall....86
5.3.4. Geochemical Signature of Carbonate Capstone Clasts within the Chinle Formation....88
5.3.5. U-Pb Age Dating of Carbonate Capstone....89
5.4. Hypotheses/Models for Lateral Caprock Emplacement....89
5.4.1. Pennsylvanian Honaker Trail Formation Hypothesis....90
5.4.2. Paradox LES Model....91
5.4.3. In-Situ Model....93
5.4.4. Halokinetic Drape-Fold Model....94
5.5. Chinle Caprock Formation by the Drape-Fold Model....95
Chapter 6: Conclusion....99
References....102
Curriculum Vita....106

List of Tables

Table 1: Classification of caprocks associated with salt diapirs according to fabric……23

Table 2: Comparison of the mean host and cement isotopic composition of capstone fabrics.....67

List of Figures

Figure 1: Crestal caprock 2
Figure 2.1: Anhydrite caprock formation 3
Figure 2.2: Carbonate caprock formation 3
Figure 3: Seismic and interpreted illustration of caprock at Epsilon diapir 5
Figure 4: *In-situ* lateral caprock model 6
Figure 5: Layered evaporite sequence (LES) model 6
Figure 6: Halokinetic drape-fold model 7
Figure 7: Regional location of Paradox Basin 9
Figure 8: Geologic map of the Gypsum Valley salt wall 14
Figure 9: Stratigraphic column of the Chinle Formation 15
Figure 10: Conceptual model of the Gypsum Valley salt shoulder 17
Figure 11: Geologic map of Gypsum Valley highlighting caprock location 19
Figure 12: Massive dolomite capstone 24
Figure 13: Massive calcite capstone 26
Figure 14: Massive gypsum capstone 27
Figure 15: Porphyritic silica-dolomite capstone 29
Figure 16: Porphyritic silica-calcite capstone 30
Figure 17: Porphyritic calcite capstone 31
Figure 18: Porphyritic gypsum capstone 33
Figure 19: Microlaminated dolomite capstone 35
Figure 20: Microlaminated calcite capstone 36
Figure 21: Microlaminated gypsum capstone 38
Figure 22: Laminated calcite capstone 39
Figure 23: Laminated dolomite capstone 41
Figure 24: Laminated silica-dolomite capstone 42
Figure 25: Banded calcite-dolomite capstone 44
Figure 26: Banded calcite capstone 45
Figure 27: Crackle breccia dolomite capstone 47
Figure 28: Mosaic breccia dolomite capstone 49
Figure 29: Mosaic breccia gypsum-dolomite capstone 50
Figure 30: Disorganized breccia dolomite capstone 52

Figure 31: Disorganized breccia calcite capstone....54
Figure 32: Geologic map of exposed capstone along the Gypsum Valley salt wall....56
Figure 33: Caprock fabric map of The Nubbin....57
Figure 34: Caprock fabric map of Box Canyon and Bridge Canyon....60
Figure 35: Caprock fabric map of Mary Jane Draw....62
Figure 36: Dolomite clasts within the Chinle Formation....64
Figure 37: $\delta^{18}O$ versus $\delta^{13}C$ cross-plot of exposed carbonate caprock at Gypsum Valley....66
Figure 38: $\delta^{18}O$ versus $\delta^{13}C$ cross-plot of carbonate capstone fabrics....68
Figure 39: $\delta^{18}O$ versus $\delta^{13}C$ cross-plot of mineral phases within carbonate capstone....71
Figure 40: Isochrons of U-Pb age dates of carbonate caprock....73
Figure 41: Carbonate caprock samples used for U-Pb age dating....74
Figure 42: Calcite capstone replacement of micritic dolomite capstone....79
Figure 43: $\delta^{18}O$ versus $\delta^{13}C$ cross-plot of primary carbonate capstone fabrics....84
Figure 44: $\delta^{18}O$ and $\delta^{13}C$ versus distance from the Nubbin....87
Figure 45: $\delta^{18}O$ versus $\delta^{13}C$ cross-plot of all carbonates exposed at Gypsum Valley....92
Figure 46: Conceptual illustration of the Gypsum Valley salt shoulder development....96
Figure 47: Schematic illustration of the caprock exposed over the modern salt shoulder....97

Chapter 1: Introduction

1.1. Caprock Formation

Caprocks associated with salt diapirs are mineral assemblages formed as salt dissolution-related insoluble residues (Murray, 1966; Kyle et al., 1987) that are typically found on the diapir crest, and occasionally in a flanking position, where they are referred to as lateral caprock (Jackson and Lewis, 2012). Caprock assemblages commonly consist of a vertically zoned layered sequence, containing in ascending order: anhydrite, gypsum, and carbonate lithologies such as limestone and dolostone (Kyle and Posey, 1991) (Figure 1). The formation of the anhydrite/gypsum caprock involves a cross-flow of halite-undersaturated phreatic water to the diapir, which causes the halite in the salt diapir to preferentially dissolve from the rising diapir. As the halite dissolves, the less soluble components of the diapir, such as $CaSO_4$ minerals (i.e. anhydrite and gypsum) accumulate as insoluble residues and accrete to the base of the developing caprock by underplating (Kyle et al., 1987; Kyle and Posey, 1991) (Figure 2.1). The formation of carbonate caprocks involves the alteration of $CaSO_4$ minerals by bacterially controlled diagenetic processes (Kyle et al., 1987). This occurs in a two-stage process: first, fluids dissolve $CaSO_4$ from the anhydrite caprock, releasing Ca^{2+} and SO_4^{2-} to solution; second, if in the presence of sulfate-reducing bacteria and organic matter, sulfate is reduced and hydrocarbons are oxidized, releasing bicarbonate and hydrogen sulfide as a result. The bicarbonate in solution bonds with calcium to precipitate calcite, and if magnesium is present, dolomite precipitates, producing a carbonate caprock (Figure 2.2) (Hallager et al., 1990; Kyle and Posey, 1991; Warren, 2006).

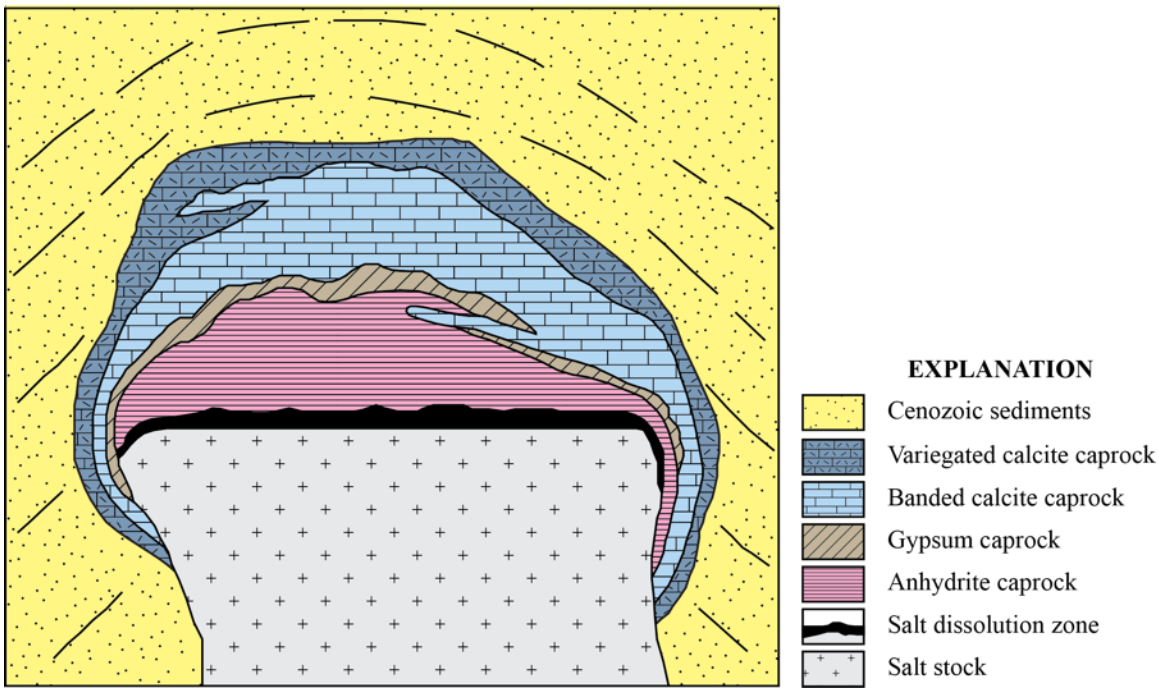

Figure 1. Cross sectional view of a Texas Gulf Coast salt dome showing generalized caprock lithologic zonation. Modified from Kyle and Posey, 1991.

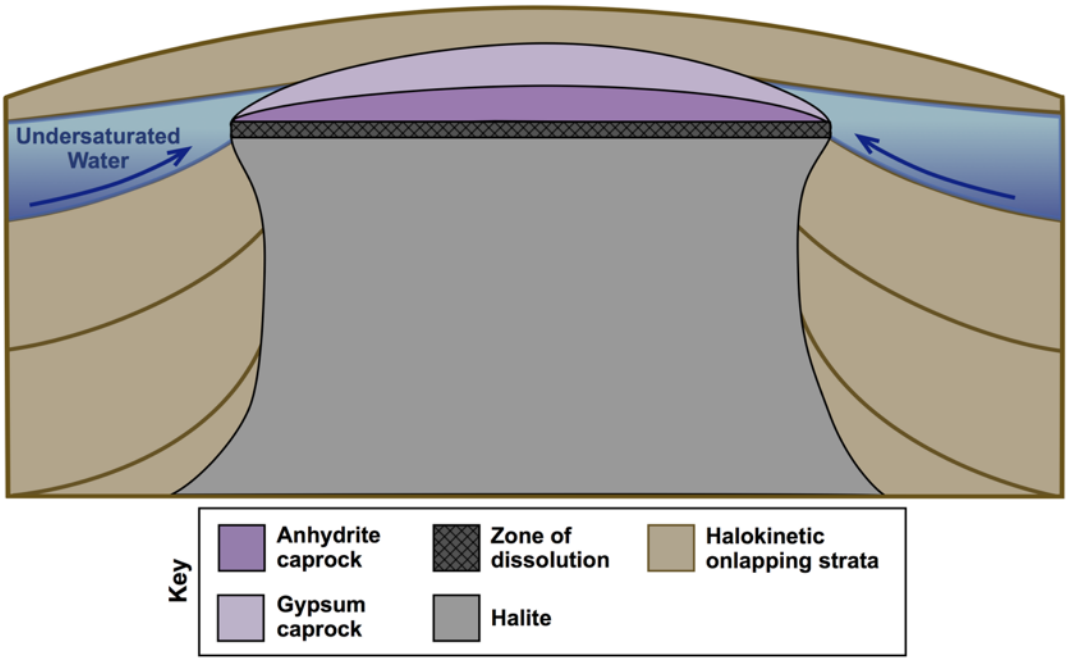

Figure 2.1. Schematic diagram of anhydrite/gypsum caprock formation. No scale implied.

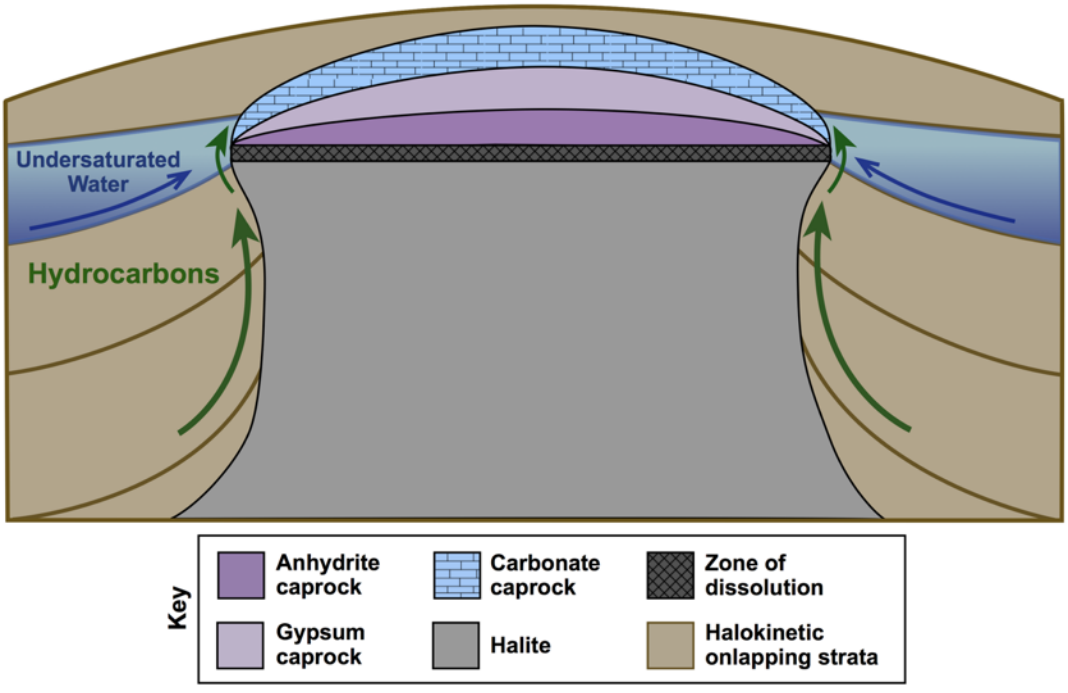

Figure 2.2. Schematic diagram of carbonate caprock formation. No scale implied.

1.2. Lateral Caprock

Lateral caprock has been identified at the Epsilon Diapir in the North Sea Egersund Basin (Jackson, et al., 2013) and at the Hockley, Boling, and Moss Bluff salt domes in the Texas Gulf Coast (Kyle and Posey, 1991) in diapir-flanking positions hundreds of meters in the subsurface (Figure 3). Currently, three general models have been proposed for the formation of lateral caprock: 1) *in-situ* model, 2) rotated layered evaporite sequence model, and 3) halokinetic drape fold ("event") model. The *in-situ* model, proposed by Evans et al. (1991), suggests that emplacement of lateral caprock is the result of unusual undersaturated deeply circulating basinal waters that flow upward along the flanks of the diapir. The outward dipping geometries of the surrounding strata assist the buoyancy-driven flow that then preferentially dissolves halite and accretes $CaSO_4$ minerals resulting in lateral caprock development (Figure 4) (Evans, 1991; Jackson, et al., 2013). The rotated layered evaporite sequence (LES) model, proposed by Schwerdther et al. (1978), suggests that a depositional/early post-depositional anhydrite-dominated evaporite sequence associated with the autochthonous depositional salt strata has been rotated upward to a position against the flank of the diapir during diapiric rise (Figure 5). Giles et al. (2012), suggest that lateral caprock initially forms in a roughly horizontal position on the crest of a diapir and is subsequently rotated to the lateral position by halokinetic drape-folding of the coupled caprock and roof strata during continued passive diapiric rise. The lateral caprock is associated with a discrete package of roof strata. Thus, the formation age of the caprock should be roughly equivalent to that of the adjacent halokinetically deformed strata. Giles et al. (2012) refers to this process as a "caprock event" (Figure 6), and a single passive diapir may have multiple caprock events. In contrast, existing models of crestal caprock formation envision caprock

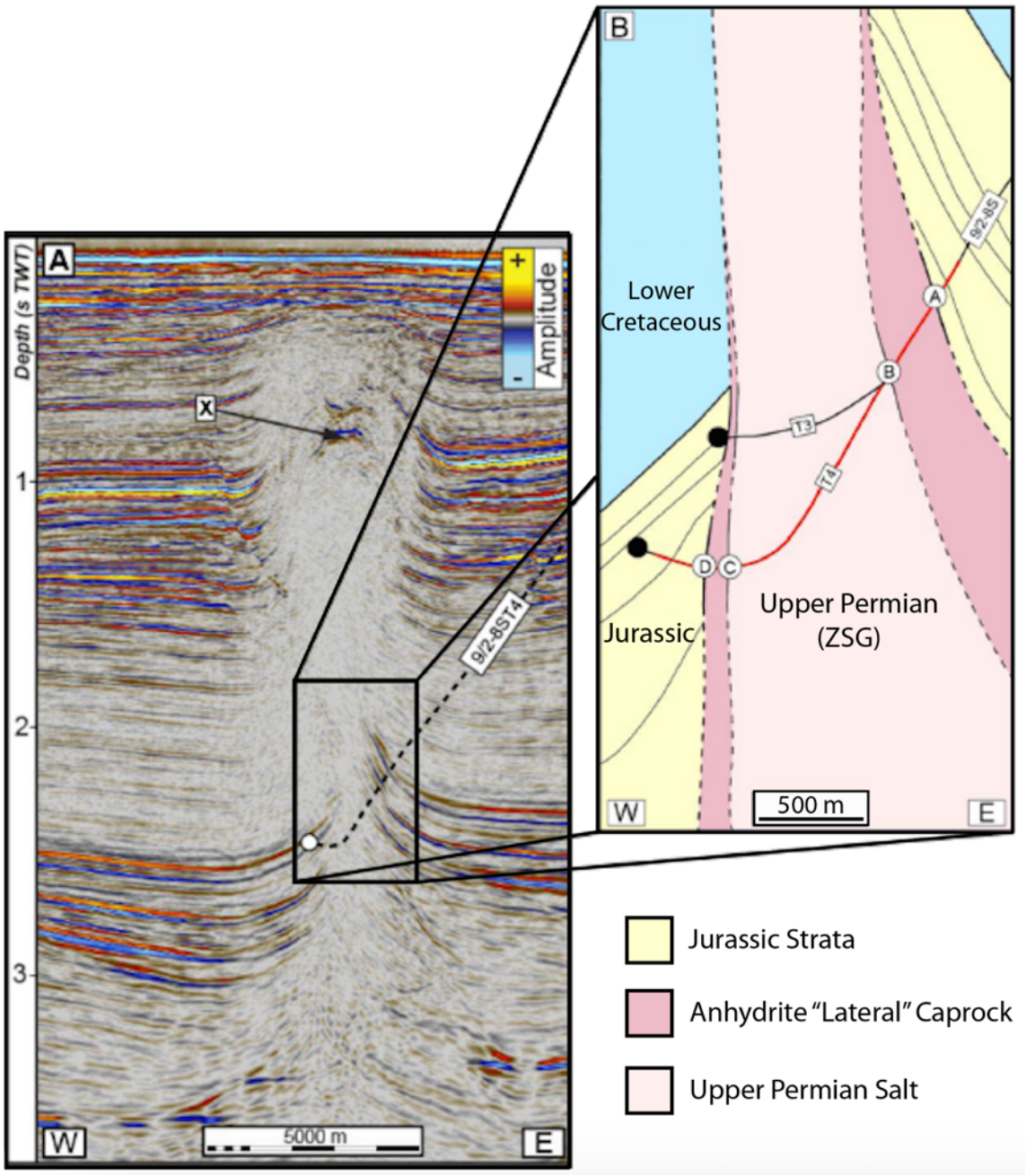

Figure 3. A. Seismic reflection, B. Seismic interpretation of the Epsilon Diapir in the Egarsund Basin, North Sea. Well 9/2-8S penetrated anhydrite caprock along the flanks of the Epsilon Diapir while drilling a Jurassic prospect (Jackson, C. A., et al, 2013).

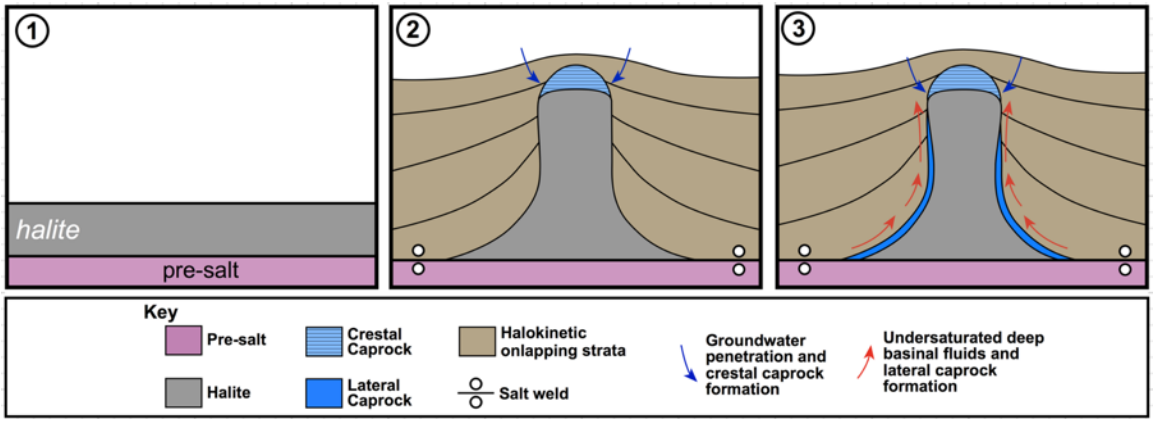

Figure 4. Conceptual model representing the *in-situ* model of lateral caprock as a mode of lateral caprock emplacement, proposed by Jackson and Lewis (2012). The model proposes that lateral caprock forms as a result of migration of undersaturated basinal fluid migration along the diapir flank. Modified from Jackson and Lewis, 2012.

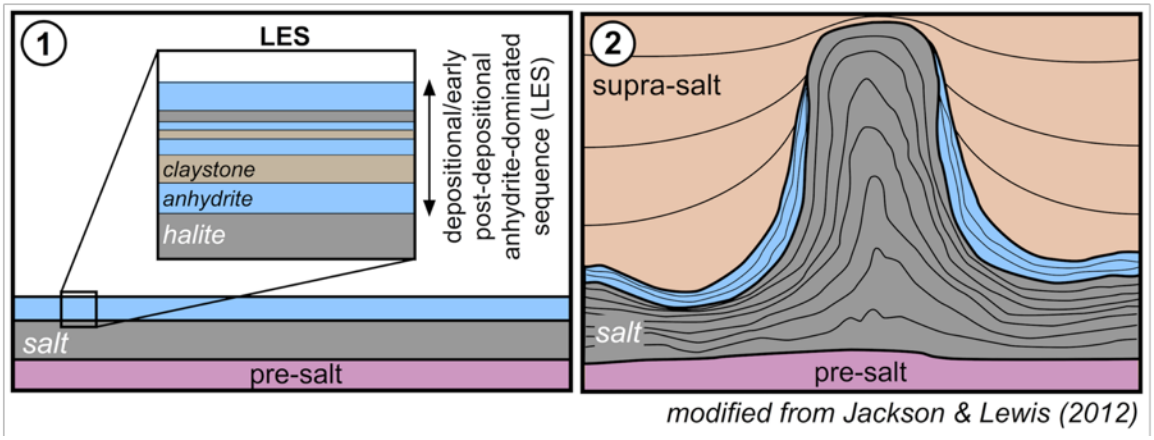

Figure 5. Simplified diagram illustrating the layered evaporite sequence (LES**)** model, proposed by Schwerdther et al. (1978) suggests that lateral caprock could essentially be a LES associated with the mother salt that has been plastered against the flank of the diapir during the rise of less dense halite. No scale is implied. Modified from Jackson and Lewis, 2012.

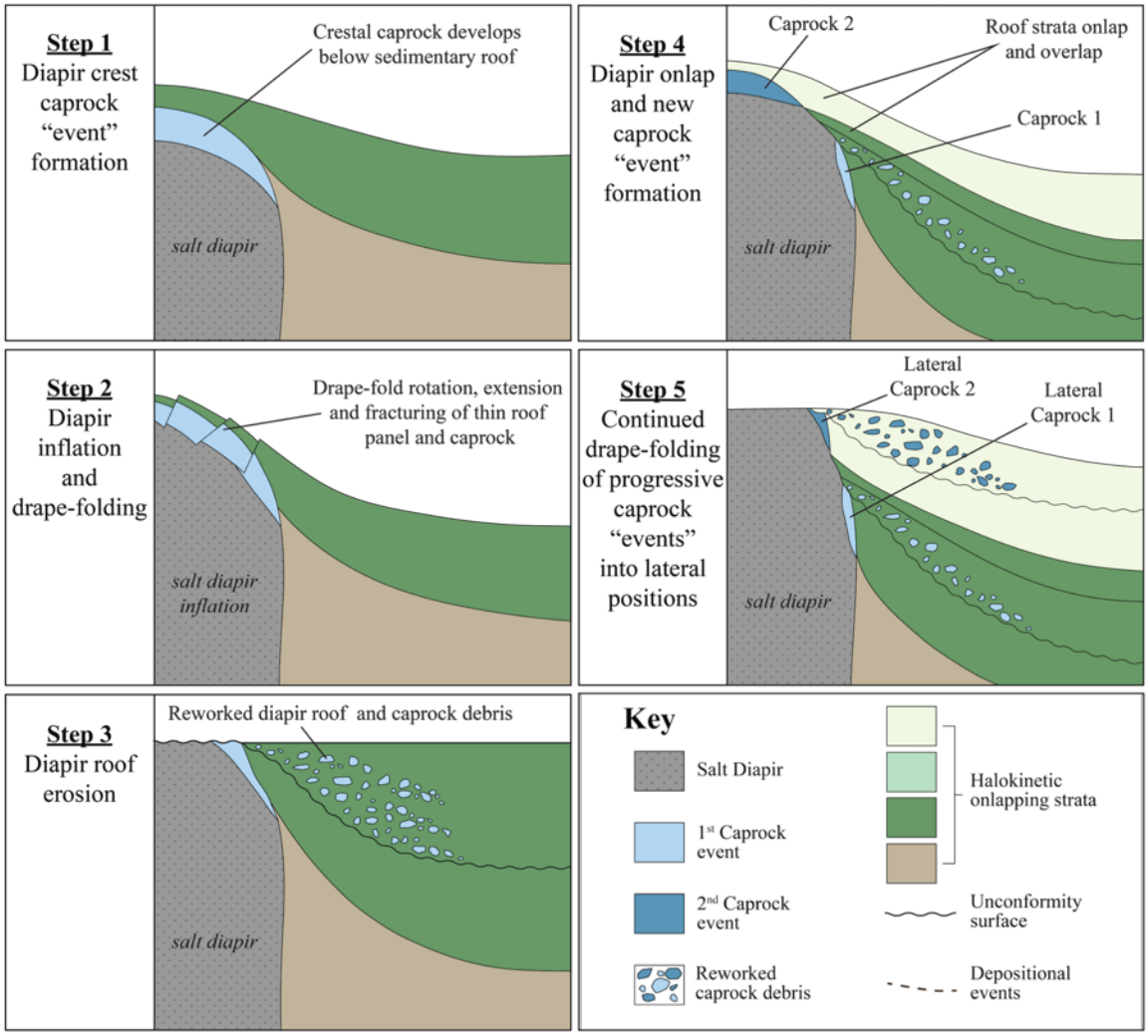

Figure 6. Conceptual diagram illustrating the halokinetic drape-fold model proposed by Giles et al. (2012) for a mode of lateral caprock emplacement, which suggests caprock forms in a crestal position during distinct periods of time and are then rotated into a lateral position as a result of halokinetic drape folding. No scale is implied. Modified from Giles et al., 2012.

generation by long-lived, crestal dissolution of halite with the caprock rising continuously along with salt during ongoing diapirism (Murray, 1966; Kyle and Posey, 1991).

The halokinetic drape-fold event model consists of four steps: 1) caprock develops in a crestal position by cross-flow of undersaturated waters; 2) continued diapiric rise and minibasin subsidence causes drape-folding of roof strata and competent caprock, which detaches from the underlying halite-dominated diapir and rotates off the crest into a lateral position; 3) topography generated by diapir inflation as diapir-rise rates exceed sedimentation rates results in erosional thinning of the roof to create an angular unconformity that truncates the underlying lateral caprock and potential incorporation of caprock clasts into the surrounding sediments; 4) increasing rates of sedimentation relative to diapiric rise lead to onlap and formation of the overlying halokinetic sequence, which may or may not develop a new crestal caprock assemblage (Giles et al., 2012).

Shock (2012) established the applicability of the halokinetic drape fold model as the mode of emplacement for the Permian Cutler Formation-age equivalent lateral caprock found at the margin of Castle Valley salt wall, Paradox Basin, Utah (Figure 7). Here, vertical layers of dolomitic and calcitic caprock separate the massive gypsum exposures of the Castle Valley salt wall from vertical to overturned strata of the Permian Cutler Formation. Fluvial channel conglomeratic facies in this Cutler strata contain caprock-derived clasts (Shock, 2012). Recently, lateral gypsum and carbonate caprock has also been documented at the Gypsum Valley salt wall in the Paradox Basin, CO, (Figure 7) (McFarland, 2016; Brunner et al., 2016; Lerer, 2017), where it is associated with 25 degree NE dipping strata of the Triassic Chinle Formation (Figure 8). McFarland (2016) and Heness *et al.* (2017) interpret carbonate clasts in the fluvial conglomerate facies to be derived from the caprock. Carbonate caprock clasts found in the halokinetic sequence of the overlying Triassic Chinle Formation are essential pieces of evidence supporting the drape

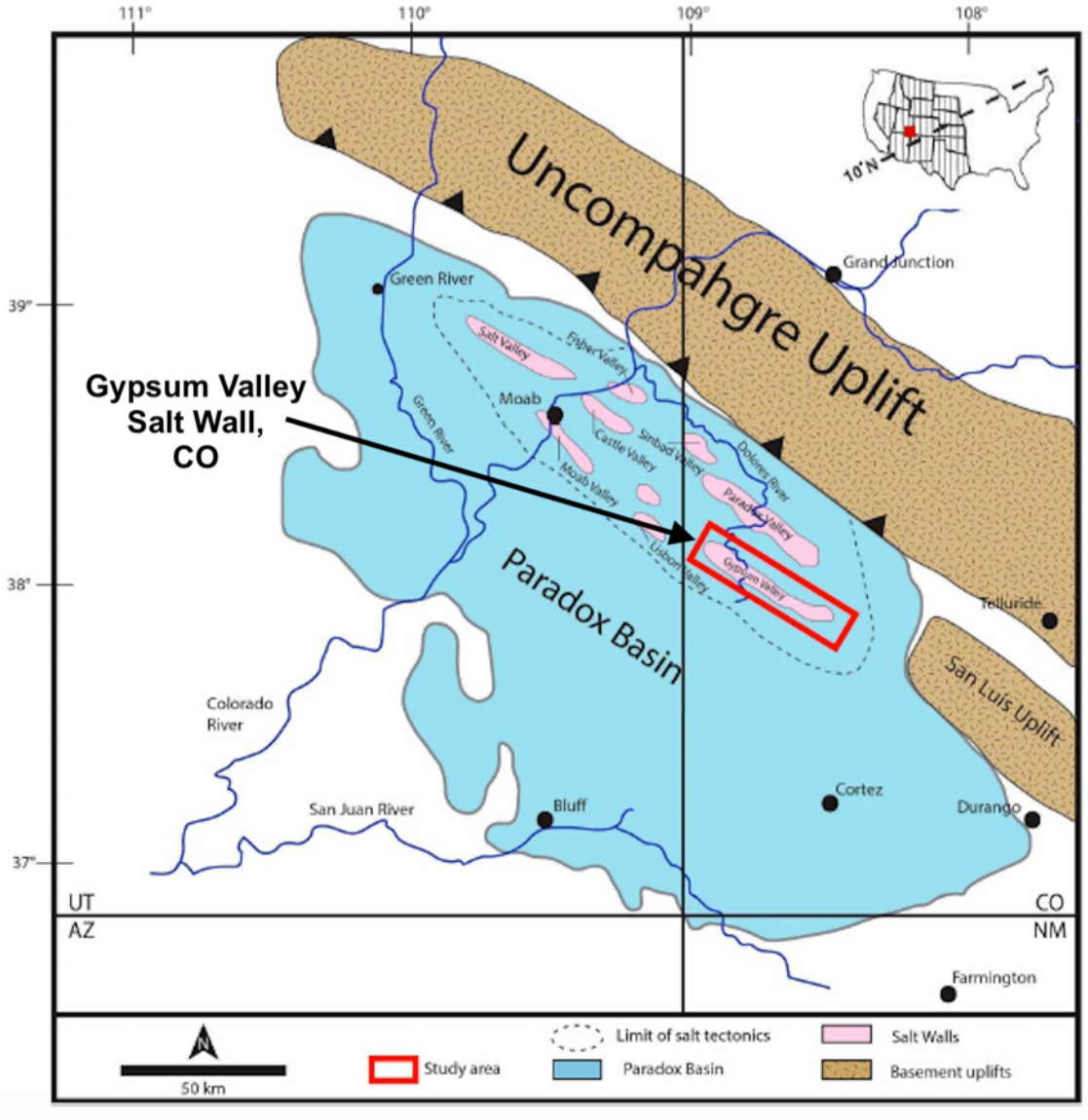

Figure 7. Location map of Paradox Basin and salt anticline province showing major uplifts and salt anticlines. Gypsum Valley salt wall study area is outlined in red. (modified from Barbeau, 2003; and Kues and Giles, 2004).

fold model. Those clasts prove that carbonate caprock was present atop the Gypsum Valley salt wall during Chinle deposition, and was partially eroded off the crest and redeposited within the Chinle. Because the Chinle Formation strata adjacent to the salt wall in which caprock clasts are encased is dipping 25 degrees to the NE; this demonstrates that the caprock and associated outboard strata have been drape-folded toward the NE.

1.3. Significance

Caprocks are relevant to the petroleum industry because they can act as reservoirs, traps, seals, or conduits for hydrocarbons, and can be potential drilling hazards if not detected pre-drill (Kyle and Posey, 1991; Enos and Kyle, 2002; Giles et al., 2012). The most famous carbonate caprock hydrocarbon reservoir is the Spindletop oil field in East Texas, which triggered the Texas oil boom (Kyle and Posey, 1991). For oil exploration, understanding the timing and the geochemical processes related to the formation of crestal and/or lateral caprock is essential – yet few studies to date have been completed that focus on this complex process. Understanding how and when these caprocks form will aid in accurately determining the timing of petroleum system elements in basins containing carbonate caprocks. Understanding caprock formation provides further insight into the dynamics between diapir-proximal halokinetic deformation and marginal fluid migration as a means by which lateral caprock forms. Additionally, it is important for understanding complex diapiric processes, and for developing accurate salt tectonic models involving halokinetic sequences, salt shoulder formation, and diapiric dissolution (Giles, et al., 2012; Mast, 2016; McFarland, 2016). Furthermore, understanding the distribution of crestal and lateral caprocks will prevent misidentification of caprock as stratigraphic units, which can result in incorrect stratigraphic cross-sections and well-top picks (Jackson and Lewis, 2012; Mast, 2016;

Rowan et al., 2016). There are also paleoclimatic and environmental implications if these are truly "events". Caprock formation requires enough rainfall to sustain an elevated groundwater table with significant flow of halite-undersaturated waters in order to account for the amount of dissolution needed to make the thickness and extent of caprock produced.

1.4. Research Objectives

The gypsum and carbonate rocks exposed at the salt-sediment interface along the northern flank of the Gypsum Valley salt wall in the Paradox Basin, CO, were originally mapped as Upper Pennsylvanian Honaker Trail Formation. The Honaker Trail is a limestone that was deposited stratigraphically above the Pennsylvanian Paradox Formation. Due to the lack of physical and geochemical similarities to the Honaker Trail Formation, the gypsum and carbonate rocks involved in this study have been determined to be caprock.

The caprock exposed at Gypsum Valley provides an excellent opportunity to study the complexities associated with caprock and its formation. This outcrop- and laboratory-based study tests competing models for the lateral emplacement of caprock located at the salt-sediment interface. The models considered are 1) *in-situ* model, 2) rotated layered evaporite sequence model, and 3) halokinetic drape-fold ("event") model.

The objectives of this study were to: 1) Determine the characteristics of the gypsum and carbonate rock located at the salt-sediment interface that are indicative of caprock; 2) Determine if the timing of caprock formation is contemporaneous with deposition of the Triassic Chinle Formation; and 3) Determine if the carbonate caprock clasts found within the overlying Chinle Formation are genetically related to the caprock exposed at the salt-sediment interface. To test these hypotheses, a multidisciplinary approach involving detailed outcrop and petrographic

documentation, $\delta^{13}C$ and $\delta^{18}O$ isotope geochemical analyses, and U-Pb dating of carbonate caprock were used to obtain a complete understanding of the formation and later lateral emplacement of the caprock at the Gypsum Valley salt wall.

1.5. Geologic Setting

The Paradox Basin is an asymmetric, intracratonic foreland basin, located in southwest Colorado and southeast Utah, which formed on the southern flank of the Uncompahgre Uplift during the Late Paleozoic Ancestral Rocky Mountain orogeny (Hite, 1960; Barbeau, 2003). The geographical boundaries of the basin are defined by the lateral extent of the Pennsylvanian Paradox Formation layered evaporite sequence (LES) (Condon, 1997; Barbeau, 2003; Trudgill, 2011). More than 20 exposed linear NE-SW trending salt walls in the northeastern part of the Paradox Basin developed from differential loading of the Paradox Formation (Figure 7). The salt was loaded by a prograding alluvial wedge of the Pennsylvanian and Early Permian Cutler Group derived from the Uncompahgre Uplift (Cater, 1970; Mack and Rasmussen, 1984, Barbeau, 2003). The trend of the salt walls has been interpreted to be largely controlled by deep-seated NW-SE trending basement faults (Trudgill *et al.,* 2004). Passive diapirism of the salt walls extended from Pennsylvanian–Permian Cutler deposition through Jurassic time when the salt walls were buried by the Morrison Formation (Doelling, 1985; Trudgill *et al.,* 2004).

This study focuses on the salt-sediment interface at the Gypsum Valley salt wall in southwestern Colorado. Gypsum Valley is a breached and collapsed, northwest-southeast trending ~35 km long and ~4 km wide salt wall. The Paradox Formation "diapir" is exposed on the valley floor in the form of residuum of massive gypsum, and local non-halite LES facies, such as black, calcareous mudstone and tan dolomite. There is no halite exposed at the surface but halite is

encountered in wells in the subsurface at Andy's Mesa and Double Eagle oil fields on the northeast margin of Gypsum Valley (Cater, 1970). Permian, Triassic, and Jurassic carbonate, fluvial, and eolian sediments are exposed along the flanks of Gypsum Valley and dip away from the core of the salt wall toward the adjacent (Dry Creek and Disappointment) mini-basins (Cater, 1970). Late stage, Neogene collapse of the Gypsum Valley roof provided the excellent exposure of carbonate caprock along the margin of the Gypsum Valley salt wall adjacent to the Triassic fluvial Chinle Formation. These exposures present a superb opportunity to study the lateral variation of carbonate caprock over an extensive area. The Owl Rock Member of the Chinle Formation onlaps and overlaps the exposed shoulder of the diapir (Figure 9) (McFarland, 2016). The lower members of the Chinle Formation are either located in the subsurface, or not present within this area of the Paradox Basin. The Moenkopi Formation, located stratigraphically below the Chinle Formation, is also present in the subsurface as indicated by well-logs adjacent to the study area in Andy's Mesa field (Cole III *et al.,* 2009). The Moenkopi Formation does not outcrop at Gypsum Valley, likely due to the large regional erosional unconformities within the Chinle Formation (Trudgill, 2011).

Gypsum Valley is geographically separated into two geomorphic defined sectors (Figure 8) marked by where the Dolores River cuts across the salt wall; Little Gypsum Valley in the northern sector, and Big Gypsum Valley in the southern sector. Carbonate caprock is exposed along the northeastern flank of the salt wall almost entirely in Little Gypsum Valley and its exposure extends to the northern edge of a wide canyon called "Hamm Canyon" within Big Gypsum Valley. The absence of caprock exposure along the majority of Big Gypsum Valley salt-sediment interface is not fully understood, but could be attributed to continued inflation of the salt

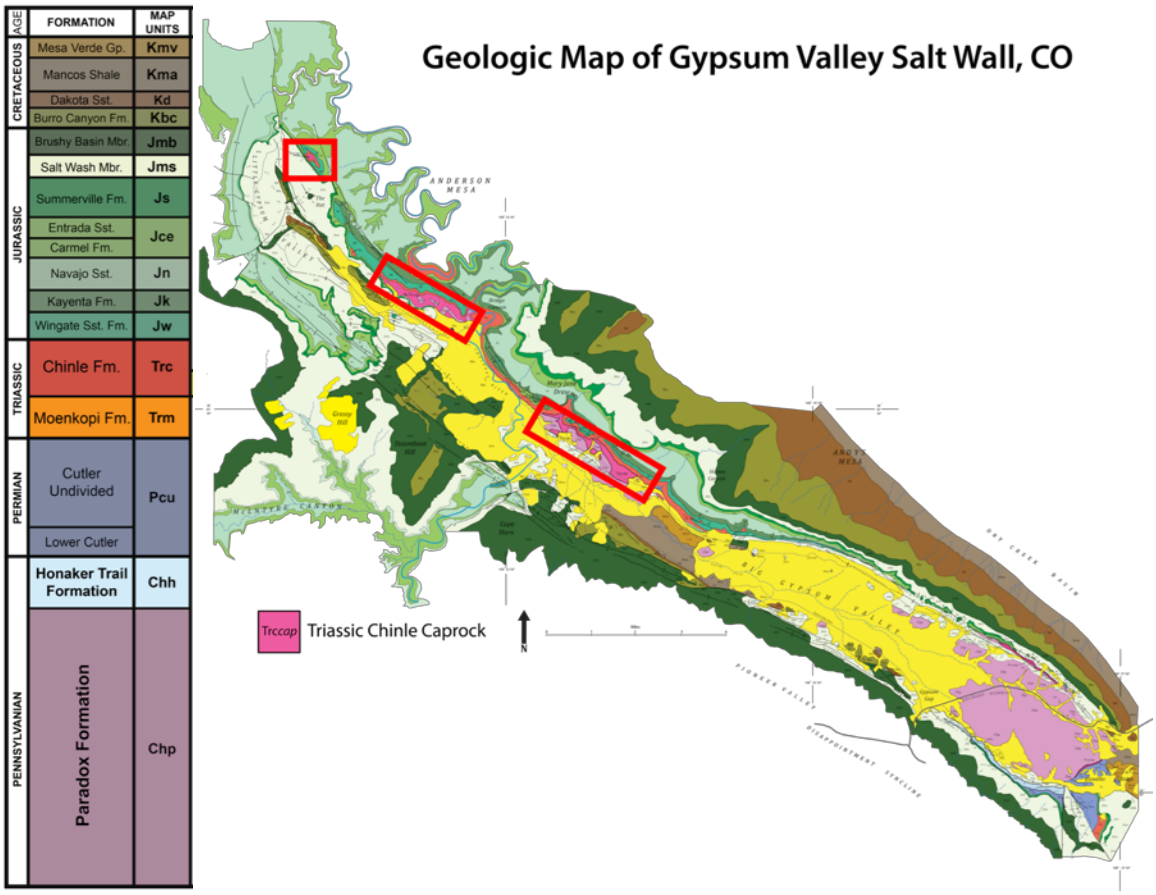

Figure 8. Geologic map of the Gypsum Valley salt wall. The red rectangles indicate the localities in which Triassic Chinle caprock has been identified and will be used in this study (modified from Giles et. al, 2016).

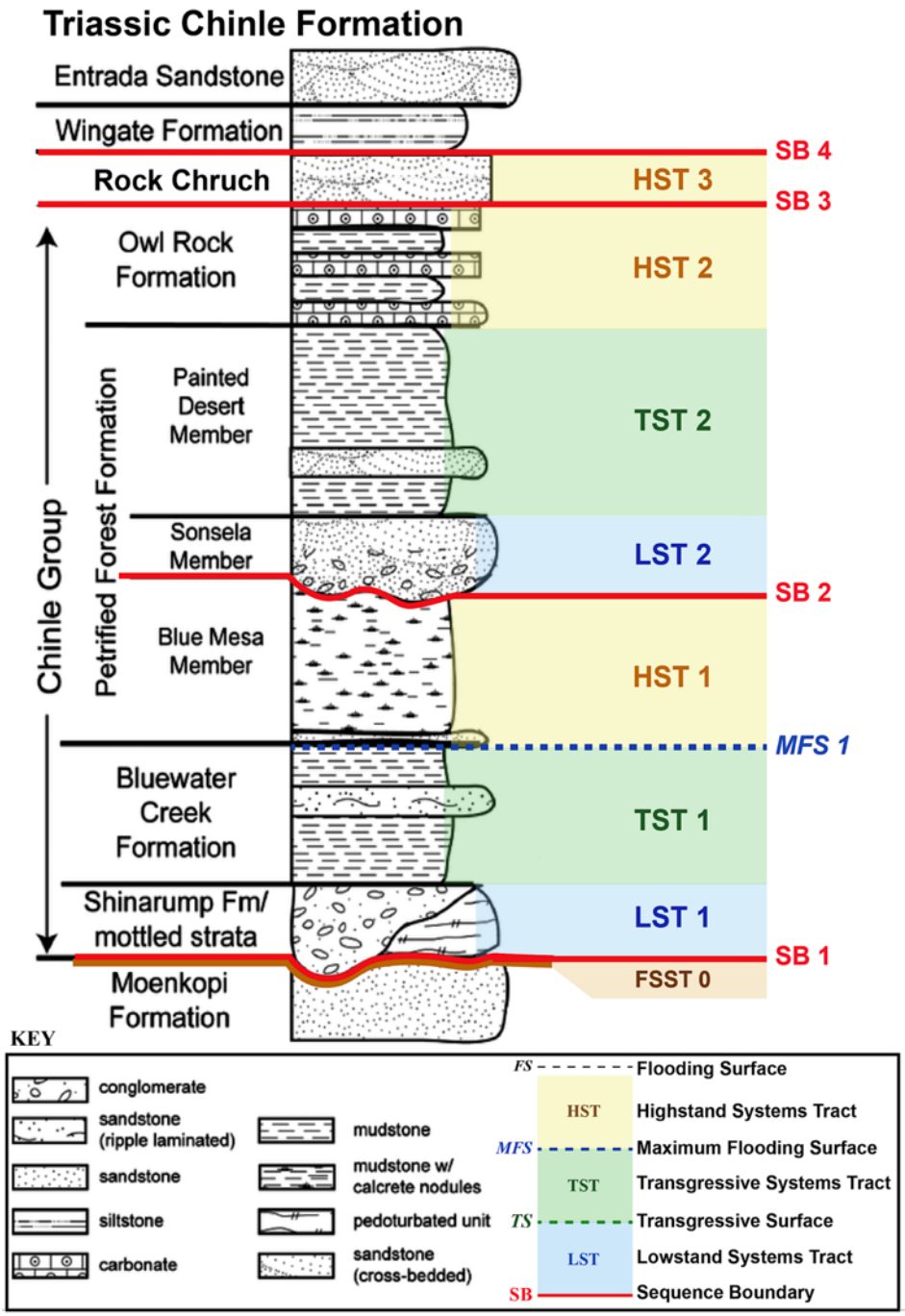

Figure 9. Generalized stratigraphic column of the Chinle Formation with interpreted systems tracts, flooding surfaces and regional sequence boundaries.

wall into Big Gypsum Valley after the Triassic-aged caprock had formed, and would now only be found in the subsurface along the flank of the wall. Another possibility for the absence of surface exposure is that the caprock only formed over the shoulder of the salt wall, which is only present along the northeastern margin of the valley (Figure 10) (McFarland, 2016).

1.6. Methods

This study involved a detailed examination of the carbonate caprock exposed along the entire length of the northern margin of the Gypsum Valley salt wall in the Paradox Basin, CO, in order to test competing models of lateral caprock emplacement. Building on previous work (Lerer, 2017), fieldwork was conducted in order to map out and interpret the distribution of caprock fabrics exposed along the salt wall. Petrographic analyses of samples collected during fieldwork were used to more precisely characterize fabrics and to determine paragenetic relationships. Stable carbon and oxygen isotopic signatures of carbonates were measured for multiple purposes: first, to compare the geochemical signatures of the caprock to carbonate clasts deposited in the outboard stratigraphy; second, to compare the geochemical signatures of caprocks formed by separate caprock "events"; and third, to understand the lateral change of isotopic signatures along the salt wall. Finally, we have employed the use of a geochemical tool in an innovative way. U-Pb age dating of the carbonate caprock at Gypsum Valley was used to assess whether or not the age of the caprock is correlative to the adjacent outboard strata and age of carbonate clasts in the outboard stratigraphy.

Detailed field mapping of the carbonate caprock exposed at the salt-sediment interface was completed. The outcrop expression of this caprock was documented to establish a comprehensive

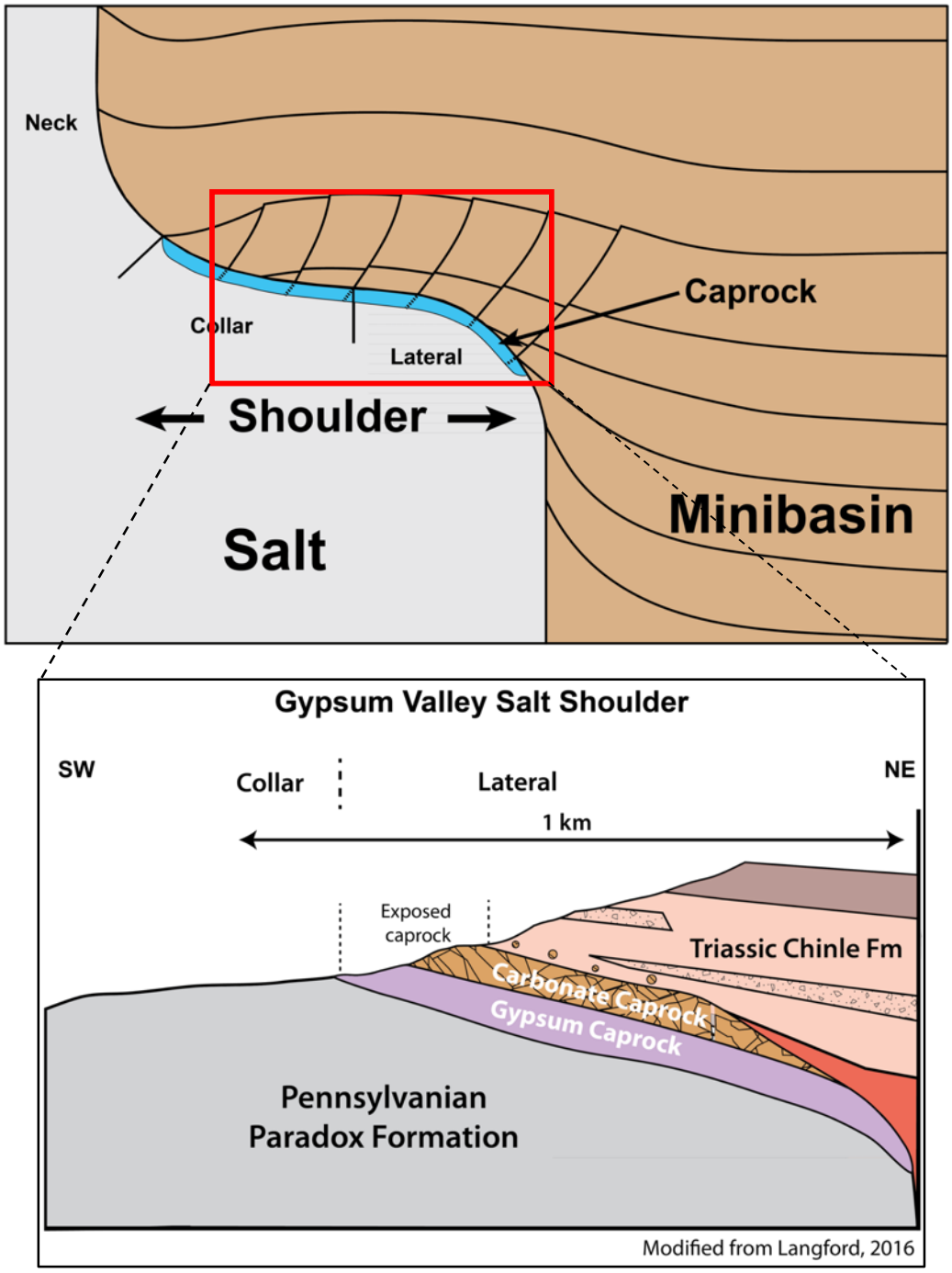

Figure 10. Top image is a conceptual model that illustrates the stratal geometries flanking and overlying a salt shoulder with an associated antiformal trap bounded by post-depositional faults. Bottom image is a schematic diagram illustrating the modern exposure of caprock atop of the Gypsum Valley salt shoulder, onlapped by the Triassic Chinle Formation.

geologic map of the fabrics and lithologies of the gypsum and carbonate caprock exposed along the entire length of the eastern flank of the Gypsum Valley salt wall. Mapping and data collection in the field was done using the application Clino on an iPhone 6. Five stratigraphic sections were measured along strike of the diapir margin in the gypsum and carbonate caprock, ending at the Triassic Chinle Formation (Figure 11). A 1.5 m Jacob staff with 0.1 m increments and a Brunton compass were used to measure the thickness and orientation of caprock and the stratigraphy overlying caprock. A 100-meter measuring tape was used to measure the lateral extent of discontinuous features in the caprock such as zones of textural or structural variability. Stratigraphic sections were recorded in detail along with their GPS coordinates. Detailed observations were recorded pertaining to lithologic and structural attributes of the exposed caprock, including: mineralogy, fabric, crystal size, fresh and weathered color, cross-cutting relationships, competency of units, lateral and stratigraphic extent of each fabric type, expression of fabric contacts, GPS location, and sample number. The location of each sample was recorded using GPS coordinates in a field notebook.

A petrographic examination of these fabrics was necessary for unambiguous mineral phases identification (i.e. calcite and dolomite), to determine the timing of progressive mineralization stages, and to document characteristics unique to each caprock fabric. Samples collected from the field were cut into billets using a rock saw at the University of Texas at El Paso in the Geological Sciences Department. Billets were labeled and sent to Spectrum Petrographic to be mounted and cut into 30μm-thick thin sections. One half of each sample was stained with potassium ferricyanide and alizarin red-S to aid in the distinction of calcite/dolomite/iron-rich calcite/iron-rich dolomite. Petrographic analysis of thin sections was completed using a Leica DM

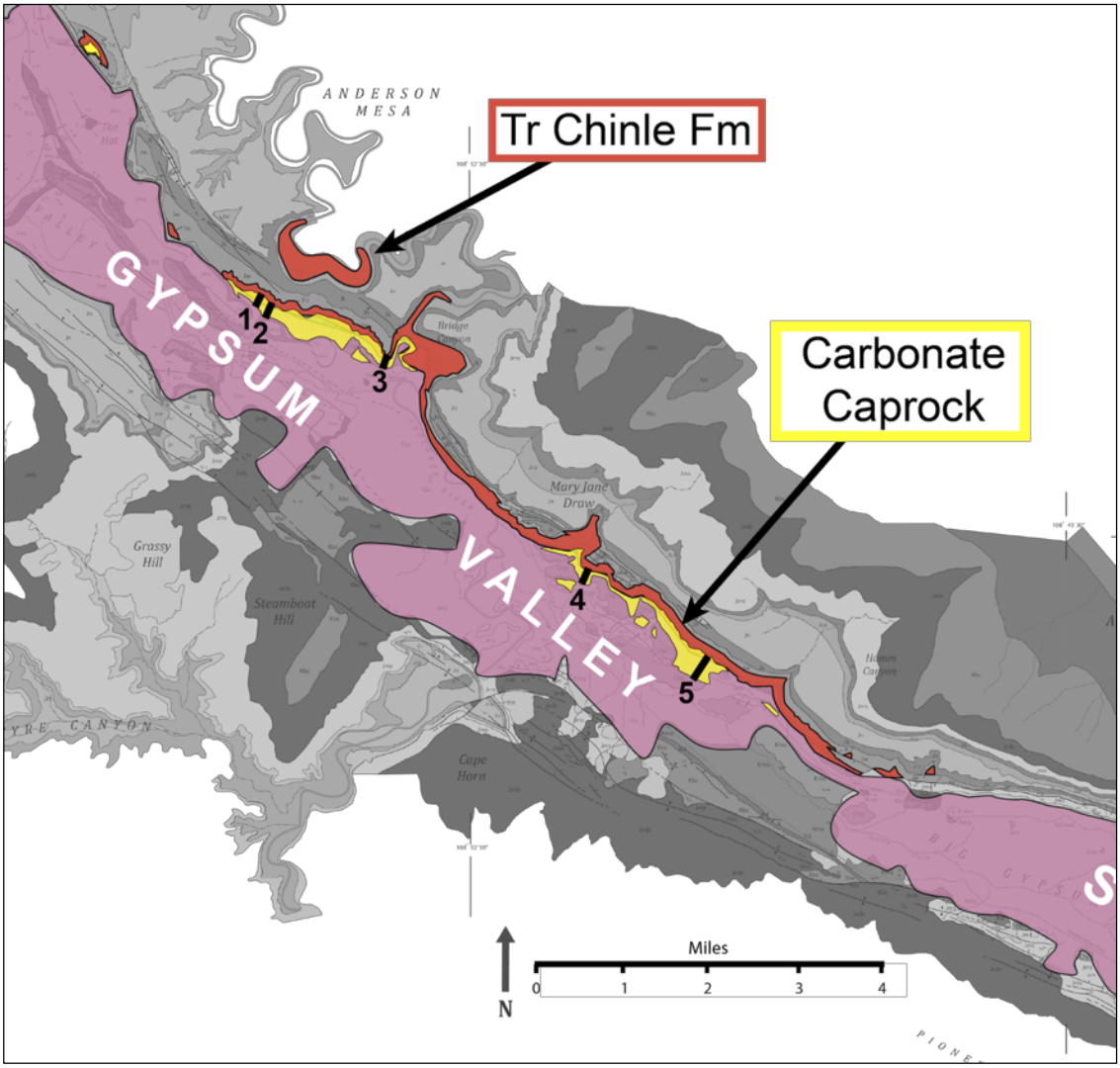

Figure 11. Geologic map of Gypsum Valley displaying the location of the 5 measured sections though gypsum and carbonate caprock. The Paradox Formation is pink, the gypsum and carbonate caprock is yellow, and the overlying Triassic Chinle Formation is orange.

750P petrographic microscope. Key features were documented, including fabric type, mineralogy, matrix, cement, porosity, sedimentary structures, and diagenetic features.

In addition to the physical attributes of carbonate caprocks and Chinle carbonate clasts, their geochemical signatures were documented. Carbonate minerals record geochemical properties of the environment in which they were precipitated and this provides essential clues about their formation. Each caprock produced by an "event" may have its own distinct geochemical signature, indicated by its carbon and oxygen isotopic values. Carbon and oxygen isotopic values were acquired from samples collected along the salt wall in order to build a geochemical database for the Gypsum Valley carbonate caprock. Preparing rock samples for isotopic analysis involved powdering each sample using a Dremel drill. Samples of approximately four milligrams were placed in plastic vials and labeled with their sample number and bulk mineralogy. A total of 49 samples were sent to the W.M. Keck Paleoenvironmental & Environmental Stable Isotope Laboratory (University of Kansas) to determine their oxygen ($\delta^{18}O$) and carbon ($\delta^{13}C$) isotope values using the phosphoric acid digestion method. Samples were calibrated to the Vienna PeeDee Belemnite (VPDB) scale. Analytical precision was monitored by daily analysis of a standard (NBS-18). Standards are run at the beginning, middle, and end of a 40-sample cue. Runs were stopped if the standard ^{18}O was more than 0.17‰ off. The $\delta^{18}O$ and carbon $\delta^{13}C$ values of the NBS-18 standard are –23.20‰ and –5.01‰, respectively.

Finally, U-Pb dating was used to determine if the age of the exposed carbonate caprock at Gypsum Valley is correlative with the outboard Triassic Chinle Formation, and provide a test for the caprock event model. Ages were obtained with the use of two independent radioactive decay systems, ^{238}U-^{206}Pb and ^{235}U-^{207}Pb, which provided crosschecks on the reliability of the ages (Rasbury and Cole, 2009). The method is based on the well–documented observation that with

time, a parent isotope decays to its daughter isotope in a predictable fashion. Linear regression through a group of samples from the same system results in a slope from which an age can be determined on the basis of the accepted decay rate for the parent isotope (Rasbury *et al.* 2009). If a system initially lacked heterogeneity and remained closed throughout time, the scatter in the data is solely caused by analytical uncertainties.

Laser ablation ICP-MS (LA-ICP-MS) analyses was conducted at the Facility for Isotope Research and Student Training (FIRST) at Stony Brook University. A 213 UV New Wave laser system coupled to an Agilent 7500cx quadrupole ICP-MS was used for the analyses. ^{238}U, ^{232}Th, and ^{208}Pb, ^{207}Pb, and ^{206}Pb isotopes were collected sequentially for 0.1 seconds each throughout 30 second ablations, along with REE, Ca, Mg, Mn, Fe and Sr. A 160 μm spot size was used for the analyses. Unknown sample spots were bracketed by at least 5 standard spots and 2 standard spots were interspersed after every 5 unknown sample spots. The WC-1 calcite standard (Roberts et al., 2017) was used as a matrix matched standard, and NIST612 was used as a cross-check on data quality and for element concentration analyses. Data were reduced in Iolite (Paton et al., 2011) using the U-Pb Geochronology 3 (or 4) data reduction scheme for U-Pb analyses. Element concentrations were processed with the Trace Element DRS in semi-quantitative mode. These data reduction schemes subtract baselines and correct for downhole fractionation and drift of the signal. For U-Pb LA-ICP-MS, reduced data are plotted on a Tera Wasserburg isochron plot using IsoExcel (Ludwig, 2003) and not corrected for common Pb. The lower intercept age is taken as the age of the sample.

Chapter 2: Classification of the Gypsum and Carbonate Caprock at the Gypsum Valley Salt Wall

Existing caprock fabric classification schemes are primarily based on outcrop and core samples from the Texas Gulf Coast domes (Kyle and Posey, 1991) where two distinct carbonate caprock fabric types are recognized: "lower banded zone" and "upper variegated zone". Although this bipartite scheme addresses the broad differences in caprock fabrics, it does not adequately describe the variability in mineralogy and fabrics found in the caprocks at Gypsum Valley. To document the wide range of textural and mineralogical properties of caprock, a new classification scheme based on fabric types was developed by the caprock research group at UTEP in order to facilitate interpretation of caprock lithologies in an organized and effective manner. The development of a comprehensive classification is the first step toward deciphering the complex diagenetic processes involved in caprock formation. Understanding the genetic history of caprock fabrics will allow for better identification and prediction of the distribution of caprock mineralogies and fabrics.

Instead of using the term caprock, which refers to the entire rock package located between the salt and the outboard stratigraphy, the term *capstone* will be used to differentiate individual caprock-rock types found within the entire caprock body. This classification scheme (Table 1) is based on the recognition of four distinct macroscopic capstone fabrics: 1) Massive: homogeneous, with micro-to-coarsely crystalline subdivisions; 2) Porphyritic: comprising two distinct crystal sizes, one significantly larger than the other; 3) Layered: subdivisions based on layer size that includes: microlaminated (1-3mm), laminated (3-10mm), and banded (>10mm); 4) Brecciated: subdivided into crackle, mosaic and disorganized, based on the degree of separation between the brecciated caprock clasts. Primary mineralogy is used as a modifier of fabric type, which typically includes anhydrite, gypsum, calcite and dolomite. Breccia clasts may internally display massive,

porphyritic or layered fabric. To address this issue, the dominant mineralogy and subordinate fabric types are attached to the overall fabric name as prefix-type modifiers (e.g. massive brecciated dolomite capstone).

TABLE 1: CLASSIFICATION OF CAPROCKS ASSOCIATED WITH SALT DIAPIRS ACCORDING TO FABRIC

MASSIVE	PORPHYRITIC	LAYERED			BRECCIATED		
		MICROLAMINATED	LAMINATED	BANDED	CRACKLE	MOSAIC	DISORGANIZED
Massive fabrics consist of a homogeneous mineralogy and crystal size, and lack any internal structure.	Porphyritic fabrics consist of two distinct crystal size populations, one significantly larger than the other.	Microlaminated fabrics consist of **1-3 mm thick laminae**.	Laminated fabrics consist of **3-10 mm thick laminae**.	Banded fabrics consist of **laminae greater than 10 mm thick**.	Crackle breccias contain clasts that display little relative displacement.	Mosaic breccias consist of clasts that are loosely fitted together. Clast bounaries are typically oriented parallel to each other.	Disorganized breccias consist of spatially independent clasts. Clast boundaries are rarely parallel to one another.
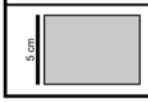	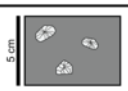			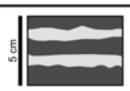	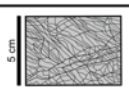	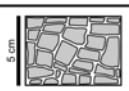	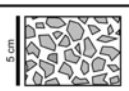

2.1. Massive Capstone

Capstone fabrics that exhibit a homogeneous mineralogy and texture (i.e. internally structureless), and have a vertical unit thickness greater than 30 mm, is termed massive.

2.1.1. Massive dolomite capstone

At Gypsum Valley, the most common mineralogy comprising the massive fabric type is micritic dolomite, but coarsely-crystalline, massive dolomite has also been found. The weathered surface of the massive dolomite capstone is most commonly light, orange-tan (Figure 12A), but has also been observed as a dark red-purple color (Figure 12B). On a fresh surface, the color ranges from black to dark purple, to light pink. The outcrop expression of this fabric type consists of resistant blocks, 0.5 - 5 m wide to 0.25 - 1.5 m tall that form small ledges. The blocks do not display a consistent orientation or dip. In thin section, (Figures 12C & D), homogeneous, anhedral, microcrystalline dolomite is observed.

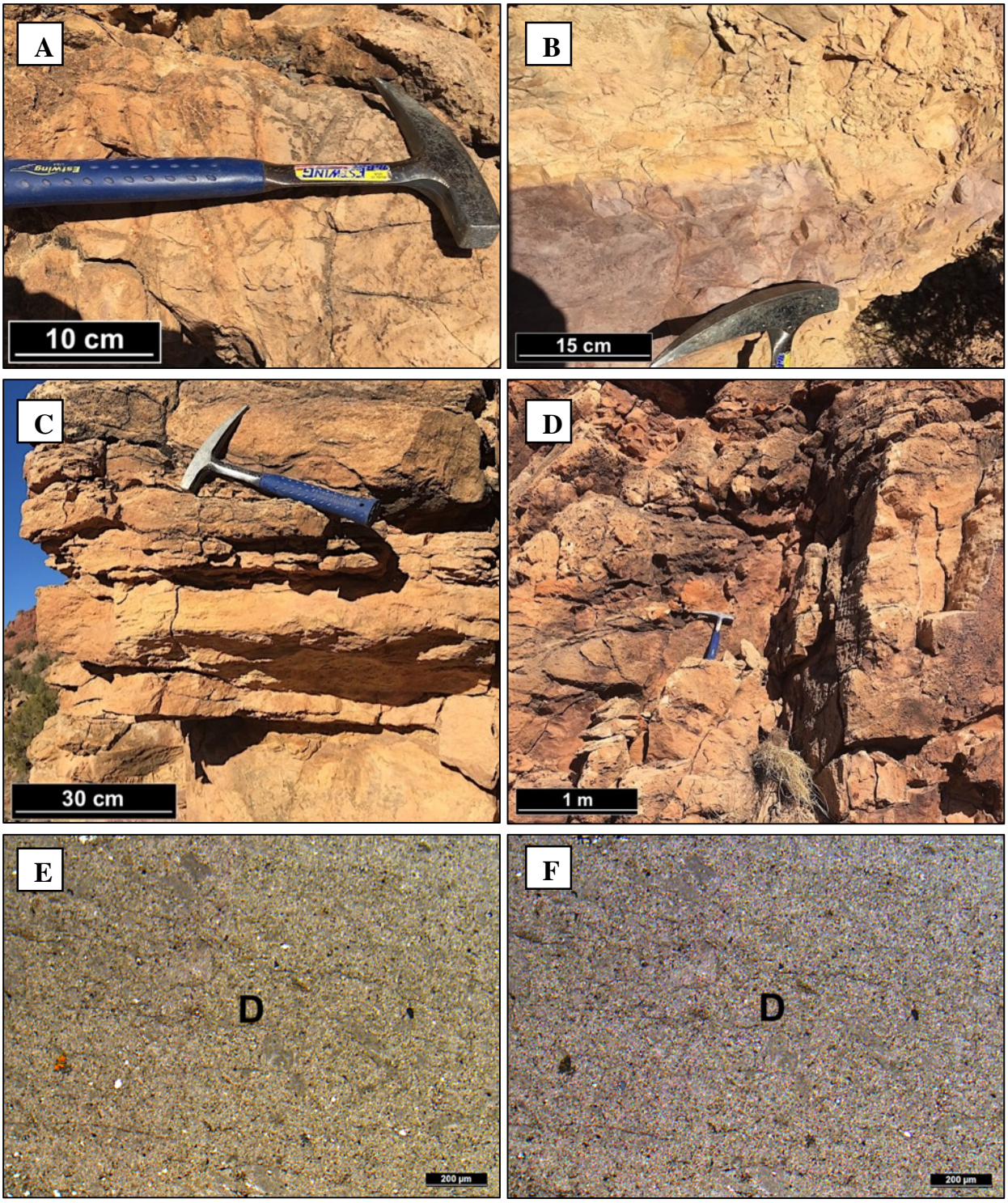

Figure 12. Massive dolomite capstone. A. Outcrop example of tan-orange microcrystalline dolomite capstone; B. Outcrop example of tan-purple microcrystalline dolomite capstone; C. & D. Outcrop examples of tan microcrystalline dolomite. Photomicrographs of microcrystalline dolomite in plane-polarized light, E, and cross-polarized light, F; scale bars = 200 µm.

2.1.2. Massive calcite capstone

Massive calcite capstone consists of primarily micritic calcite, although coarsely-crystalline calcite is also found. The weathered surface is typically light gray and contains local, 1-5mm thick, white coarsely-crystalline calcite veins (Figure 13A). The fresh surface is also gray to light gray in color. The outcrop expression is much more recessive than its dolomitic counterpart, only rarely occurring as ledge-forming blocks. The fabric is most commonly expressed as recessive 2 - 6 cm wide cobbles scattered on a recessive carbonate-dominated slope at the gypsum-carbonate caprock contact (Figure 13B). In thin section (Figures 13C & D), this fabric is homogeneous and consists of anhedral, microcrystalline to coarsely-crystalline calcite.

2.1.3. Massive gypsum capstone

Massive gypsum capstone typically consists of anhedral to subhedral, fine- to coarsely-crystalline gypsum and forms low, rolling hills within the gypsum caprock interval on outcrop. It is white to gray on fresh and weathered surfaces (Figure 14A & B). This fabric makes up 95% of the entire gypsum caprock at Gypsum Valley. In thin section (Figures 14C & D), this fabric is homogeneous and contains microcrystalline to coarsely-crystalline, anhedral gypsum crystals.

2.2. Porphyritic Capstone

Capstone with a fabric forming a unit greater than 30 mm thick and consisting of two distinct crystal sizes is termed porphyritic. The groundmass of this fabric is typically very finely crystalline. The larger crystal size is commonly a pseudomorph of a preexisting mineralogy, but occasionally consists of a larger crystal size of the same mineralogy as the groundmass (e.g. gypsum rosettes in a finely-crystalline gypsum groundmass).

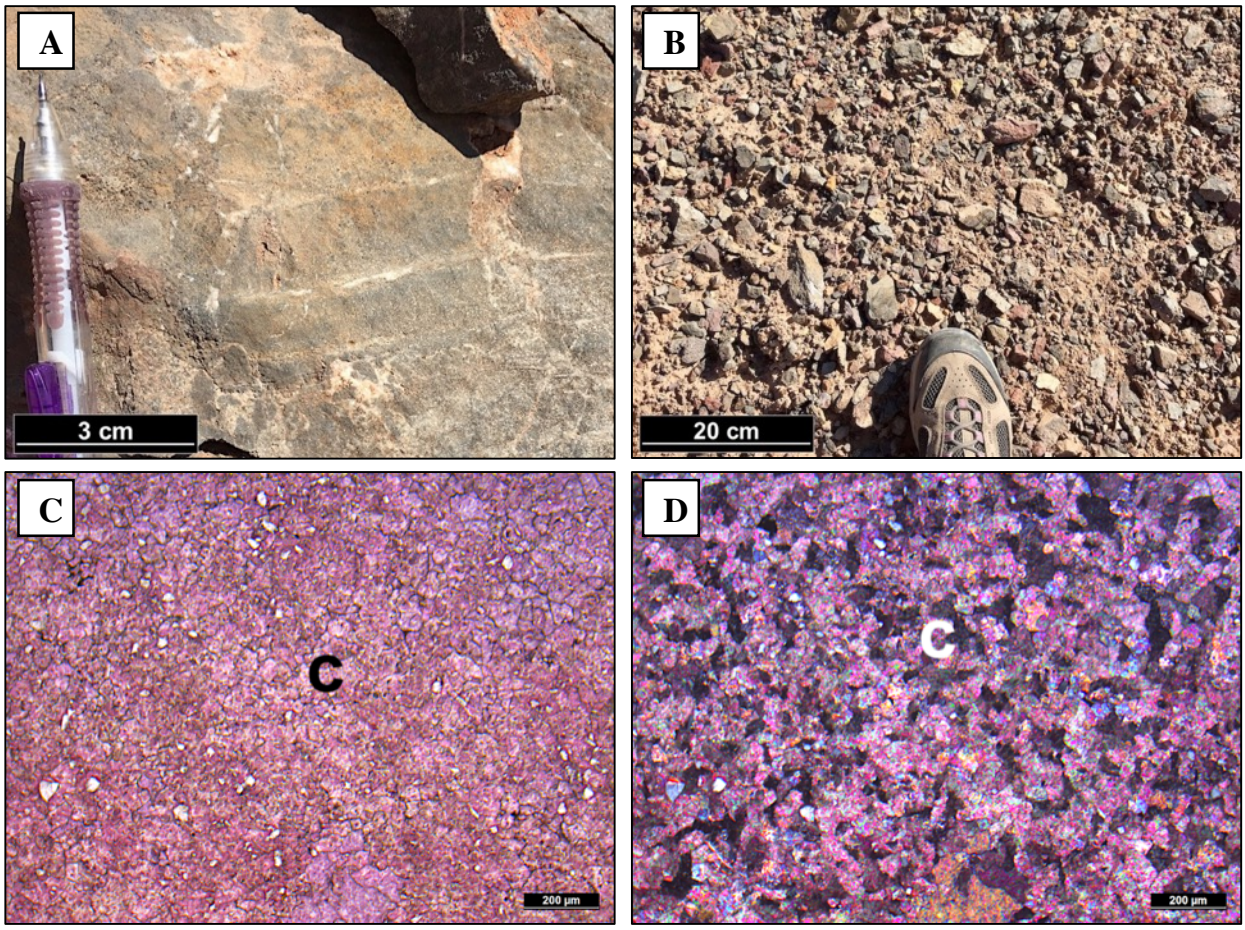

Figure 13. Massive calcite capstone. A. Outcrop example of gray, microcrystalline, calcite capstone containing white calcite veins; B. Outcrop expression of recessive calcite capstone; Photomicrographs of fine-medium crystalline calcite (C) in plane-polarized light, C, and cross-polarized light, D; scale bars = 200 µm.

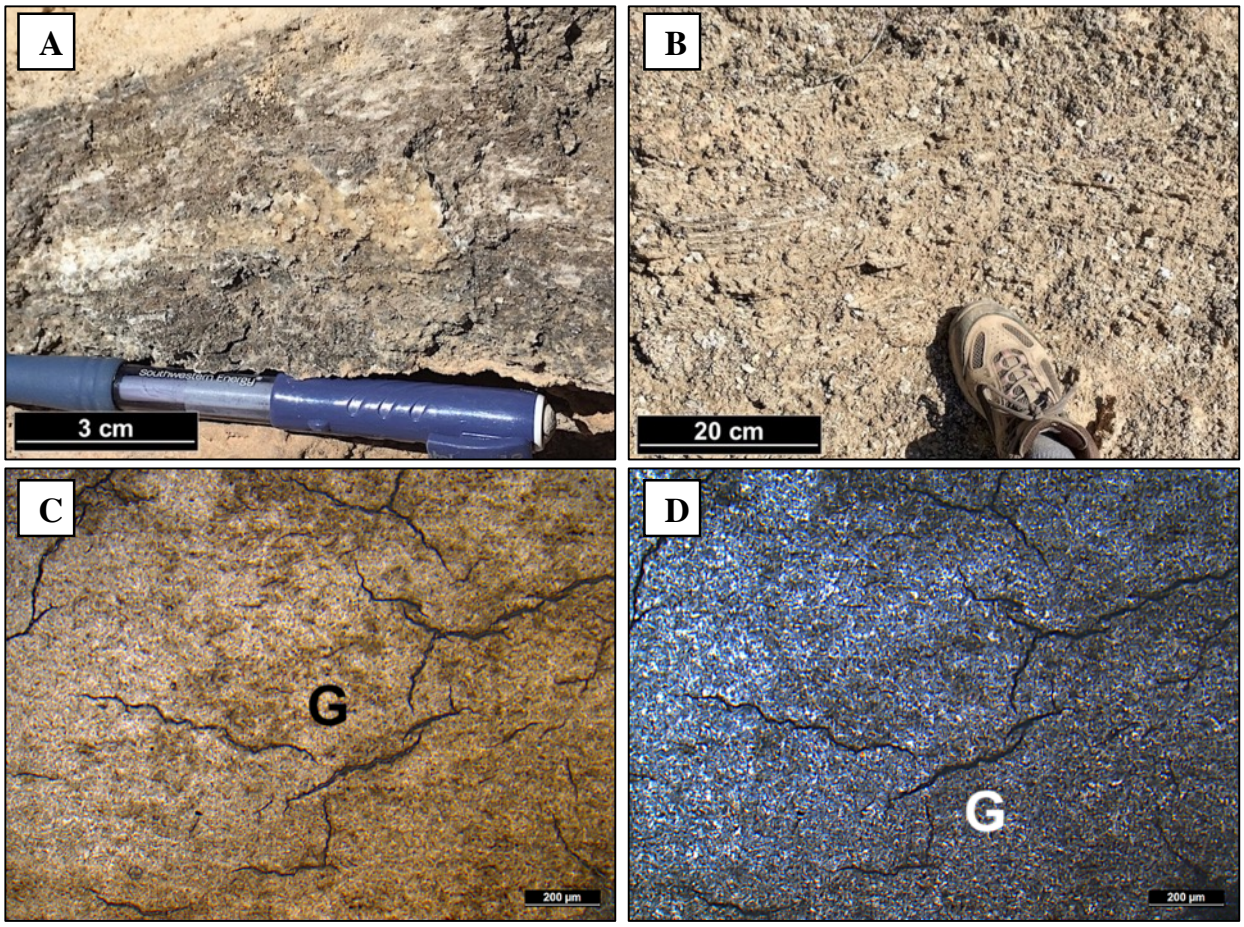

Figure 14. Massive gypsum capstone. A. Outcrop expression of massive gypsum capstone. B. Outcrop expression of recessive gypsum capstone. Photomicrographs of fractured microcrystalline gypsum (G) in plane-polarized light, C, and cross-polarized light, D; scale bars = 200 µm.

2.2.1. Porphyritic silica-dolomite capstone

This fabric type is composed of millimeter to centimeter-wide white silica nodules suspended in a microcrystalline tan dolomite matrix (Figure 15A & B). The shape of the white silica nodules varies from circular to elongated lenses that range from 2 – 10 mm in length. The silicified nodules are commonly concentrated within 2 – 15 cm tall "beds" within the dolomite capstone where they form silicified clusters enclosed in a microcrystalline dolomite matrix. In thin section (Figure 15C & D), the silica is in the form of chert and chalcedony replacement of dolomite.

2.2.2. Porphyritic silica-calcite capstone

This fabric type is composed of white silica nodules suspended in a gray micritic calcite matrix (Figure 16A & B). The white silica nodules are typically lenticular to circular in shape and are ~0.5 – 2 cm wide. The silicified nodules are commonly concentrated within a 10 – 25 cm "beds" within the calcite capstone. The outcrop expression of this fabric is characterized by 10 – 20 cm wide, semi-resistant, isolated outcrops. In thin section (Figure 16C & D), a large, ~ 2 mm wide silicified nodule is surrounded by a calcite matrix (red). Within the silicified nodule, many scattered isolated lath-shaped anhydrite pseudomorphs are filled by calcite. The nodular shape of silicified zones appears to be pseudomorphs of gypsum rosettes.

2.2.3. Porphyritic calcite capstone

This fabric is composed entirely of calcite, where coarsely-crystalline calcite clusters are suspended in a microcrystalline calcite matrix (Figure 17A & B). The microcrystalline calcite matrix is typically light to dark gray on outcrop. The coarsely-crystalline calcite clusters are white in color and range from 2 – 10 mm in length and, like the previous porphyritic fabrics, are clustered

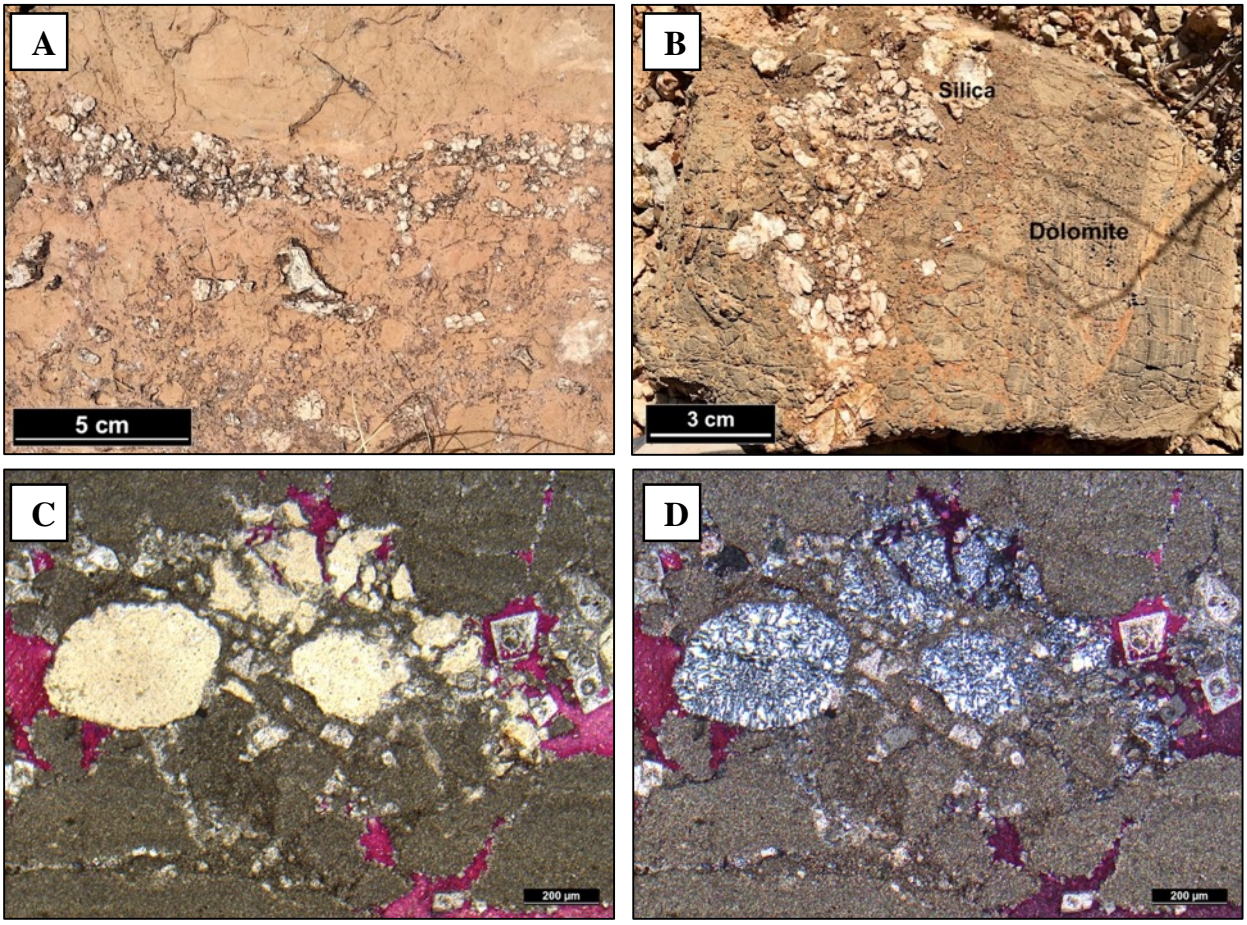

Figure 15. Porphyritic silica-dolomite capstone. A. Outcrop example of microcrystalline, light tan dolomite capstone containing a "bed" of 1-6 mm wide, white silica nodules; B. Outcrop example of microcrystalline crackle breccia dolomite capstone containing scattered, 1-10 mm wide, white silica nodules. Photomicrographs of a porphyritic silica-dolomite capstone comprised of an elongate, patchy cluster of silicified nodules (S) in a micritic dolomite matrix (D) in plane-polarized light, C, and cross-polarized light, D, scale bars = 200 µm.

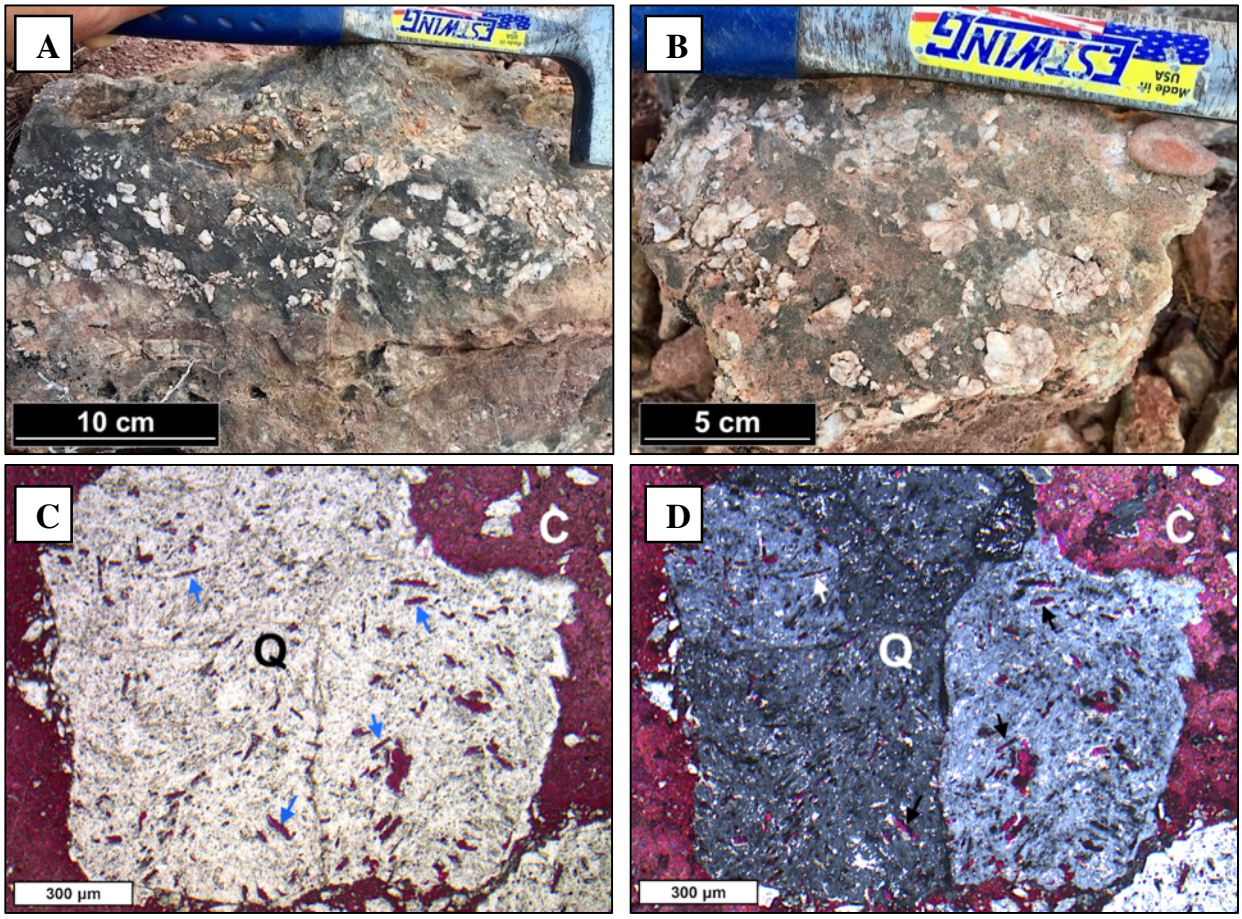

Figure 16. Porphyritic silica-calcite capstone. A. Outcrop example of a porphyritic silica-calcite capstone, consisting of a gray micritic calcite matrix encasing white silicified lens-shaped nodules; B. Outcrop example of blocky, round, silicified nodules in a microcrystalline calcite matrix. Photomicrographs of a porphyritic silica-calcite capstone in plane-polarized light, C, and cross-polarized light, D. Scale bars = 300 µm. These photomicrographs show a silicified blocky, rosette-like nodule (S) in a micritic calcite matrix (red) (C). Within the silicified nodule, many scattered isolated lath-shaped anhydrite pseudomorphs are filled by calcite (arrows).

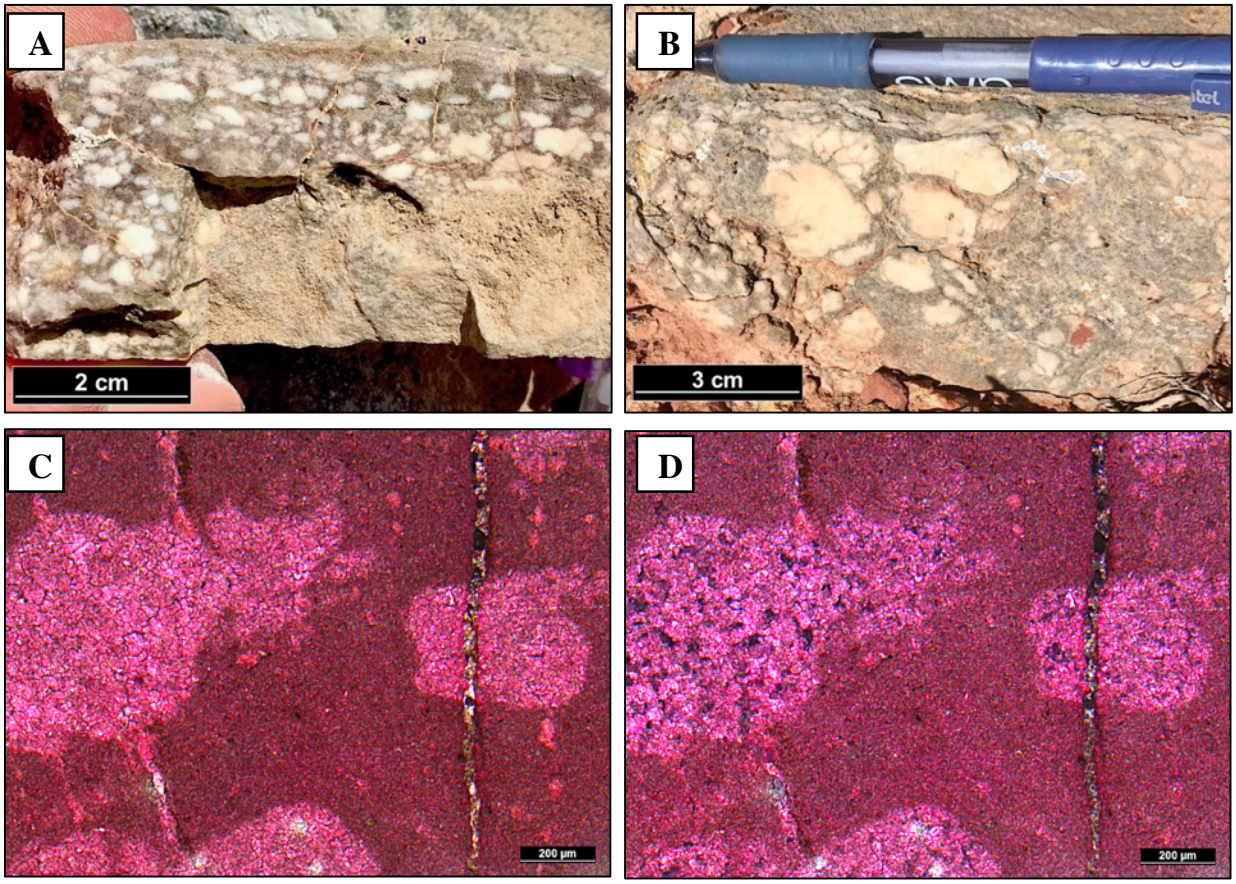

Figure 17. Porphyritic calcite capstone. Images A. and B. are outcrop example of a porphyritic calcite capstone consisting of a finely crystalline calcite matrix (grayish-tan) with coarsely crystalline calcite clusters (white). Photomicrographs of porphyritic calcite capstone consisting of medium to coarsely crystalline calcite clusters in a micritic calcite matrix. Plane-polarized light, C, and cross-polarized light, D, scale bars = 200 µm.

in 2 – 5 cm "beds". The outcrop expression of this fabric is characterized by recessive, 10 – 15 cm wide cobbles within the greater slope forming carbonate caprock. In thin section (Figure 17C & D), blocky, slightly elongated clusters of anhedral, coarsely-crystalline calcite are seen suspended in a microcrystalline calcite matrix.

2.2.4. Porphyritic gypsum capstone

The porphyritic gypsum capstone fabric, originally observed by Lerer (2017), is composed entirely of gypsum and consists of dark gray gypsum rosettes within a light gray, finely-crystalline gypsum matrix (Figure 18A). The gypsum rosettes are a 2 – 5 mm wide and are scattered throughout the sample. This fabric is not common within the gypsum caprock, but when observed, it is characterized by a small, ~0.5 m patch of slightly more resistant gypsum capstone within the greater recessive gypsum caprock. In thin section (Figure 18B), the dominant texture is a microcrystalline aggregate of 10 – 100 μm sized, interlocking anhedral gypsum crystals. The microcrystalline matrix is locally aligned around the peripheral of 1 – 2 mm wide, subhedral, coarsely-crystalline gypsum rosettes.

2.3. Layered Capstone

Capstone fabrics that have an apparent visual layering to them, identifiable by either alternating color, crystal size, or mineralogy, are termed layered. Subdivisions are based on the thickness of individual laminae, termed microlaminated, laminated, or banded. The orientation of the majority of the layered fabrics within gypsum and carbonate capstone parallels that of the adjacent halokinetically drape-folded Chinle Formation.

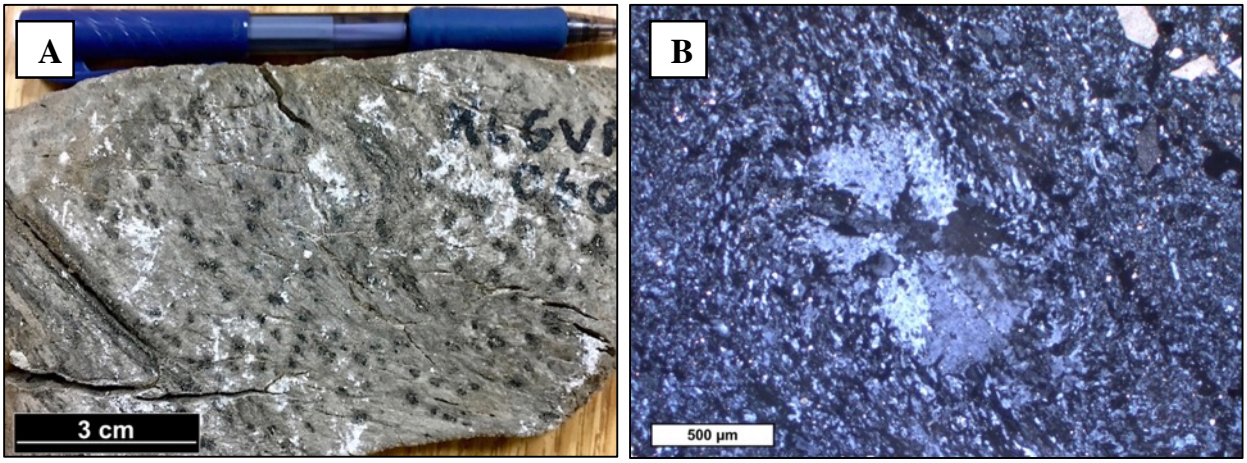

Figure 18. Porphyritic gypsum capstone. A. Hand sample of a porphyritic gypsum capstone, consisting of a finely crystalline gypsum matrix (light gray) with coarsely crystalline gypsum rosettes (dark gray); B. Cross-polarized photomicrograph of image A., finely crystalline gypsum matrix encasing gypsum rosettes. Scale bar = 500 µm. Sample collected and photomicrograph taken by Lerer, 2017.

2.3.1. Microlaminated Capstone

Caprock displaying horizontal, 1 – 3 mm thick laminae are termed microlaminated. Laminations are typically recognized by internal crystal size variations, organic content variations, or by interchanging mineralogies indicated by a change in laminae color. The orientation of laminae most commonly parallel the orientation of the adjacent outboard strata.

2.3.1.1. Microlaminated dolomite capstone

The most common layered fabric at Gypsum Valley is the microlaminated dolomite capstone. This fabric consists of thin, parallel, 1 – 2 mm thick dolomite laminae (Figure 19A & B). The weathered surface ranges from light to dark-orange-tan in color, and the color of the fresh surface is typically black, but dark purplish-red and light pink shades have been observed. The outcrop expression of this fabric is characterized by resistant, 0.5 – 2 m tall, 1 – 5 m wide, blocks of dolomite capstone. Petrographically, laminae are defined by either alternating inclusion-rich and inclusion-poor laminae; or alternating finely-crystalline and medium to coarsely-crystalline laminae (Figure 19C & D).

2.3.1.2. Microlaminated calcite capstone

Microlaminated calcite capstone is texturally very similar to its dolomite counterpart but differs in that it is composed entirely of calcite and is light to medium gray in color (Figure 20A & B). The outcrop expression of this fabric is characterized by 20 – 40 cm wide, semi-resistant isolated outcrops within the greater slope forming carbonate caprock. Petrographically, laminations are defined by alternating organic-rich, micritic calcite laminae and inclusion-free, coarsely-crystalline calcite laminae (Figure 20C & D).

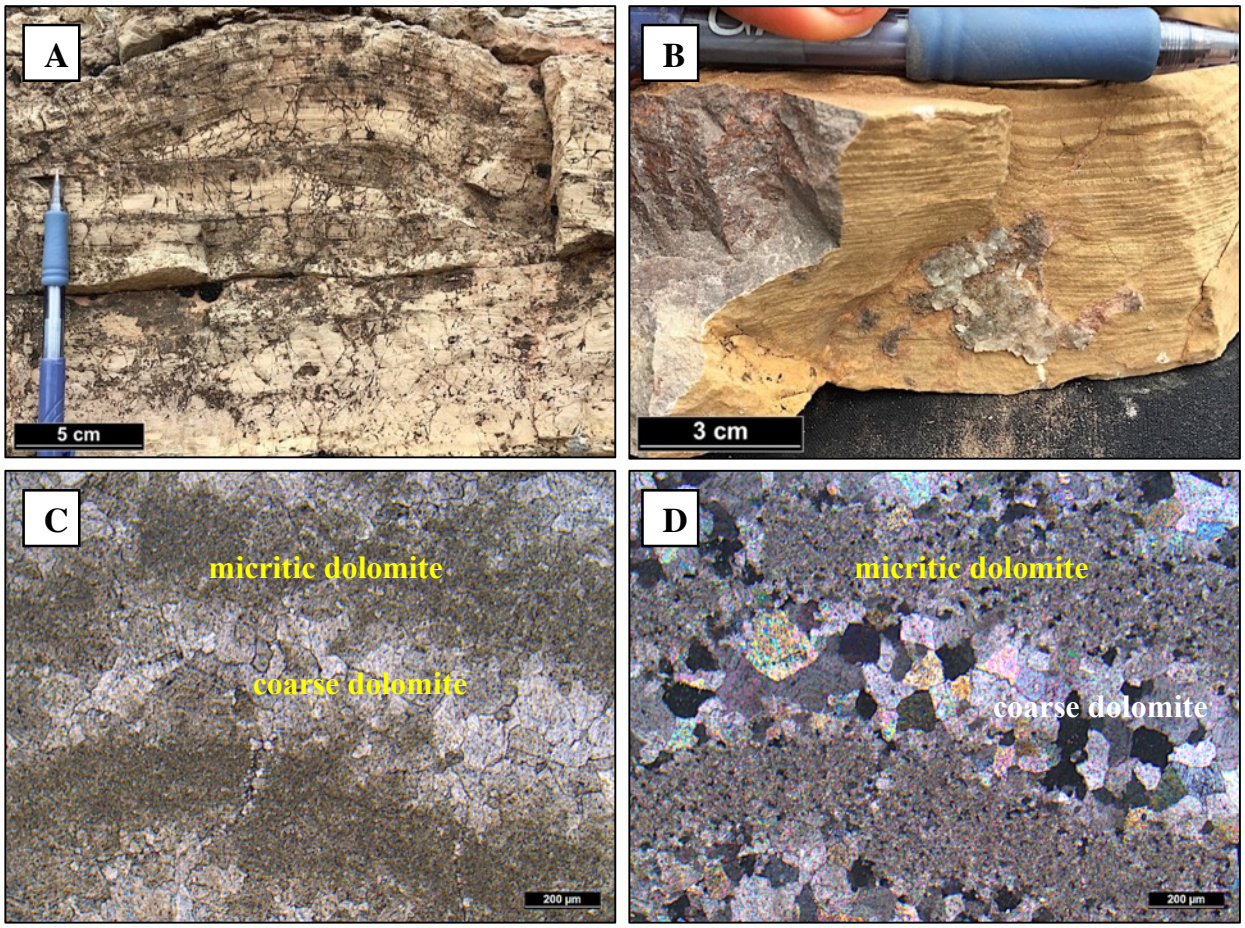

Figure 19. Microlaminated dolomite capstone. A. Outcrop example of a tan microlaminated dolomite capstone; B. Outcrop example of a fresh (red-purple) and weathered (orange-tan) surface of the microlaminated dolomite fabric. Photomicrographs of the laminations in plane-polarized light, C, and cross-polarized light, D, scale bars = 200 µm. Laminations defined by interlayered inclusion-rich micritic dolomite laminae and coarsely crystalline, anhedral to subhedral dolomite laminae.

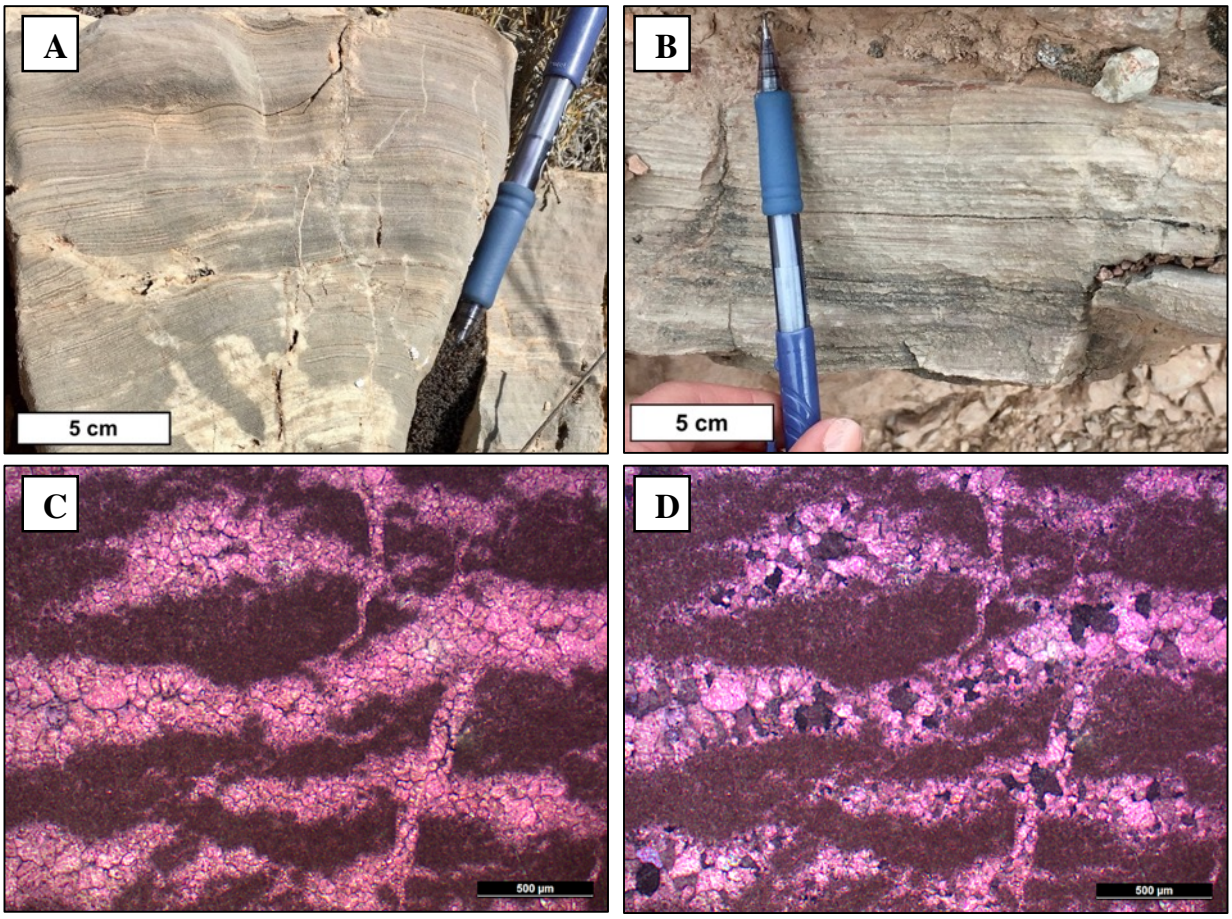

Figure 20. Microlaminated calcite capstone. Images A & B are outcrop examples of light gray, microlaminated calcite capstone. Photomicrographs of the laminations in plane-polarized light, C, and cross-polarized light, D, scale bars = 500 µm. Laminations defined by interlayered inclusion-rich micritic calcite laminae and coarsely crystalline calcite laminae.

2.3.1.3. Microlaminated gypsum capstone

This fabric consists of 1 – 2 mm thick, horizontal to concordant, stacked lamina of very finely crystalline gypsum. The laminae are visually striking (Figure 21A & B) due to their black color within the light gray to white gypsum matrix. On outcrop, this fabric is characterized by a small, ~0.5 m patch of slightly more resistant gypsum capstone within the greater recessive gypsum caprock. In thin section, the dominant texture is a microcrystalline equigranular aggregate of gypsum crystals (Figure 21C & D) with the black-colored laminae containing residual dark organic matter, which could be dead oil.

2.3.2. Laminated Capstone

Capstone displaying horizontal layers of 3 – 10 mm thick laminae are termed laminated. Laminae are obvious even on outcrop scale due to the alternating color of the laminae. This is typically attributed to alternating crystal sizes, but occasionally due to alternating mineralogy. Plastic deformation is common within this fabric in the form of small-scale folds and irregular and discontinuous laminations.

2.3.2.1. Laminated calcite capstone

Laminated calcite capstone is the most common of the laminated fabric types at Gypsum Valley. It is characterized by 5 – 10 mm thick, parallel, equal thickness laminae of alternating crystal size. The laminae alternate between gray and white laminae (Figure 22A); the gray color corresponds to coarsely-crystalline calcite, and the white color corresponds to finely-crystalline calcite. Although the color of the alternating laminae is most typically gray and white, dark pink to purple laminae has been observed as well (Figure 22B & C). Laminae occasionally show plastic deformation in the form of undulating/enterolithic and folded structures (Figure 22B).

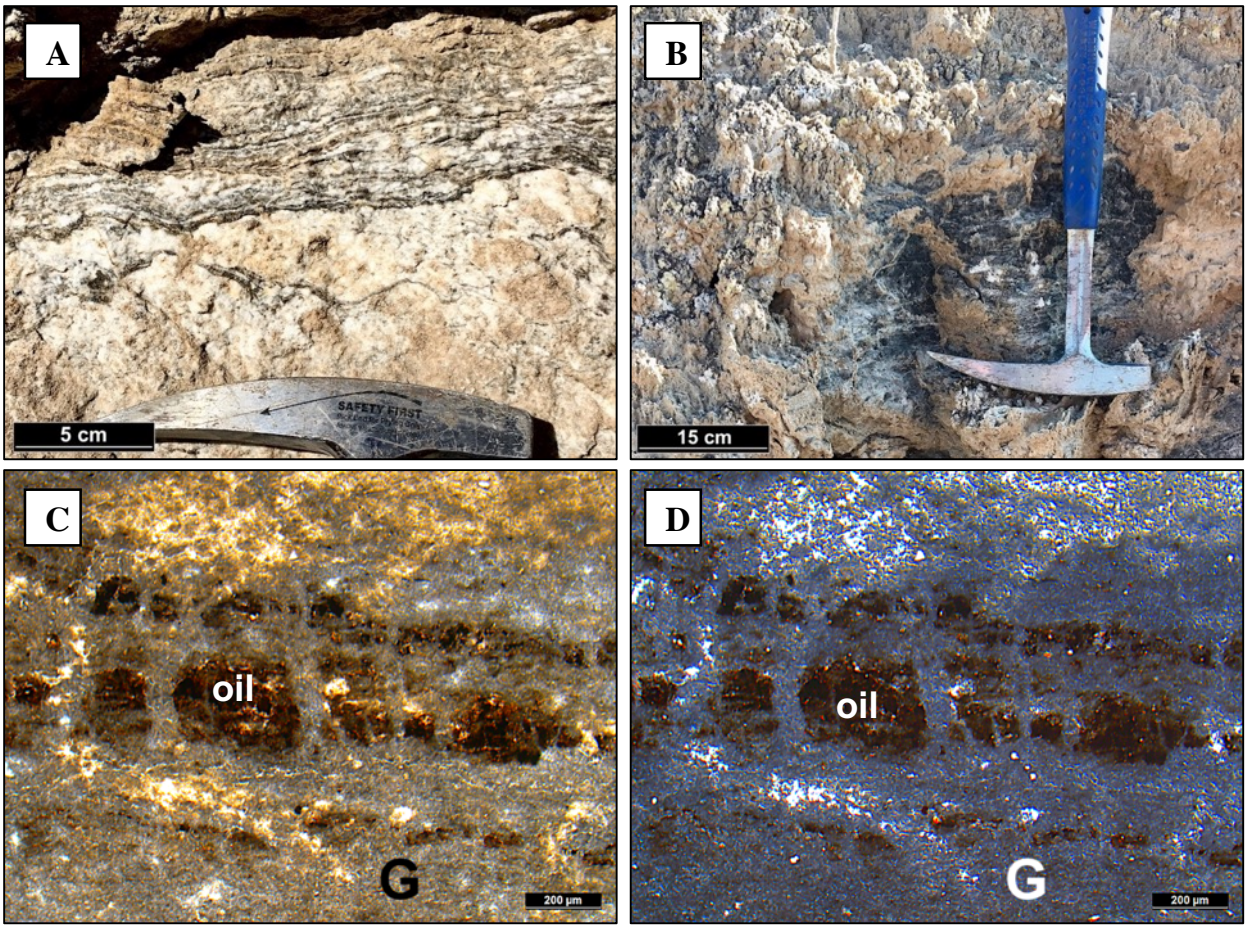

Figure 21. Microlaminated gypsum capstone. A. Outcrop example of a microlaminated gypsum capstone consisting of black, oil-filled gypsum laminae within a white gypsum matrix; B. Example of a small, black, microlaminated gypsum capstone outcrop within the greater, recessive gypsum caprock. Photomicrographs of the laminations in image A., in plane-polarized light, C, and cross-polarized light, D, scale bars = 200 µm. Laminations defined by oil-filled gypsum laminae (dark brown) in a finely crystalline gypsum matrix (G).

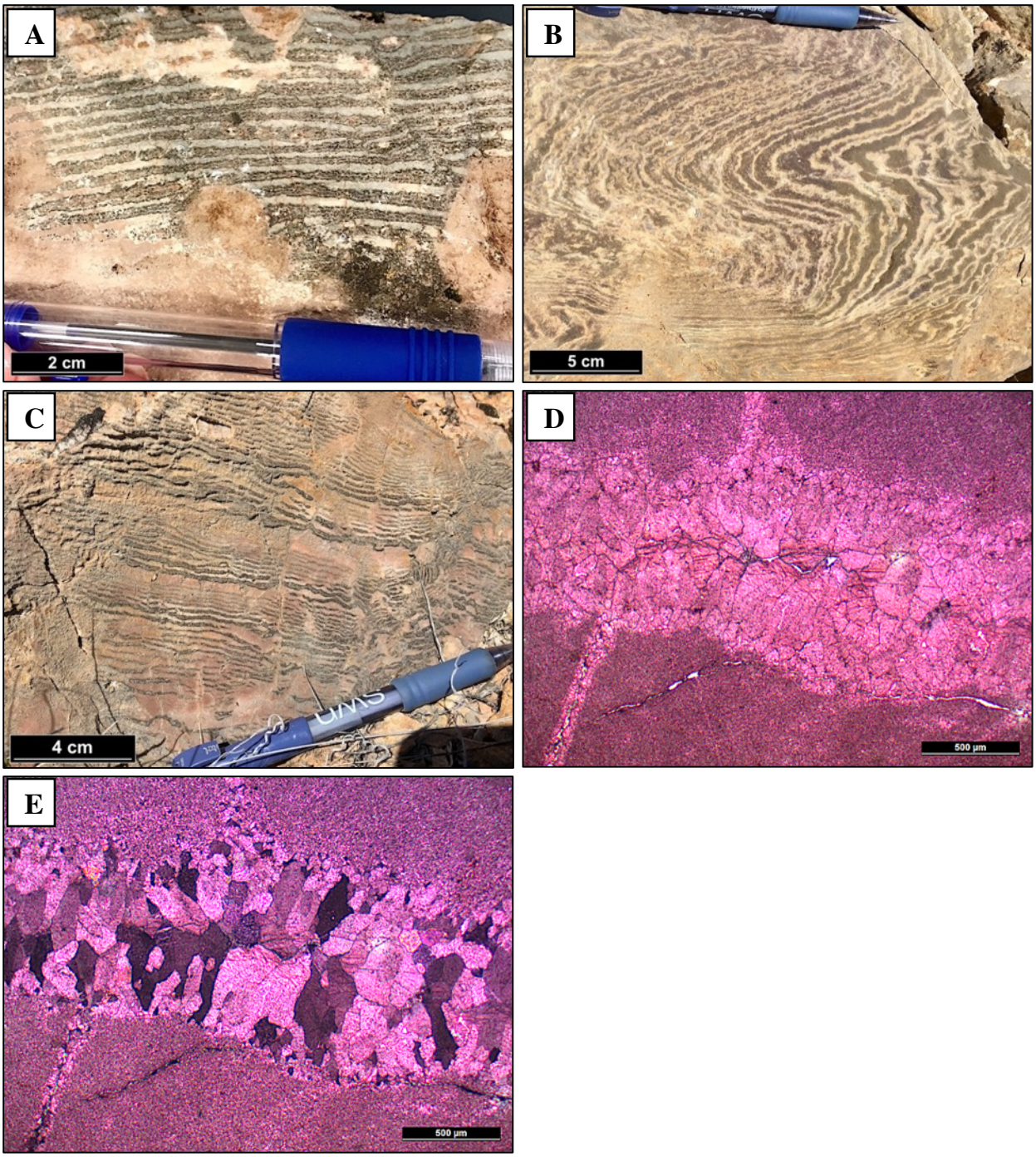

Figure 22. Laminated calcite capstone. Images A - C are outcrop examples. A. Isopachous calcite laminae, light gray laminae consist of finely crystalline calcite, dark gray laminae consist of coarsely crystalline calcite; B. Outcrop example of heavily deformed, folded calcite laminae within a laminated calcite capstone; C. Outcrop example of a laminated calcite capstone with large-scale, repeating bands of segmented laminae that thin upward. Photomicrographs of the laminations in plane-polarized light, D, and cross-polarized light, E, scale bars = 500 µm. The contact between the microcrystalline and coarsely-crystalline laminae is clearly seen.

On outcrop, this fabric is expressed as semi-resistant, 0.25 – 2 m wide isolated outcrops within the greater slope forming carbonate caprock. Petrographically, the contact between the two crystal sizes is sharp, and the coarsely-crystalline calcite laminae appear to grow upward from the microcrystalline calcite substrate to form medium to coarsely-crystalline calcite laminae (Figure 22D & E).

2.3.2.2. Laminated dolomite capstone

Laminated dolomite capstone is characterized by 3 – 10 mm thick laminae of alternating colors. On weathered surfaces this fabric displays the orange-tan color typical for all dolomitic caprock fabrics at Gypsum Valley. On fresh surfaces the thinner laminae are a dark pink-red color, and the thicker laminae are light pink in color (Figure 23A & B). On outcrop this fabric is expressed as resistant, 0.5 – 1 m wide isolated exposures within the greater slope forming carbonate caprock. In thin section, the thicker, light pink laminae are composed of fine- to coarsely-crystalline, anhedral, equigranular ferroan dolomite (blue stained). Whereas, the dark pink laminae are composed of finely-crystalline, equigranular non-ferroan dolomite.

2.3.2.3. Laminated silica-dolomite capstone

Laminated silica-dolomite capstone is characterized by 4 – 10 mm thick, dark brown dolomite laminae alternating with nodular white silica laminae. The dolomite laminae are often wavy and bend around the lens-shaped silica laminae (Figure 24A). Petrographically, microcrystalline silica is seen growing between micritic dolomite laminae (Figure 24B & C). On outcrop, this fabric forms resistant 0.1 – 0.5 m wide ledges within the slope-forming carbonate caprock.

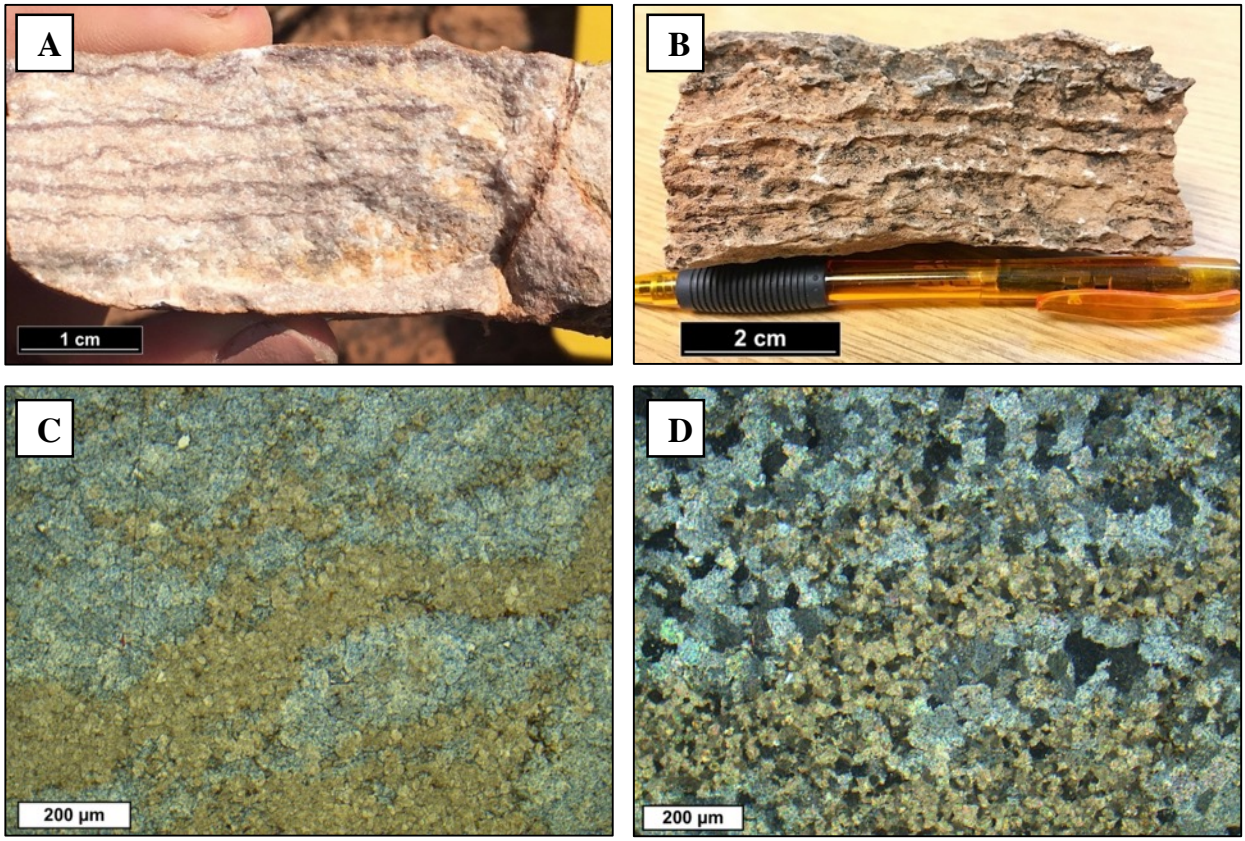

Figure 23. Laminated dolomite capstone. A. Fresh surface of a laminated dolomite capstone, laminae defined by alternating light pink and dark pink dolomite; B. Weathered surface of image A., dolomite is orange-tan in color and laminations are defined by differential weathering. Photomicrographs of the laminations in plane-polarized light, C, and cross-polarized light, D, scale bars = 200 µm. Laminations defined by finely-crystalline, equigranular, dolomite laminae composed of interlayered iron-rich (stained blue) and iron-poor dolomite.

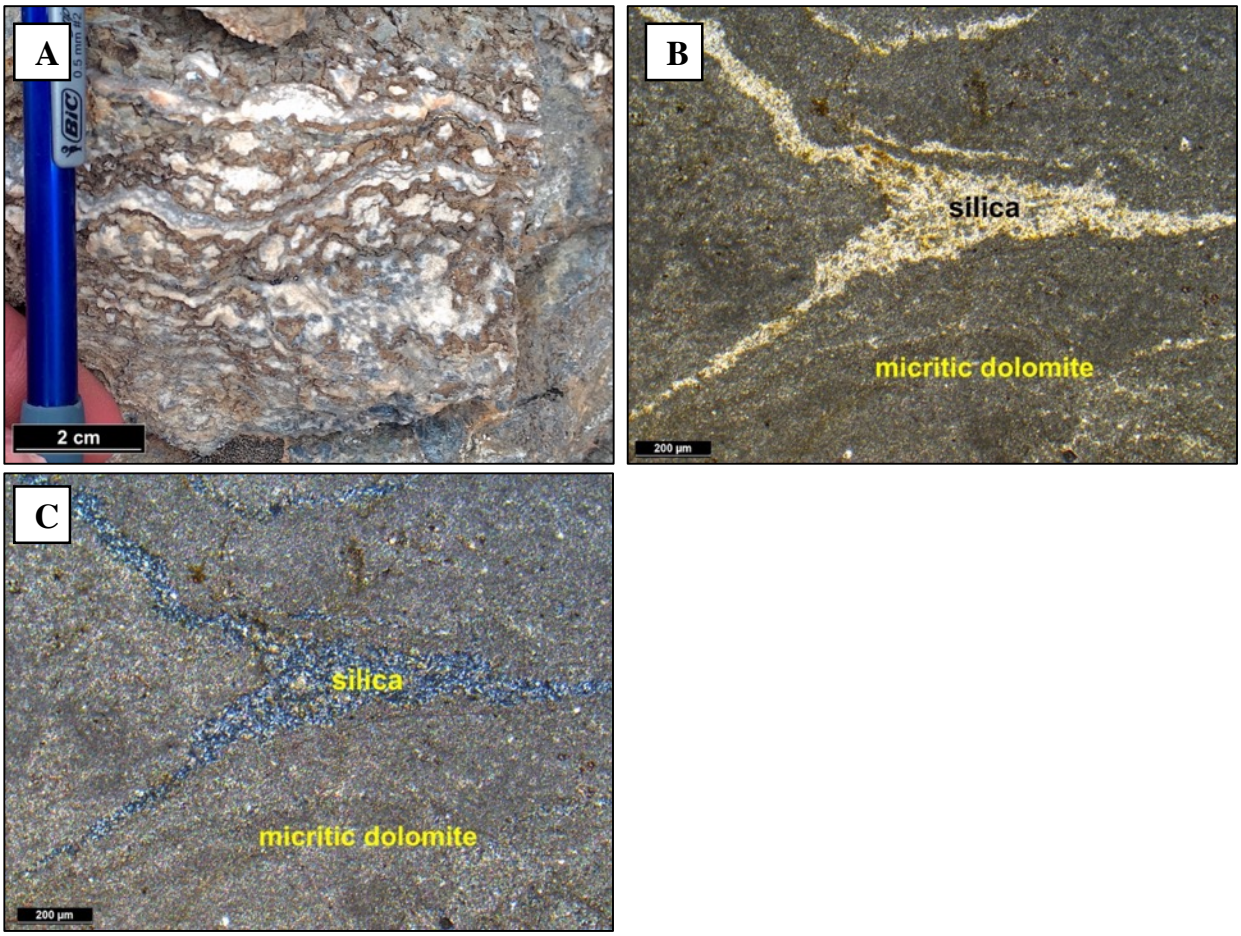

Figure 24. Laminated silica-dolomite capstone. A. Outcrop example of laminated silica-dolomite capstone, the dolomite laminae are dark brown and are deformed by the nodular, white silica laminae. Photomicrographs of the laminations in plane-polarized light, C, and cross-polarized light, D, scale bars = 200 µm. Microcrystalline silica laminae (S) is seen between finely-crystalline dolomite laminae (D).

2.3.3. Banded Capstone

Capstone characterized by >10 mm thick layering is termed banded. The bands are most commonly defined by alternations in crystal size of the same or varying mineralogy.

2.3.3.1. Banded calcite-dolomite capstone

This fabric is characterized by 10 – 20 mm thick, isopachous to disk-shaped bands composed of fine- to coarsely-crystalline dolomite alternating with calcite bands. The coarsely-crystalline bands are dominantly dolomite and are light pink-purple in color. They typically consist of two halves, an upper and lower, with a visible central seam between them (Figure 25A & B). Each half consists of sub-euhedral, elongate dolomite crystals growing toward the other half and meeting at the central seam. The calcite bands are light tan in color and are fine- to coarsely-crystalline with subordinate anhedral, finely-crystalline dolomite as well. On outcrop, this fabric is expressed as 2 m by 1 – 3 m wide resistant blocks within the slope-forming carbonate caprock. Petrographically, the dolomite crystals are stained blue and display curved, baroque crystal facies that come into sharp contact with the calcite crystals (Figure 25C & D). Dark black residual organic matter (possibly petroleum) is also commonly found within this fabric type.

2.3.3.2. Banded calcite capstone

This fabric is characterized by 10 – 25 mm thick calcite bands of alternating crystal size, visually displayed by alternating gray and white bands. Gray bands contain finely-crystalline calcite and white bands contain coarsely-crystalline calcite. The white bands of coarse-crystalline calcite occasionally display internal sigma-shaped veins (Figure 26A). The contact between the white and gray bands is sharp (Figure 26C & D). The crystal size in the white band increases from medium– to coarsely-crystalline away from the contact with the gray band. On outcrop, banded

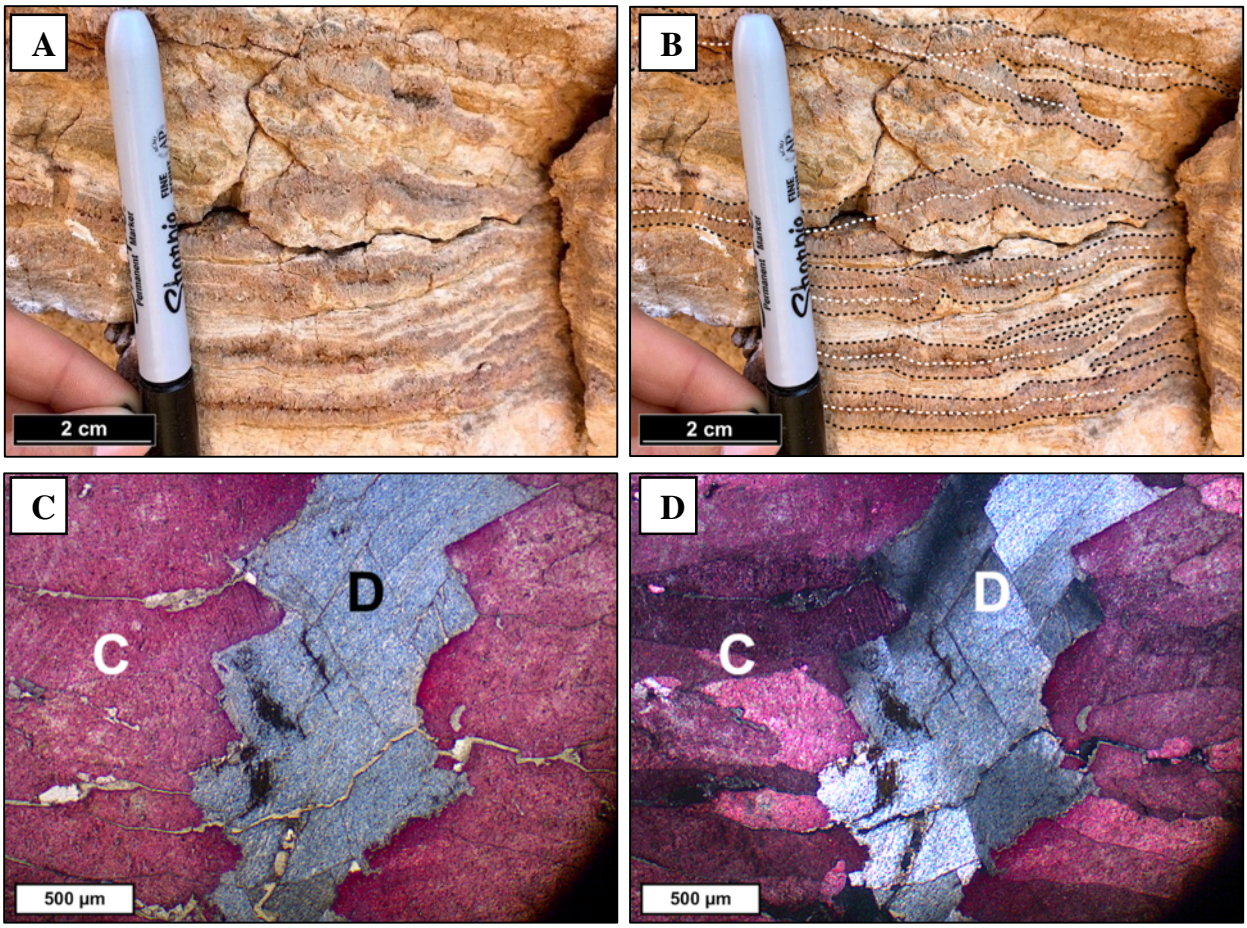

Figure 25. Banded calcite-dolomite capstone. Images A & B are outcrop examples of banded calcite-dolomite capstone, tan laminae are microcrystalline dolomite and calcite, the pink laminae are coarsely-crystalline, baroque dolomite. Image B annotates the coarsely-crystalline dolomite bands, outlined in black; and the visible central seam that separates the two halves is white. Photomicrographs of the laminations in plane-polarized light, C, and cross-polarized light, D, scale bars = 500 µm. Coarsely-crystalline calcite (C) laminae (red) in contact with coarsely-crystalline, Fe-dolomite (D) (blue); outline of euhedral dolomite crystals filled with dark organic matter.

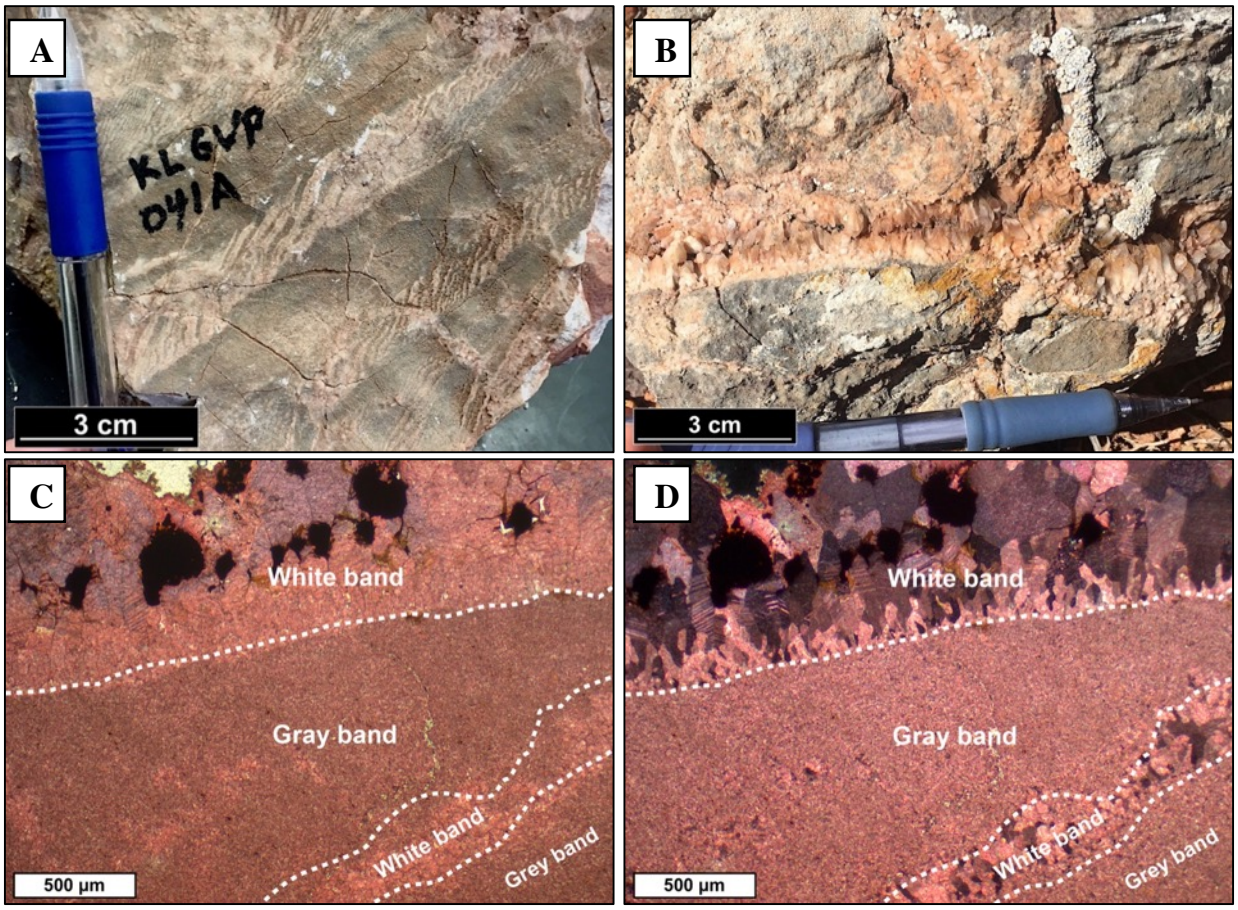

Figure 26. Banded calcite capstone. A. Outcrop example of banded calcite capstone, dark gray laminae consist of finely crystalline calcite, light gray laminae consist of coarsely crystalline, segmented calcite; B. Outcrop example of banded calcite capstone consisting of light pink, coarsely-crystalline, dog tooth calcite laminae within a light gray, microcrystalline calcite matrix. Photomicrographs of the laminations in plane-polarized light, C, and cross-polarized light, D, scale bars = 500 µm. The contact between the microcrystalline and coarsely-crystalline laminae is seen; dead oil is seen trapped within the coarsely-crystalline laminae.

calcite capstone is expressed as semi-resistant, 0.25 – 0.75 m wide, isolated outcrops within the greater slope-forming carbonate caprock.

2.4. Brecciated Capstone

Capstone composed of cemented angular fragments is classified as brecciated. Subdivisions of brecciated capstone are based on the degree of separation between capstone fragments, which may be closely, loosely, or spatially independent. These include crackle breccia (Morrow, 1982), mosaic breccia and disorganized breccia. The internal texture of the brecciated clasts consists of previously defined capstone fabrics (i.e. massive, porphyritic, layered, or brecciated). Intraclast cement composition is most commonly a later-stage coarsely-crystalline calcite, but coarsely-crystalline dolomite, gypsum, and silica have been observed. The brecciated clasts are most commonly microcrystalline massive or microlaminated dolomite.

2.4.1. Crackle Breccia Capstone

Brecciated capstones that display little to no dislocation between internal capstone fragments are termed crackle breccias (Figure 27). The dislocation between fragments ranges from 1 – 3 mm so that cement surrounding clasts are a network of veins.

2.4.1.1. Crackle brecciated dolomite capstone

Dolomitic crackle breccia capstone is the most abundant fabric type within the carbonate caprock exposed at Gypsum Valley. The weathered surface of this fabric is an orange-tan color (Figure 27A-D). The color of the fresh surface varies from jet black to dark purple to light pink to white. The brecciated fragments are typically angular, often with little to no visible cement between the fragments. The fabric of the brecciated fragments is microcrystalline massive or

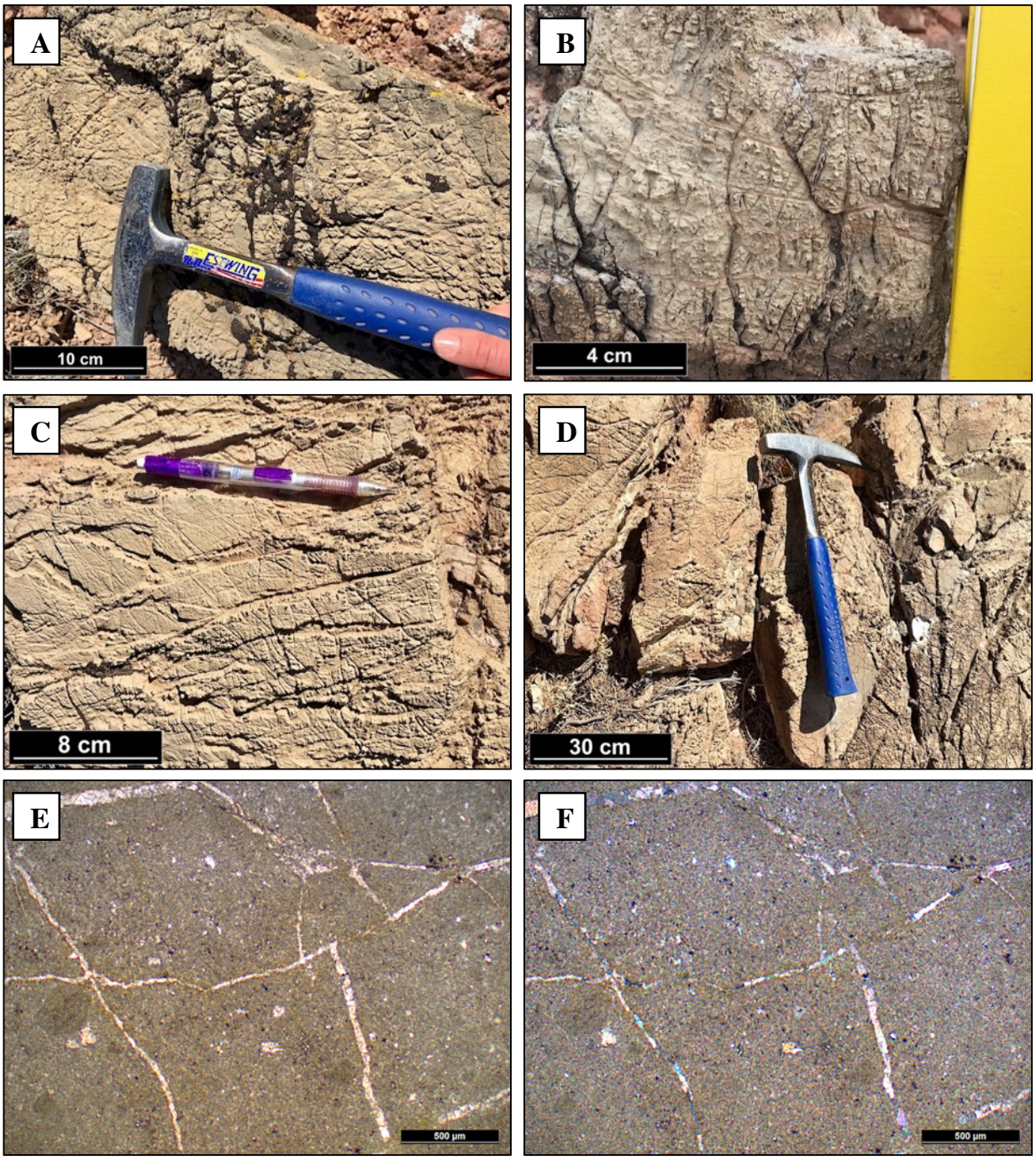

Figure 27. Crackle breccia dolomite capstone. Images A-D are outcrop/hand sample examples of the crackle breccia capstone fabric; all samples are composed of microcrystalline dolomite. Photomicrographs of crackle breccia in plane-polarized light, E, and cross-polarized light, F, scale bars = 500 µm. Microcrystalline dolomite brecciated fragments are cemented together by coarsely-crystalline dolomite.

microlaminated dolomite capstone. Intra-fragment cement composition is most commonly a late stage, coarsely-crystalline dolomite, but coarsely-crystalline calcite and finely-crystalline silica has been observed (Figure 27E & F). The outcrop expression of this fabric is characterized by resistant, 0.5 – 2 m tall, 1 – 3 m wide, blocks of dolomite capstone within the greater slope-forming carbonate caprock.

2.4.2. Mosaic Breccia Capstone

Brecciated capstone that contains fragments that are largely, but not entirely displaced are termed mosaic breccias (Morrow, 1982) (Figure 21). Most mosaic breccias consist of ~90% original capstone fragments/groundmass and ~10% fracture-filling cement. The internal texture of the brecciated fragments consists of previously defined capstone fabrics (i.e. massive, porphyritic, or layered).

2.4.2.1. Mosaic breccia dolomite capstone

This fabric consists of dolomitic breccia fragments, cemented together by either calcite, dolomite, or silica (Figures 28A & B). The most common capstone fabric type of the brecciated fragments consists of either massive or microlaminated, finely-crystalline dolomite. On outcrop, this fabric is expressed as 0.5 – 1.5 m tall, 0.5 – 4 m wide, resistant ledges within the greater, slope-forming carbonate caprock. In thin section, microcrystalline dolomite fragments are largely, but not entirely, displaced from one another. Cement between the brecciated fragments is most commonly composed of late-stage, blocky calcite cement (Figures 28C & D), but dolomite and quartz cement have also been observed.

2.4.2.2. Mosaic breccia gypsum-dolomite capstone

This fabric, originally documented by Lerer (2017), consists of dolomitic breccia fragments cemented together by gypsum (Figures 29A). The fabric type of the brecciated fragments consists

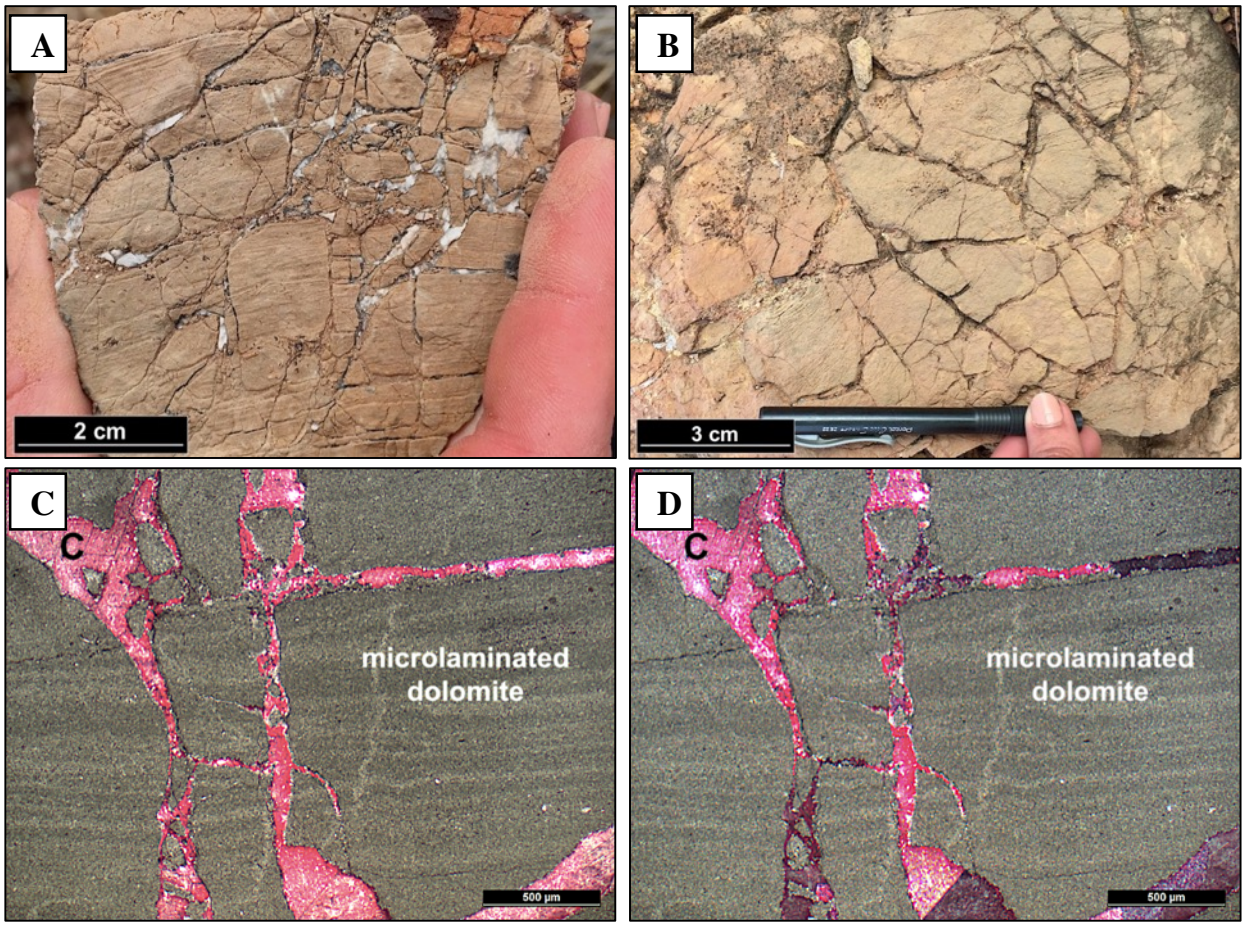

Figure 28. Mosaic breccia dolomite capstone. A. Outcrop example of tan, microlaminated dolomite capstone fragments with white calcite vein fill; B. Outcrop example of massive, microcrystalline dolomite capstone fragments cemented together by dolomite. Photomicrographs of mosaic breccia dolomite capstone in plane-polarized light, C, and cross-polarized light, D, scale bars = 500 µm. Subangular microlaminated dolomite capstone fragments cemented by calcite (C) (red).

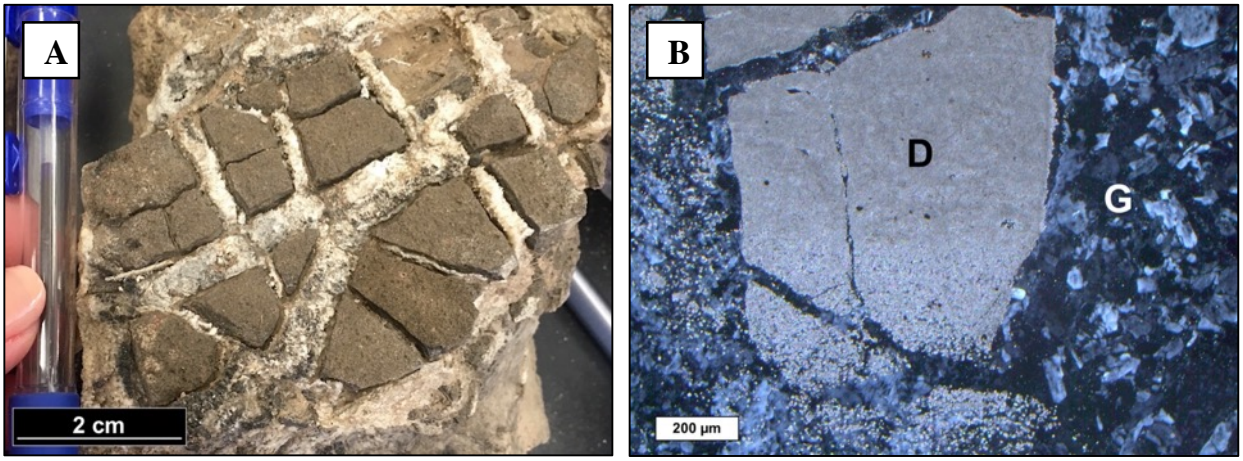

Figure 29. Mosaic breccia gypsum-dolomite capstone. A. Outcrop example consisting of brown, microcrystalline dolomite fragments within a white gypsum matrix; B. Cross-polarized photomicrograph of image A., microcrystalline dolomite fragment within a gypsum matrix; dolomite (D) is being replaced by gypsum (G), scale bar = 200 µm. Sample collected and photomicrograph taken by Lerer, 2017.

of massive, finely-crystalline dolomite. On outcrop, this fabric is expressed as 10 – 20 cm wide, semi-resistant blocks found at the contact between the gypsum and carbonate capstone. In thin section, a blocky, microcrystalline dolomite fragment is seen floating in a matrix/cement of medium-coarsely crystalline, equigranular gypsum crystals (Figures 29B). The contact between the dolomite and gypsum ranges from sharp to gradational. Where the contact is gradational, it appears that the dolomite is being replaced by the gypsum.

2.4.3. Disorganized Breccia Capstone

Brecciated capstones that display a large degree of dislocation between fragments are termed disorganized breccias. Most disorganized breccias consist of ~70% original capstone fragments/groundmass and ~30% fracture-filling veins, and typically consist of a wide range of fragment sizes.

2.4.3.1. Disorganized brecciated dolomite capstone

This fabric consists of dolomitic breccia fragments, cemented together by either calcite or dolomite (Figure 30A & B). The most common capstone fabric type of the brecciated fragments is either massive or microlaminated, finely-crystalline dolomite. Brecciated fragments are often largely displaced and the orientation of fragments is variable between fragments. On outcrop, this fabric is expressed as 0.5 – 1.5 m tall, 0.5 – 1 m wide, resistant blocks within the greater, slope-forming carbonate caprock. In thin section, microcrystalline dolomite fragments vary in size and orientation, and their spatial relationship to one another is also variable. Cement between the brecciated fragments is most commonly composed of late-stage, blocky calcite or dolomite (Figure 30C & D).

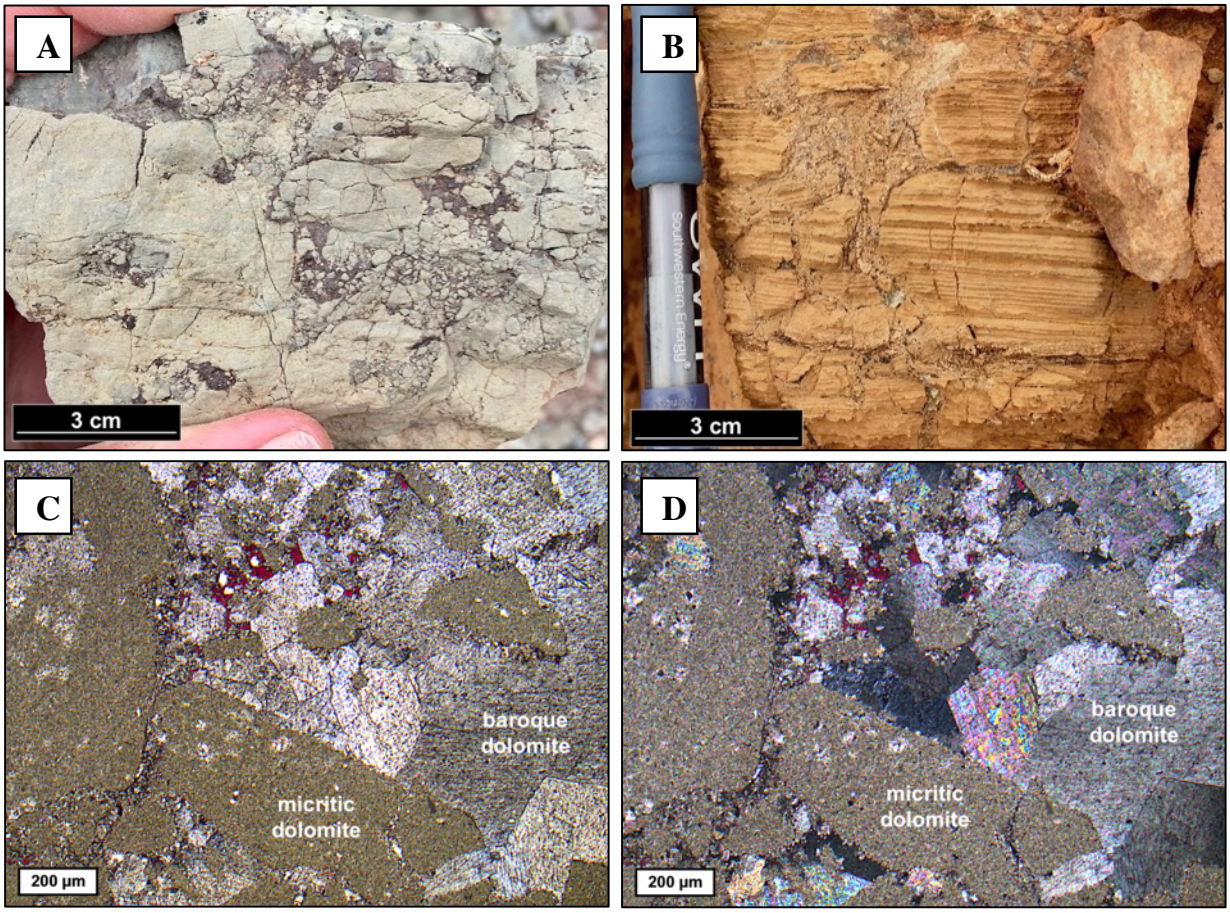

Figure 30. Disorganized breccia dolomite capstone. A. Tan massive dolomite breccia fragments within a red-purple dolomite matrix; B. Microlaminated dolomite fragments within a dolomite matrix. Photomicrographs of disorganized breccia dolomite capstone in plane-polarized light, C, and cross-polarized light, D, scale bars = 200 µm. Brecciated fragments are composed of microcrystalline dolomite with subhedral to euhedral baroque dolomite cement between fragments. Minor late stage calcite in pores (red).

2.4.3.2. Disorganized brecciated calcite capstone

This fabric consists of subrounded, massive calcite fragments cemented together by coarsely-crystalline calcite (Figure 31A & B). The color of the brecciated fragments range from dark purple to dark gray to light gray. The coarsely-crystalline cement between fragments is almost always white. On outcrop, this fabric is expressed as semi-competent, 0.25 – 1 m wide blocks within the greater, slope-forming carbonate caprock. Petrographically, the brecciated fragments, composed of finely-crystalline calcite, can be seen in contact with the coarsely-crystalline calcite cement (Figure 31C & D).

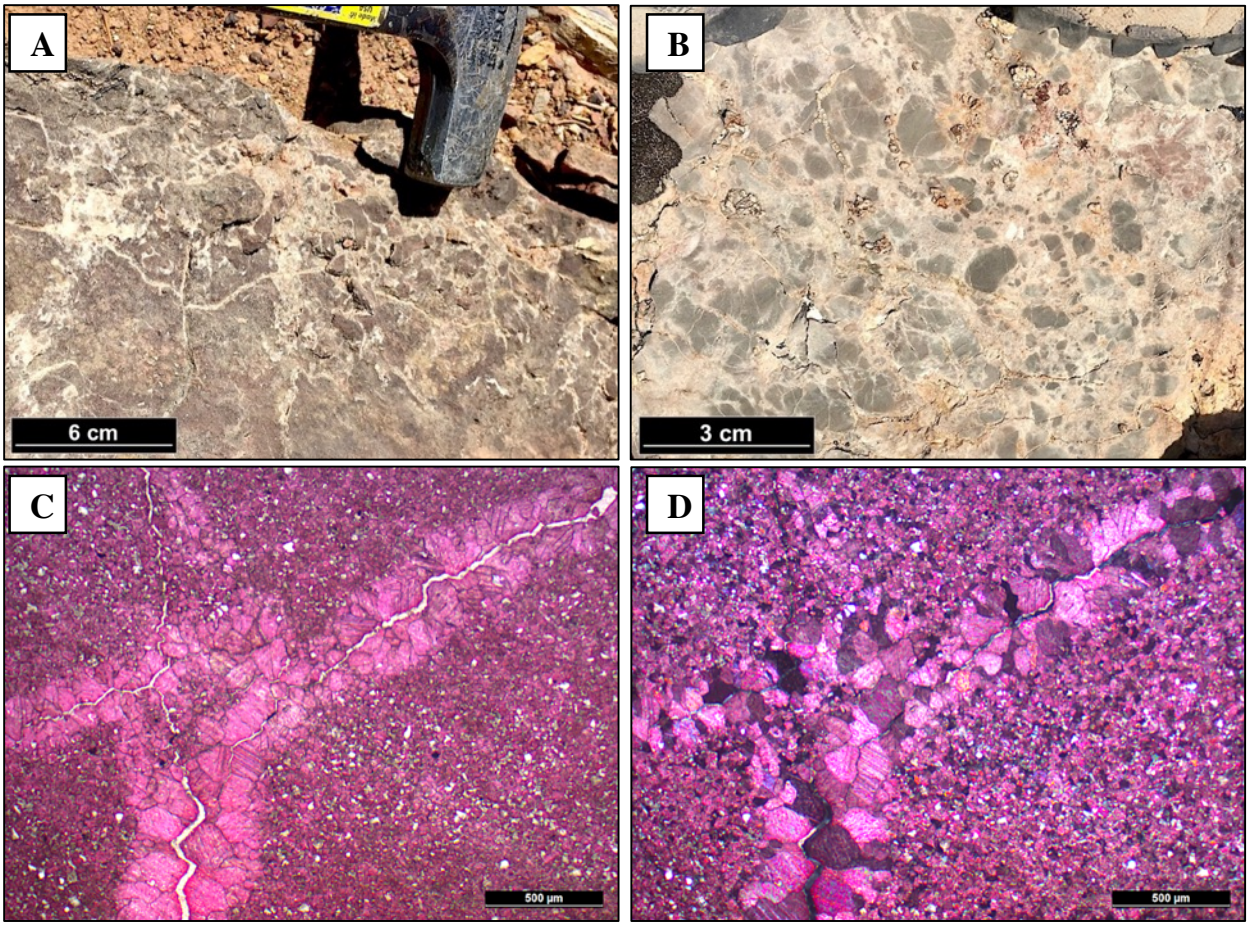

Figure 31. Disorganized breccia calcite capstone. A. Outcrop example of massive, dark-purple calcite fragments cemented together by white calcite cement. B. Outcrop example of massive, dark to light gray calcite fragments in a white calcite matrix. Photomicrographs of disorganized breccia calcite capstone in plane-polarized light, C, and cross-polarized light, D, scale bars = 500 µm. Subangular, finely-crystalline calcite fragments are cemented together by coarsely-crystalline calcite.

Chapter 3: Distribution of Capstone Fabrics along the Gypsum Valley Salt Wall

The northeastern flank of Gypsum Valley salt wall contains exposures of a combined 8 kilometers (measured parallel to the trend of the salt wall) of gypsum and carbonate caprock (Figure 32). The width of the exposed caprock varies from a few meters up to 850 m wide. The caprock is situated at the salt-sediment interface, with the diapir exposed on the southwestern margin of the caprock, and the Triassic Chinle Formation exposed along the northeastern margin. Caprock is not continuously exposed along the entire flank of the salt wall, but it is exposed primarily at three localities referred to here as: 1) The Nubbin, 2) Bridge Canyon and 3) Mary Jane Draw (Figure 32). The Nubbin is located at the northern end of the Gypsum Valley salt wall and contains the smallest exposure of caprock of all the localities, totaling about 500 m in length. The next caprock exposure to the south is the Bridge Canyon locality, located ~4.7 km to the southeast of the Nubbin, and contains about 3,750 m in length of caprock. The final location along the salt wall that contains exposed caprock is Mary Jane Draw. This locality is ~5.3 km to the southeast of Bridge Canyon, and contains the largest exposure of caprock, totaling about 4,000 m in length. Where exposed, the caprock is characterized by dominantly slope-forming, rolling hills that are in contact with the adjacent cliff-forming Triassic Chinle Formation.

3.1. The Nubbin

The Nubbin is a NW-SE trending amphitheater that exposes a window of caprock 530 m long (measured parallel to the trend of the salt wall), by 150 m wide (measured perpendicular to the trend of the salt wall) (Figure 33). The Nubbin caprock is completely surrounded by the Chinle Formation. Only carbonate caprock is exposed in this locality likely because the window has not eroded down through the carbonate caprock to expose the presumably underlying gypsum caprock.

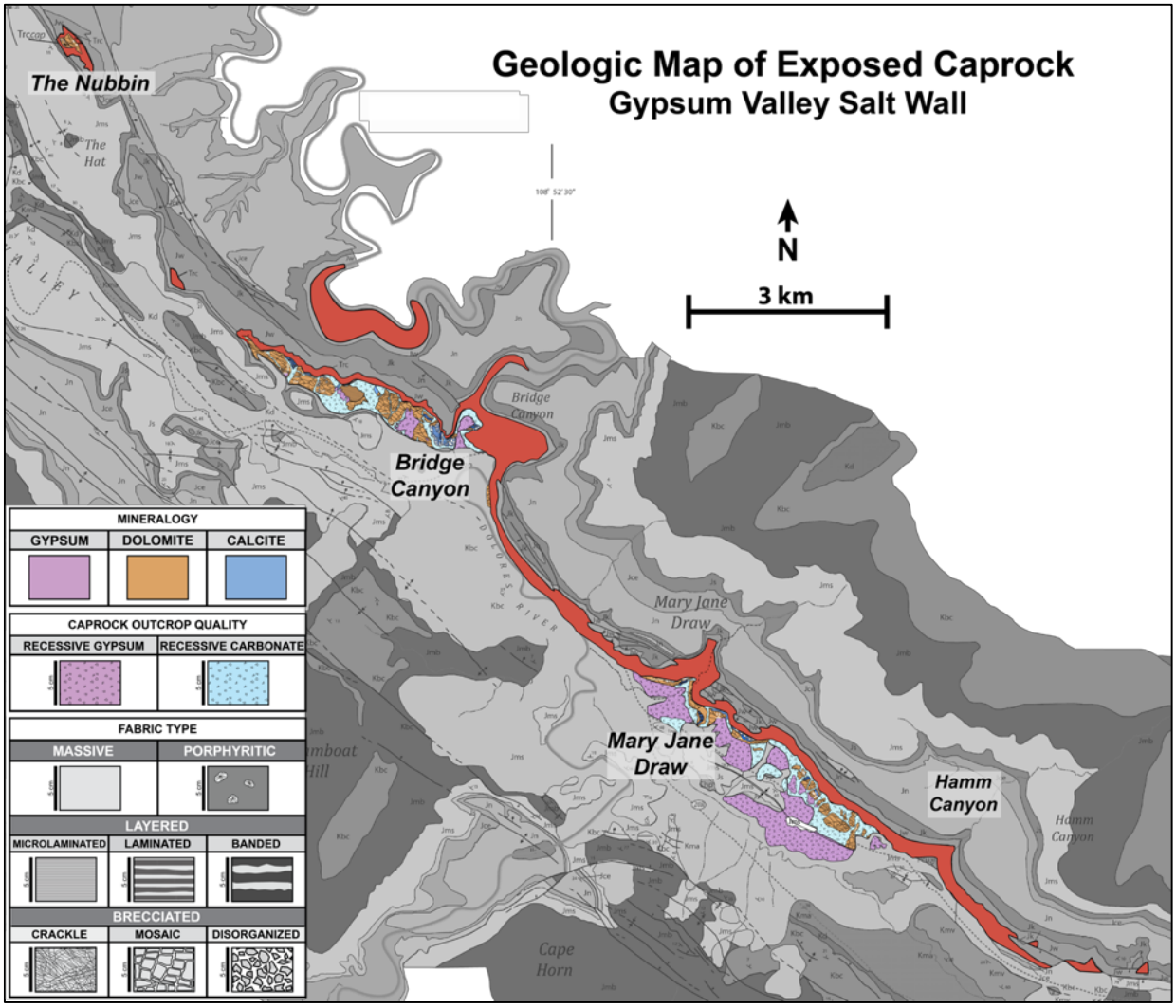

Figure 32. Geologic map of the exposed gypsum and carbonate caprock along the Gypsum Valley salt wall. Three main localities along the wall were studied. From NW to SE these include the Nubbin, Bridge Canyon, and Mary Jane Draw, respectively. The gypsum caprock is purple, the calcite caprock is dark blue, and the dolomite caprock is tan. Light blue colors indicate recessive carbonates (predominantly calcitic). Their associated fabrics are super-imposed over those colors. The Triassic Chinle Formation is highlighted in red.

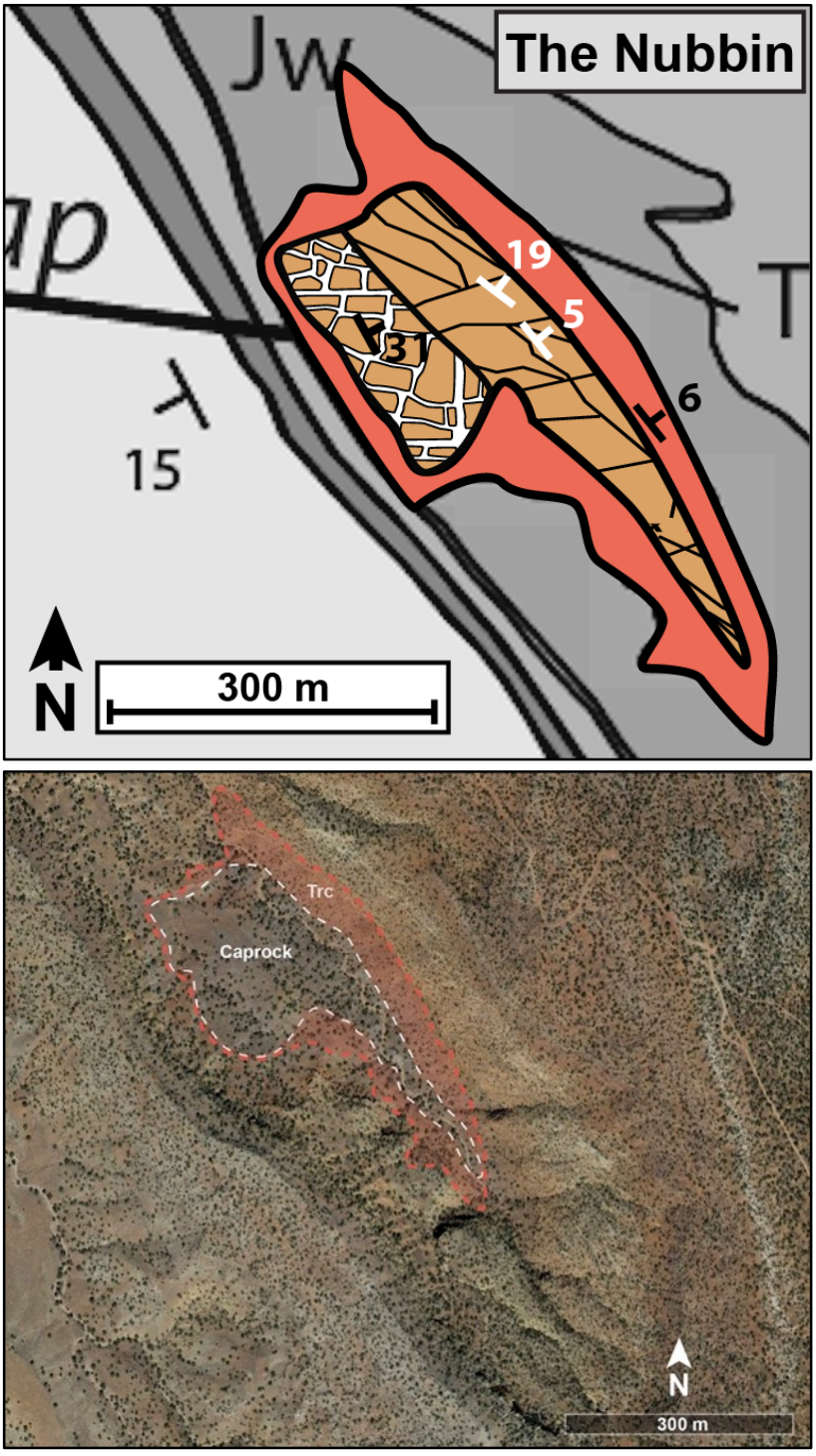

Figure 33. Caprock fabric map of The Nubbin. The top image is a geologic map of the caprock fabrics and surrounding geologic formations. The bottom image is a Google Earth image of the Nubbin area, with the Triassic Chinle formation (Trc) annotated in orange, and the outline of the caprock annotated in white.

The caprock here is composed entirely of dolomite of two different fabric types. Along the northeast margin, crackle breccia dolomite capstone is present, and the western margin is composed of mosaic breccia dolomite capstone. This area of caprock exposure displays the least amount of diagenetic alteration of the original microcrystalline dolomite capstone. The only evidence of alteration is the brecciation of the western portion of the caprock.

3.2. Box Canyon - Bridge Canyon

The Box Canyon to Bridge Canyon locality represents a caprock exposure 3,750 m long (measured parallel to the trend of the salt wall), and ranges from a few meters to 400 m wide (measured perpendicular to the trend of the salt wall) (Figure 34). Gypsum and carbonate caprock are exposed along this transect. This transect is characterized by "blocks" of more competent dolomite and calcite capstone surrounded by slope-forming, massive calcite and gypsum capstone.

3.2.1. Box Canyon

The western 1,400 m of this transect is named Box Canyon and is composed almost entirely of carbonate caprock. Here, the caprock is positioned between the Chinle Formation along the northern margin, and down-dropped blocks of Jurassic stratigraphy (Glen Canyon Group, San Raphael Group and the Morrison Formation) along the southern margin. The dominant fabric type of the exposed caprock in Box Canyon is crackle breccia dolomite capstone. The other fabrics exposed at this locality include: massive gypsum capstone; porphyritic silica-dolomite capstone; microlaminated dolomite capstone; laminated calcite capstone; banded calcite capstone; crackle breccia dolomite capstone; and mosaic brecciated dolomite capstone. The porphyritic silica-dolomite capstone is superimposed on the crackle breccia at the most northeastern portion of Box

Canyon. The laminated and banded calcite capstone is exposed in a narrow zone at the caprock-Chinle contact. Interestingly, the fabric type of the competent dolomite blocks corresponds to crackle breccia dolomite capstone and the other carbonate capstone fabrics are either located around the edges of the blocks or at the caprock-Chinle Formation contact.

3.2.2. Bridge Canyon

The eastern portion of the caprock exposure transect is considered Bridge Canyon. Here, the caprock lies nonconformably below the Chinle Formation along the northern margin and extends to the southwest until it is covered by Quaternary alluvium (Figure 34). Both gypsum and carbonate caprock are exposed here. The dominant fabric type is crackle breccia dolomite capstone, outcropping as large competent blocks that form subtle topographic highs. A series of diapir-parallel, steeply dipping down to the south, normal faults are present in the adjacent Chinle Formation and extend up through the Jurassic Navajo Formation (McFarland, 2016). It is not clear if the faults extend down into the underlying caprock or not. The carbonate caprock located directly inboard (south) of these faults exhibit a diverse array of fabrics and mineralogies. The fabrics observed here include: massive calcite capstone, porphyritic silica-calcite capstone, microlaminated calcite capstone, laminated calcite capstone, and disorganized breccia calcite capstone. The remainder of the carbonate caprock within this exposure is characterized by gray, recessive, massive calcite capstone. The gypsum caprock exposed at this locality is entirely recessive, and is white-gray in color, and is dominantly covered by microbial, cryptic soil.

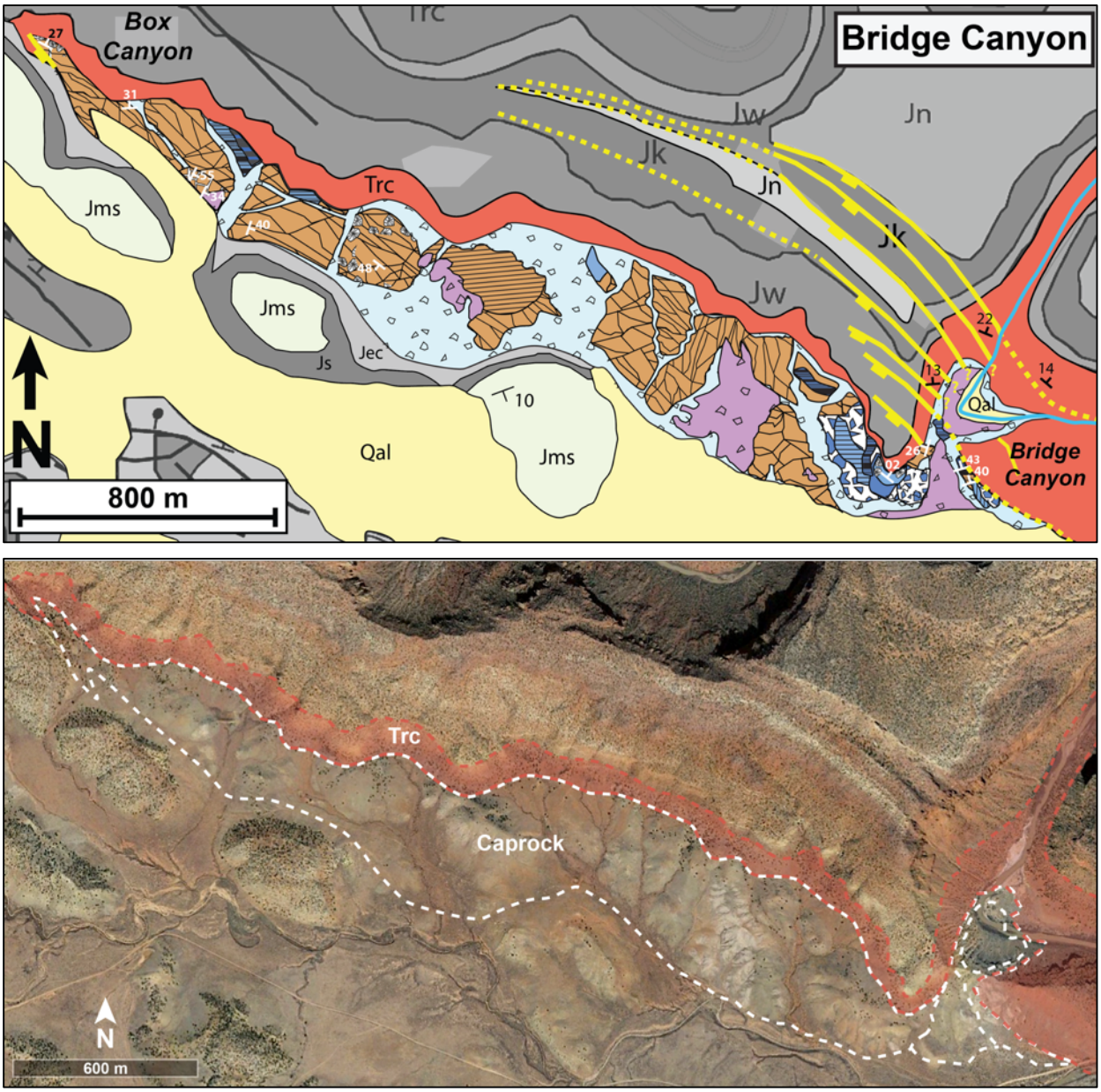

Figure 34. Caprock fabric map of Box Canyon (west) and Bridge Canyon (east). The top image is a geologic map of the caprock fabrics and surrounding geologic formations (Trc = Triassic Chinle Fm; Jw = Jurassic Wingate Fm; Jk = Jurassic Kayenta Fm; Jn = Jurassic Navajo Fm; Jec = Jurassic Entrada/Carmel Fm; Js = Jurassic Summerville Fm; Jms = Jurassic Morrison Fm-Salt Wash Mbr). Yellow lines indicate normal faults within the overlying stratigraphy. The bottom image is a Google Earth image of Box to Bridge Canyon area, with the Triassic Chinle formation (Trc) annotated in orange, and the outline of the caprock annotated in white.

3.3. Mary Jane Draw

The Mary Jane Draw locality represents a caprock exposure 4,000 m long (measured parallel to the trend of the salt wall), and ranges from a few meters to 850 m wide (measured perpendicular to the trend of the salt wall) (Figure 35). Gypsum and carbonate caprock are exposed at the Mary Jane Draw locality (Lerer, 2017). Here, the caprock is positioned between the Chinle Formation along the northeastern margin, and down-dropped blocks of Jurassic stratigraphy (Glen Canyon Group, San Raphael Group and the Morrison Formation), and Quaternary alluvium covering the diapir along the southern margin. This locality has the largest exposure of gypsum caprock, which is characterized by slope-forming, rolling hills of white to gray gypsum. Cryptic soil formation on the gypsum caprock is very common. The dominant carbonate caprock fabric exposed at this locality is crackle breccia dolomite capstone. Similar to Bridge Canyon, a series of diapir-parallel, steeply dipping, normal faults are present in the adjacent Chinle Formation and extend up through the Jurassic Navajo Formation (Stokes, *et al.,* 1948). It is not clear if the faults extend down into the underlying caprock or not. The carbonate caprock located directly inboard (southwest) of these faults, at the caprock-Chinle contact, and especially along the dry river bed of Mary Jane Draw, exhibit a diverse array of fabrics and mineralogies. The fabrics exposed here include: massive dolomite capstone, microlaminated dolomite capstone, disorganized breccia dolomite capstone, porphyritic silica-calcite capstone, microlaminated calcite capstone, laminated silica-dolomite capstone, laminated calcite capstone, and disorganized breccia calcite capstone.

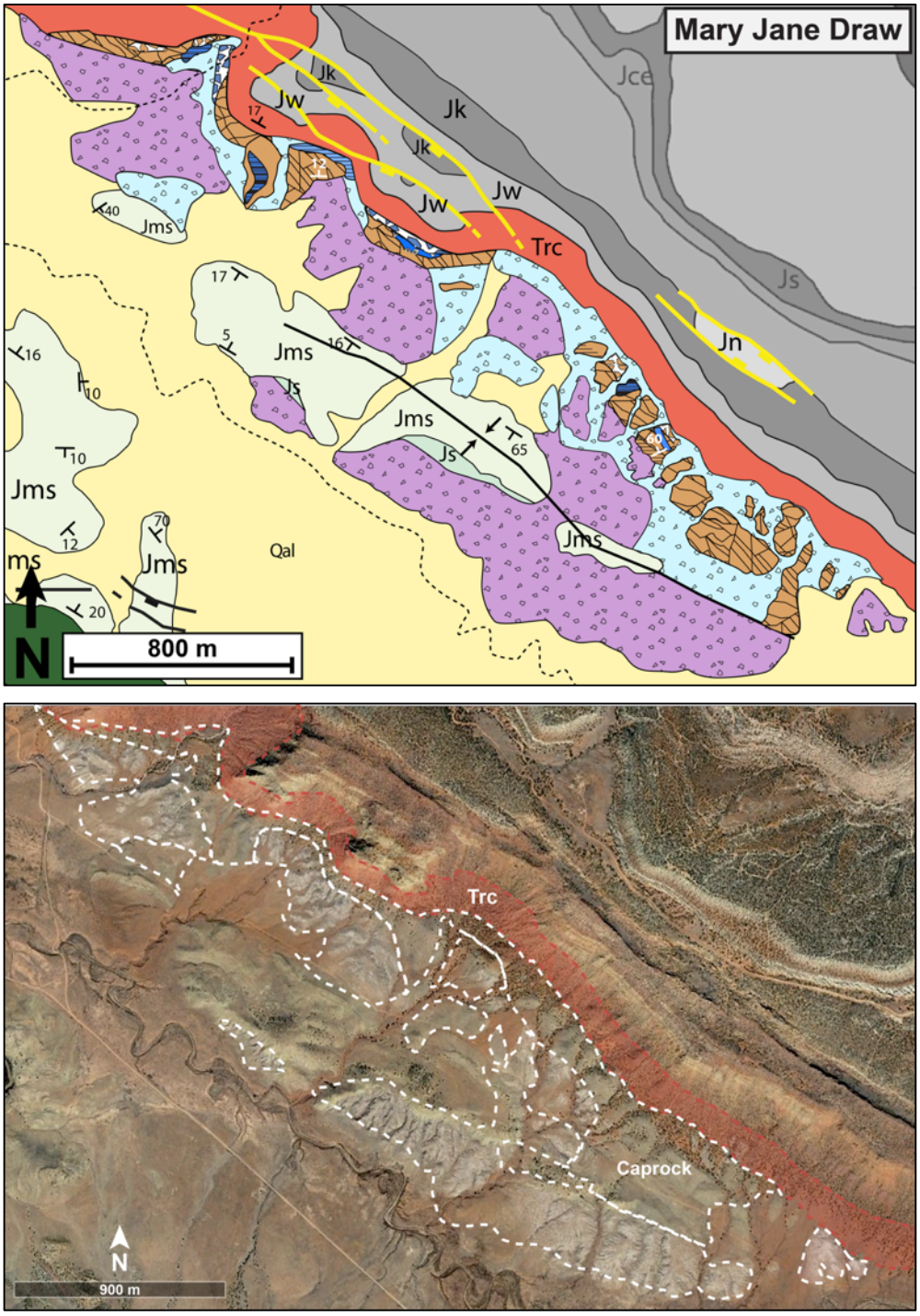

Figure 35. Caprock fabric map of Mary Jane Draw. The top image is a geologic map of the caprock fabrics and surrounding geologic formations (Trc = Triassic Chinle Fm; Jw = Jurassic Wingate Fm; Jk = Jurassic Kayenta Fm; Jn = Jurassic Navajo Fm; Jec = Jurassic Entrada/Carmel Fm; Js = Jurassic Summerville Fm; Jms = Jurassic Morrison Fm-Salt Wash Mbr). The bottom image is a Google Earth image of the Mary Jane Draw area, with the Triassic Chinle formation (Trc) annotated in orange, and the outline of the caprock annotated in white.

3.4. Carbonate Caprock Clasts

The Triassic Chinle Formation unconformably overlies the Gypsum Valley salt wall on the northeast margin in Little Gypsum Valley atop a salt shoulder (McFarland, 2016). A salt shoulder is a low-angle segment of the salt-sediment interface where the margin of a passive diapir steps abruptly inboard (Hearon *et al.,* 2015). Locally, the contact between the caprock and the Chinle Formation is an erosional, scoured surface, spatially-associated with fluvial sandstones of the Chinle Formation (Figure 36A). These sandstones and conglomerates contain tan, massive, micritic dolomite clasts within channelized facies. McFarland (2016) identified three halokinetic sequences within the Chinle Formation on the salt shoulder at Gypsum Valley, each locally bound by an angular unconformity < 5º. Interestingly, all three halokinetic sequences within the Chinle Formation contain micritic dolomite clasts within fluvial channel fill sandstones and conglomerates. McFarland (2016) interpreted these clasts to have originated from the carbonate caprock located inboard of the Chinle Formation, as that is the only dolomitic unit proximal to the Chinle Formation. The dolomitic clasts look identical to the massive and microlaminated dolomite capstone (Figure 36B) are rounded to subangular and 1 to 10 cm in diameter. Petrographically, the clasts are composed of microcrystalline dolomite (Figure 36C & D).

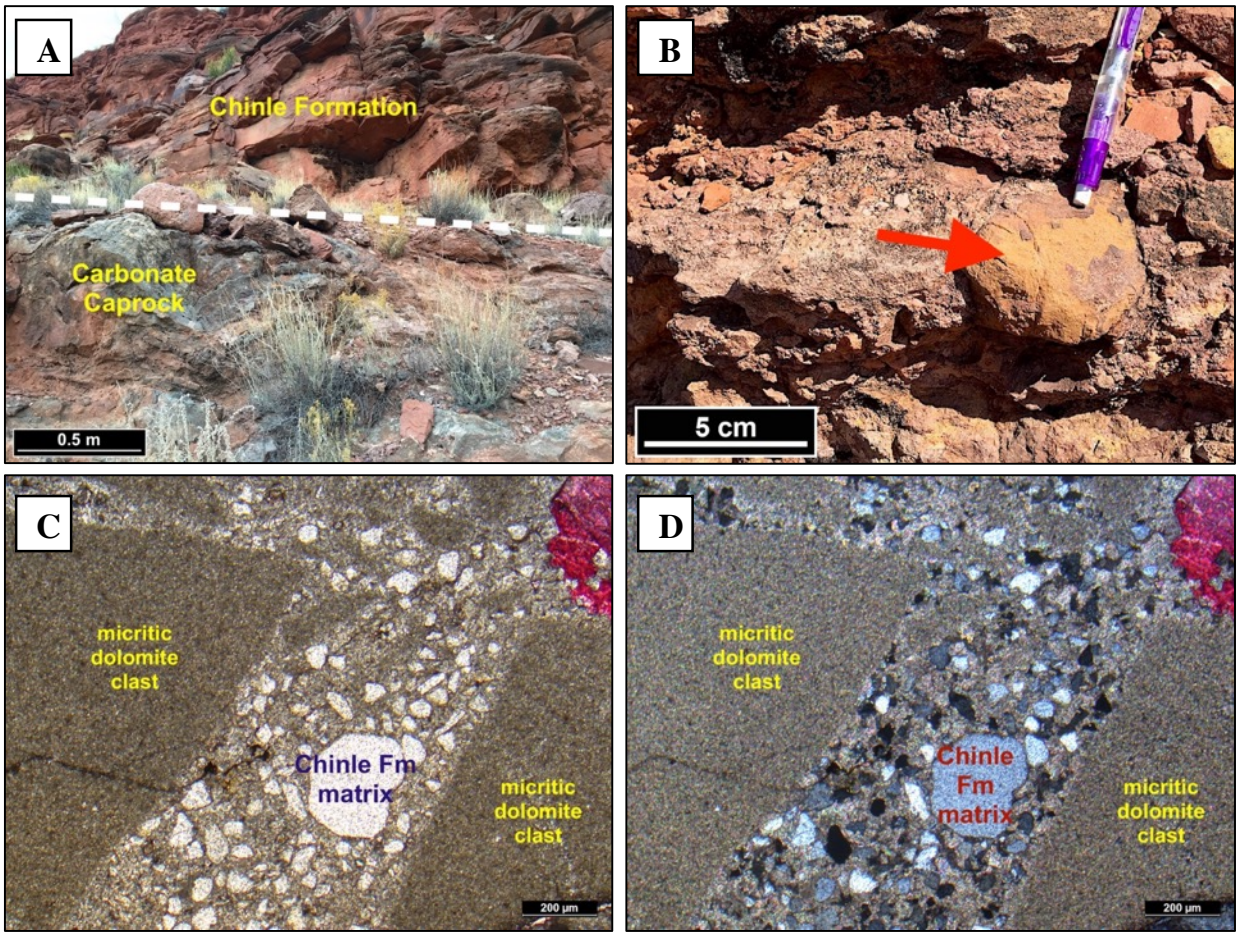

Figure 36. Microcrystalline dolomite clasts within fluvial channel sands of the Chinle Formation. **A.** Outcrop photographic of the contact between the Chinle Formation and carbonate caprock. **B.** Outcrop photograph of a tan, microcrystalline dolomite clast within the Chinle Formation. Photomicrographs of the dolomitic clasts in plane-polarized light, **C**, and cross-polarized light, **D**, scale bars = 200 µm. Quartz sand from the Chinle Formation surrounds the microcrystalline dolomite clasts.

Chapter 4: Geochemical Observations of Gypsum Valley Carbonate Caprock

Carbon and oxygen isotope analyses of exposed carbonate caprock were used to determine the origin of the carbon and oxygen within carbonate and to infer paragenetic relationships found within the different carbonate caprock fabrics. Additionally, carbon and oxygen isotope analyses of carbonate caprock clasts found within fluvial channels of the overlying Triassic Chinle Formation were used to determine if the clasts originated from exposed carbonate caprock atop the Gypsum Valley salt wall during Chinle deposition (Figure 37). Many paragenetic phases are present within these carbonates, and these phases presumably precipitated within different settings with different isotopic signatures. To address this complexity, detailed petrographic mapping was completed prior to micro-sampling of specific phases within these carbonate caprocks for geochemical analysis.

Two cross-plots of $\delta^{18}O$ versus $\delta^{13}C$ were used to identify trends and/or clusters in the isotopic signatures of carbonate caprock that could be attributed to environments of formations or post–formation diagenetic alteration. One cross plot separated data by petrographic observations and the other separated data by capstone fabric type.

4.1. $\delta^{18}O$ versus $\delta^{13}C$ cross-plot: carbonate capstone fabrics

The first $\delta^{18}O$ versus $\delta^{13}C$ cross-plot displays a comparison of the stable isotopic compositions of individual carbonate capstone fabric types (Table 2) (Figure 38). The cross-plot indicates: 1) The only massive calcite capstone sampled exhibits a $\delta^{18}O$ value of –16.49 ‰ and a $\delta^{13}C$ value of –8.49 ‰; 2) The porphyritic calcite capstone exhibits $\delta^{18}O$ values ranging from –5.10 ‰ to –4.81 ‰ and $\delta^{13}C$ values ranging from –9.05 ‰ to –8.24 ‰; 3) The only porphyritic

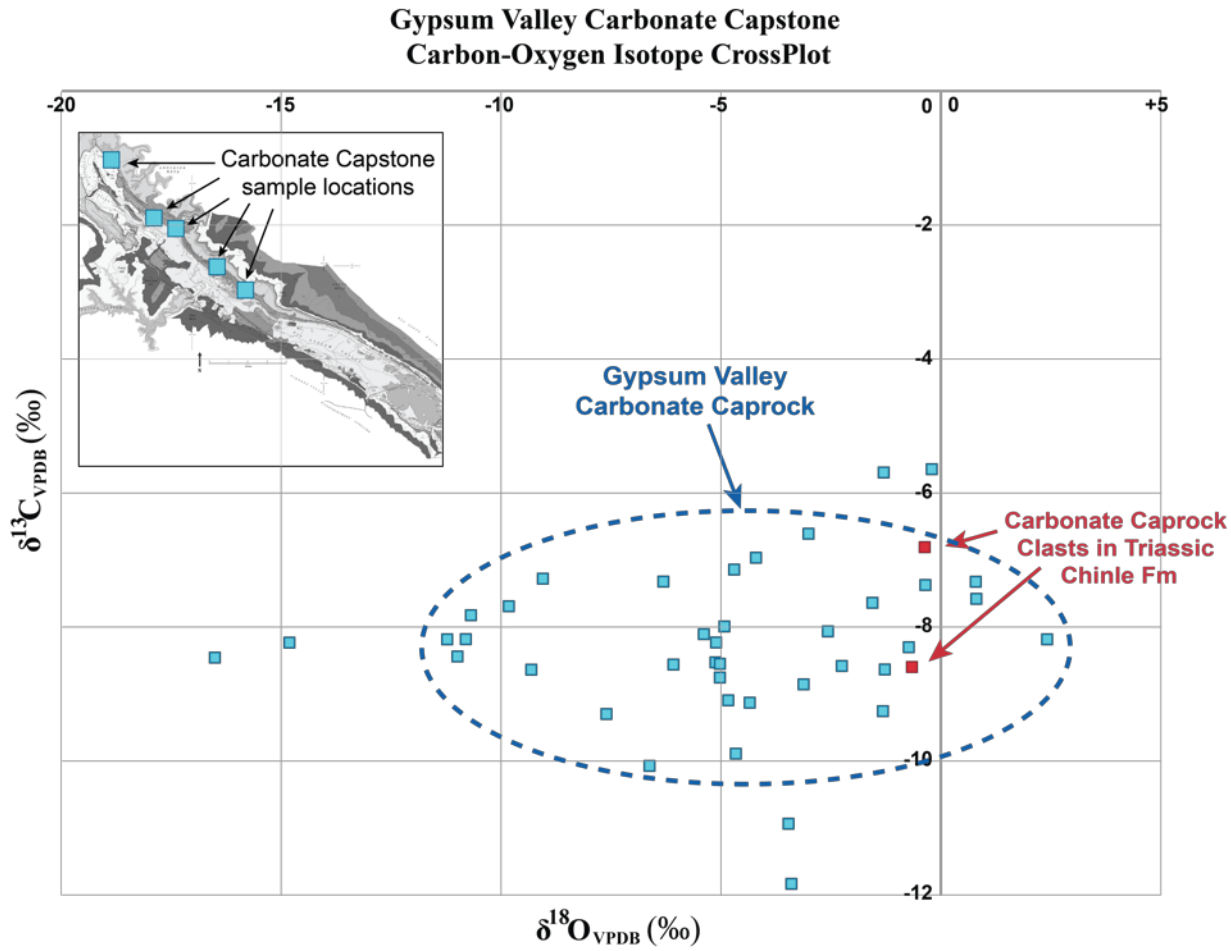

Figure 37. Cross-plot of the $\delta^{18}O$ versus $\delta^{13}C$ values of exposed carbonate caprock along the salt-sediment interface (blue), carbonate caprock clasts found within fluvial channels of the overlying Triassic Chinle Fm (red). Samples were collected from numerous locations along the salt wall, denoted on inset map.

Table 2: Comparison of the mean host and cement isotopic composition of carbonate capstone fabrics

	Host Mineralogy				Cement Mineralogy			
	Micritic Dolomite		Micritic Calcite		Coarsely-Crystalline Calcite		Baroque Dolomite	
Carbonate Capstone Fabric	**$\delta^{18}O$ VPDB**	**$\delta^{13}C$ VPDB**	**$\delta^{18}O$ VPDB**	**$\delta^{13}C$ VPDB**	**$\delta^{18}O$ VPDB**	**$\delta^{13}C$ VPDB**	**$\delta^{18}O$ VPDB**	**$\delta^{13}C$ VPDB**
Massive Dolomite	-2.25 ‰	-8.54 ‰					-11.01 ‰	-8.27 ‰
Porphyritic Silica-Dolomite	-1.35 ‰	-5.69 ‰					-10.43 ‰	-7.76 ‰
Microlaminated Dolomite	-1.40 ‰	-6.85 ‰					-9.56 ‰	-8.18 ‰
Laminated Dolomite	-6.96 ‰	-7.61 ‰					-10.98 ‰	-8.42 ‰
Laminated Silica-Dolomite	-3.44 ‰	-11.86 ‰						
Crackle Breccia Dolomite	-2.63 ‰	-7.57 ‰					-10.84 ‰	-8.22 ‰
Mosaic Breccia Dolomite	-3.07 ‰	-8.84 ‰			-4.55 ‰	-7.48 ‰		
Disorganized Brecciated Dolomite	-1.18 ‰	-8.45 ‰			-2.79 ‰	-7.42 ‰		
Massive Calcite					-16.5‰	-8.49‰		
Porphyritic Silica-Calcite			-4.95 ‰	-8.82 ‰				
Porphyritic Calcite			-5.02 ‰	-8.62 ‰	-4.87 ‰	-8.65 ‰		
Microlaminated Calcite			-0.30 ‰	-7.37 ‰	2.41 ‰	-8.18 ‰		
Laminated Calcite			-5.30 ‰	-8.13 ‰	-6.98 ‰	-9.28 ‰		
Banded Calcite-Dolomite					-3.55 ‰	-10.89 ‰	-14.89 ‰	-8.23 ‰
Banded Calcite			-5.05 ‰	-8.73 ‰				
Disorganized Brecciated Calcite			0.73 ‰	-7.33 ‰	-6.35 ‰	-7.63 ‰		

Carbonate Capstone Clasts Found within Triassic Chinle Formation	**$\delta^{18}O$ VPDB**	**$\delta^{13}C$ VPDB**
Massive Dolomite	-0.57 ‰	-8.62 ‰
Microcrystalline Dolomite	-0.34 ‰	-6.84 ‰

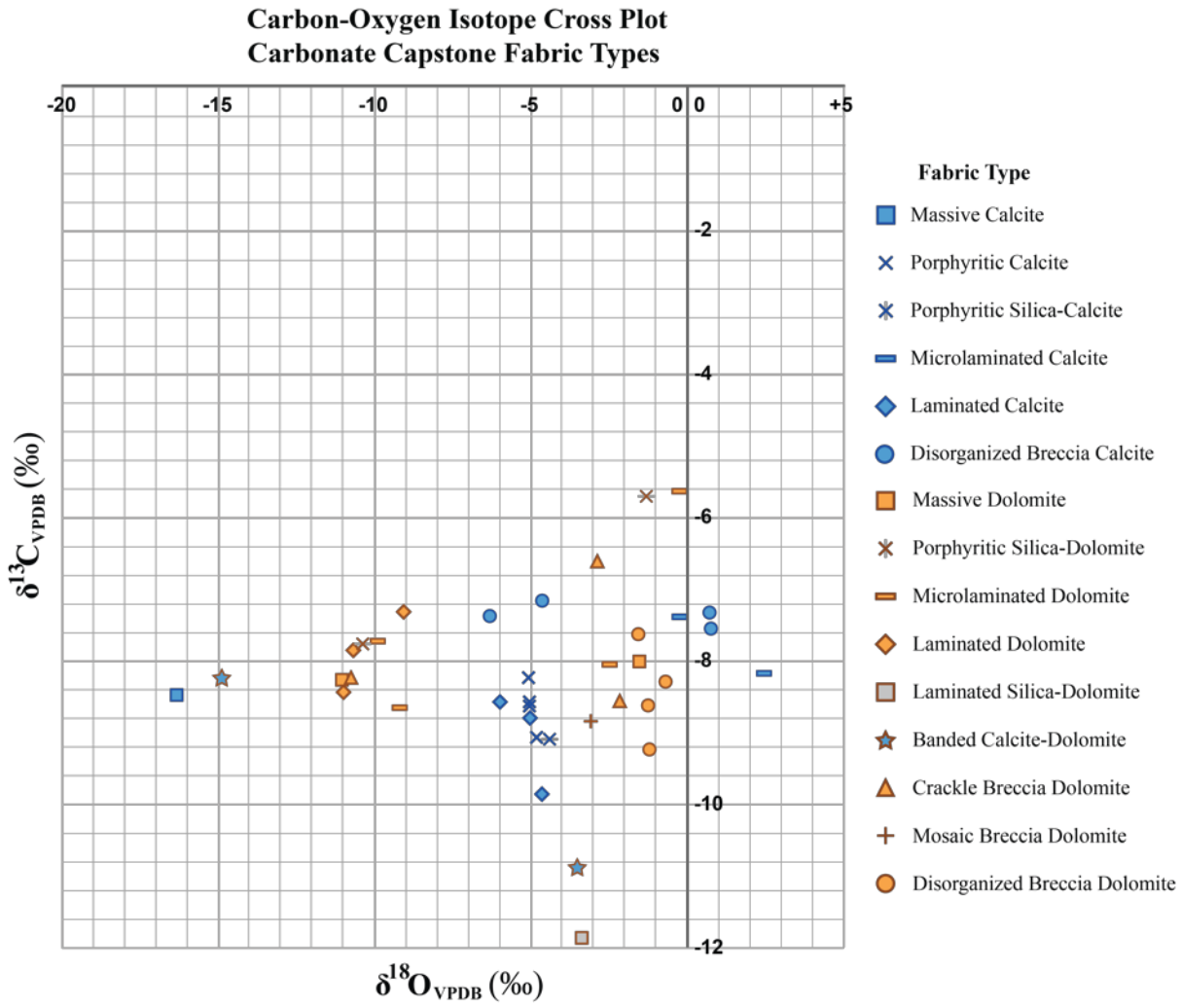

Figure 38. Carbonate isotope cross-plot of $\delta^{18}O$ versus $\delta^{13}C$ comparing the geochemical signatures of the carbonate capstone fabrics. The stable isotope compositions of the dolomitic capstone fabrics are illustrated in orange, and the calcitic capstone fabrics are illustrated in blue.

silica–calcite capstone sample exhibits a $\delta^{18}O$ value of –4.44 ‰ and a $\delta^{13}C$ value of –9.10 ‰; 4) The microlaminated calcite capstone fabric exhibits $\delta^{18}O$ values ranging from –0.30 ‰ to +2.41 ‰ and $\delta^{13}C$ values ranging from –8.18 ‰ to –7.37 ‰; 5) The only laminated calcite capstone fabric sampled exhibits a $\delta^{18}O$ value of –4.67 ‰ and a $\delta^{13}C$ value of –9.85 ‰; 6) The disorganized breccia calcite capstone exhibits $\delta^{18}O$ values ranging from –6.35 ‰ to +0.77 ‰ and $\delta^{13}C$ values ranging from –7.55 ‰ to –7.16 ‰; 7) The only massive dolomite capstone sampled exhibits a $\delta^{18}O$ value of –11.01 ‰ and a $\delta^{13}C$ value of –8.27 ‰; 8) The porphyritic silica-dolomite capstone exhibits $\delta^{18}O$ values ranging from –10.43 ‰ to –1.35 ‰ and $\delta^{13}C$ values ranging from –7.76 ‰ to –5.69 ‰; 9) The microlaminated dolomite capstone exhibits $\delta^{18}O$ values ranging from –9.88 ‰ to –0.26 ‰ and $\delta^{13}C$ values ranging from –8.64 ‰ to –5.63 ‰; 10) The laminated dolomite capstone fabric exhibits $\delta^{18}O$ values ranging from –10.98 ‰ to –8.23 ‰ and $\delta^{13}C$ values ranging from –9.20 ‰ to –7.31 ‰; 11) The laminated silica-dolomite capstone exhibits a $\delta^{18}O$ value of –3.44 ‰ and a $\delta^{13}C$ value of –11.86 ‰; 12)The banded calcite-dolomite capstone exhibits $\delta^{18}O$ values ranging from –14.89 ‰ to –3.55 ‰ and $\delta^{13}C$ values ranging from –10.89 ‰ to –8.23 ‰; 13) The crackle breccia dolomite capstone exhibits $\delta^{18}O$ values ranging from –10.84 ‰ to –2.25 ‰ and $\delta^{13}C$ values ranging from –8.54 ‰ to –6.60 ‰; 14) The mosaic breccia dolomite capstone exhibits $\delta^{18}O$ values ranging from –4.90 ‰ to –3.07 ‰ and $\delta^{13}C$ values ranging from –8.84 ‰ to –6.98 ‰; 15) The disorganized breccia dolomite capstone exhibits $\delta^{18}O$ values ranging from –1.55 ‰ to –0.70 ‰ and $\delta^{13}C$ values ranging from –9.23 ‰ to –7.63 ‰.

4.2. $\delta^{18}O$ versus $\delta^{13}C$ cross-plot: carbonate capstone petrographic observations

Precise petrographic observations and documentation of the mineralogies present within carbonate capstone are critical to identifying different diagenetic processes and paragenetic

relationships. Petrographically, four dominant carbonate mineralogies were identified: two comprise unreplaced "primary" capstone material, which are micritic dolomite and micritic calcite; and two involve later-stage cementation and/or replacement events, which are baroque dolomite and coarsely-crystalline calcite. A $\delta^{18}O$ versus $\delta^{13}C$ cross–plot was made to compare the geochemical signatures of these four mineralogies (Figure 39). The cross–plot indicates the following: 1) The stable isotopic composition of the micritic dolomite exhibits $\delta^{18}O$ values ranging from –9.88 ‰ to –0.26 ‰ and $\delta^{13}C$ values ranging from –11.86 ‰ to –5.63 ‰; 2) The stable isotopic composition of the micritic calcite exhibits $\delta^{18}O$ values ranging from –5.30 ‰ to +0.73 ‰ and $\delta^{13}C$ values ranging from –9.85 ‰ to –7.33 ‰; 3) The stable isotopic composition of the coarsely–crystalline calcite cements exhibit $\delta^{18}O$ and $\delta^{13}C$ values ranging from –16.49 ‰ to +2.41 ‰ and –10.89 ‰ to –6.98 ‰, respectively; 4) The stable isotopic composition of the baroque dolomite cements exhibit $\delta^{18}O$ values ranging from –14.89 ‰ to –10.43 ‰ and $\delta^{13}C$ values ranging from –8.42 ‰ to –7.76 ‰.

4.3. Carbon and oxygen isotopic signature of carbonate clasts found within the Chinle Formation

In order to identify where the dolomitic clasts found within the Chinle Formation originated, oxygen and carbon stable isotope analyses were completed on two samples. One sample was collected from the Chinle Formation at the Mary Jane Draw locality; the stable isotopic composition of the micritic dolomite within the clast exhibited a $\delta^{18}O$ value of –0.57 ‰ and a $\delta^{13}C$ value of –8.62 ‰. The other sample was collected from the Chinle Formation at the Nubbin locality; the stable isotopic composition of the micritic dolomite within the clast exhibited a $\delta^{18}O$ value of –0.34 ‰ and a $\delta^{13}C$ value of –6.84 ‰ (Figure 36).

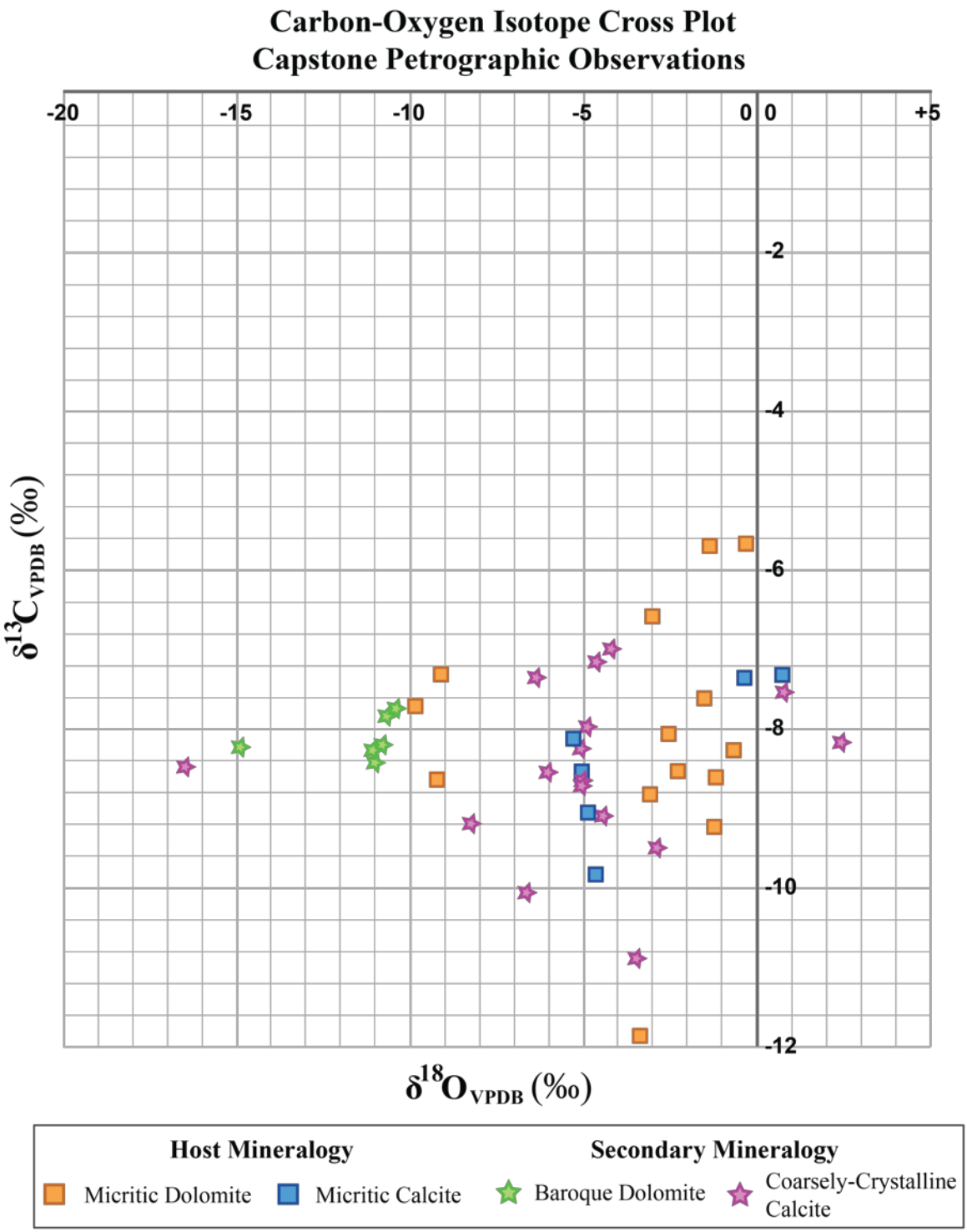

Figure 39. Cross-plot of the $\delta^{18}O$ versus $\delta^{13}C$ values pertaining to specific mineral phases. Unreplaced micritic dolomite and calcite are illustrated by orange and blue squares, respectively. Baroque dolomite cement values are illustrated by green stars, and coarsely-crystalline calcite cements are illustrated by purple stars.

4.4. U-Pb age dating of carbonate capstones

To gain information regarding the age of carbonate capstone formation we used uranium-lead dating of the carbonate capstone to constrain the age of its formation (Figure 40). Four samples taken from carbonate capstone at Gypsum Valley were analyzed for U-Pb dating (Figure 41). The U-Pb isochron generated for sample GVP-01 corresponds to an age of 82 ± 20 Ma; error under 15% (Fig. 41A). The U-Pb isochron generated for sample GVP-03 corresponds to an age of 213 ± 34 Ma (error under 15%) (Fig. 41B). The U-Pb isochron generated for sample GVP087 corresponds to an age of 100 ± 60 Ma (error under 8%) (Fig. 41C). The U-Pb isochron generated for sample GVP–02 corresponds to an age of 209 ± 36 Ma (error under 12%) (Fig. 41D). The oldest of these ages average ~211 Ma. The stratigraphic unit at Gypsum Valley that corresponds to this age is the Triassic Chinle Formation, which is the same unit that lies above the carbonate capstone.

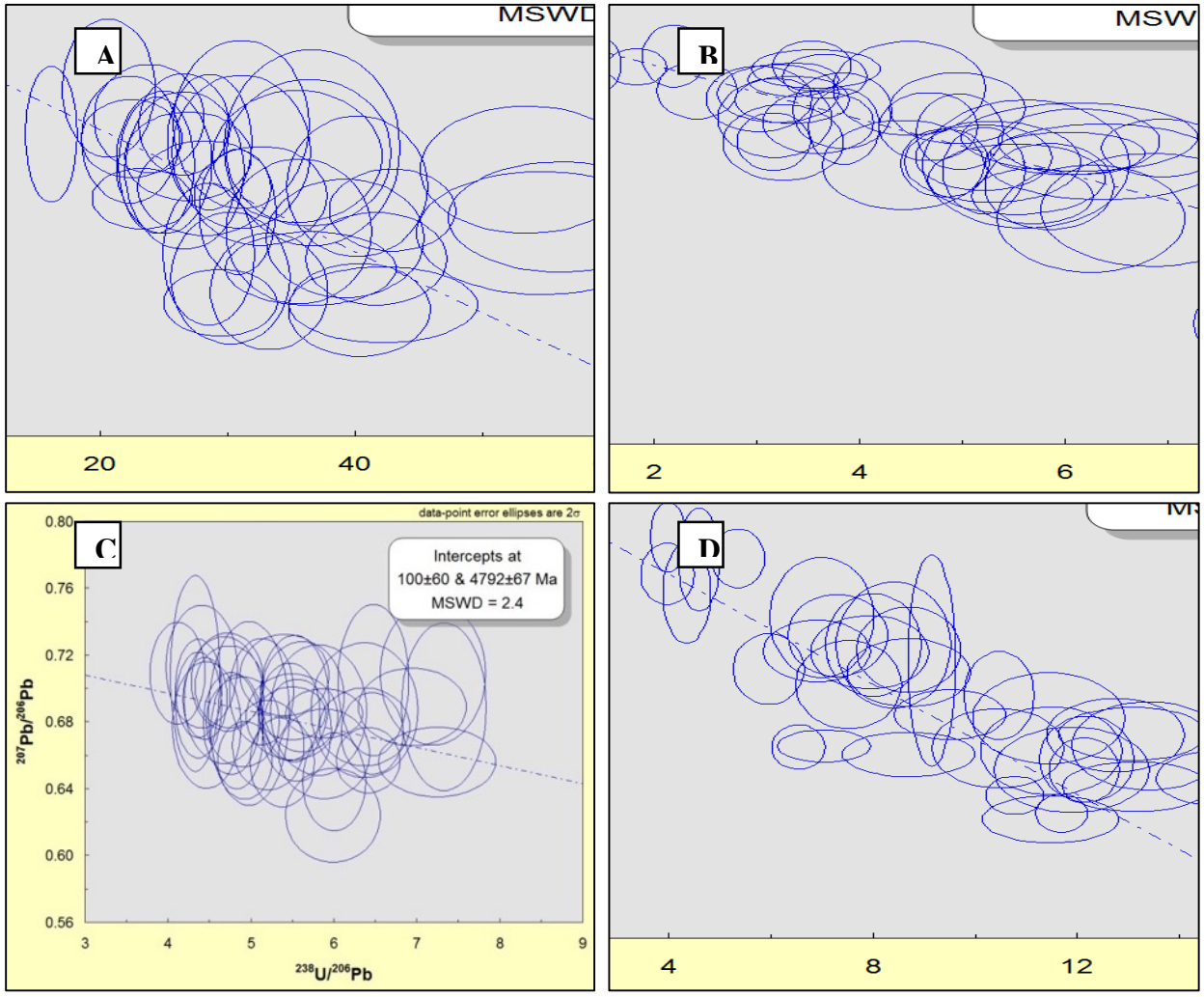

Figure 40. Isochrons of U-Pb age dates of carbonate capstone at Gypsum Valley. The Isochron intercepts at two points, at one point representing the youngest age a sample represents, and the other, the oldest (i.e. roughly the age of the Earth). Data point error ellipses are 2 sigmas. MSWD = mean squared weight deviate. A. Isochron generated for sample GVP-01, error under 15%; U-Pb age date = 82 ± 20 Ma. B. Isochron generated for sample GVP-03, error under 15%; U-Pb age date = 213 ± 34 Ma. C. Isochron generated for sample GVP087, error under 8%; U-Pb age date = 100 ± 60 Ma. D. Isochron generated for sample GVP-02, error under 12%; U-Pb age date = 209 ± 36 Ma.

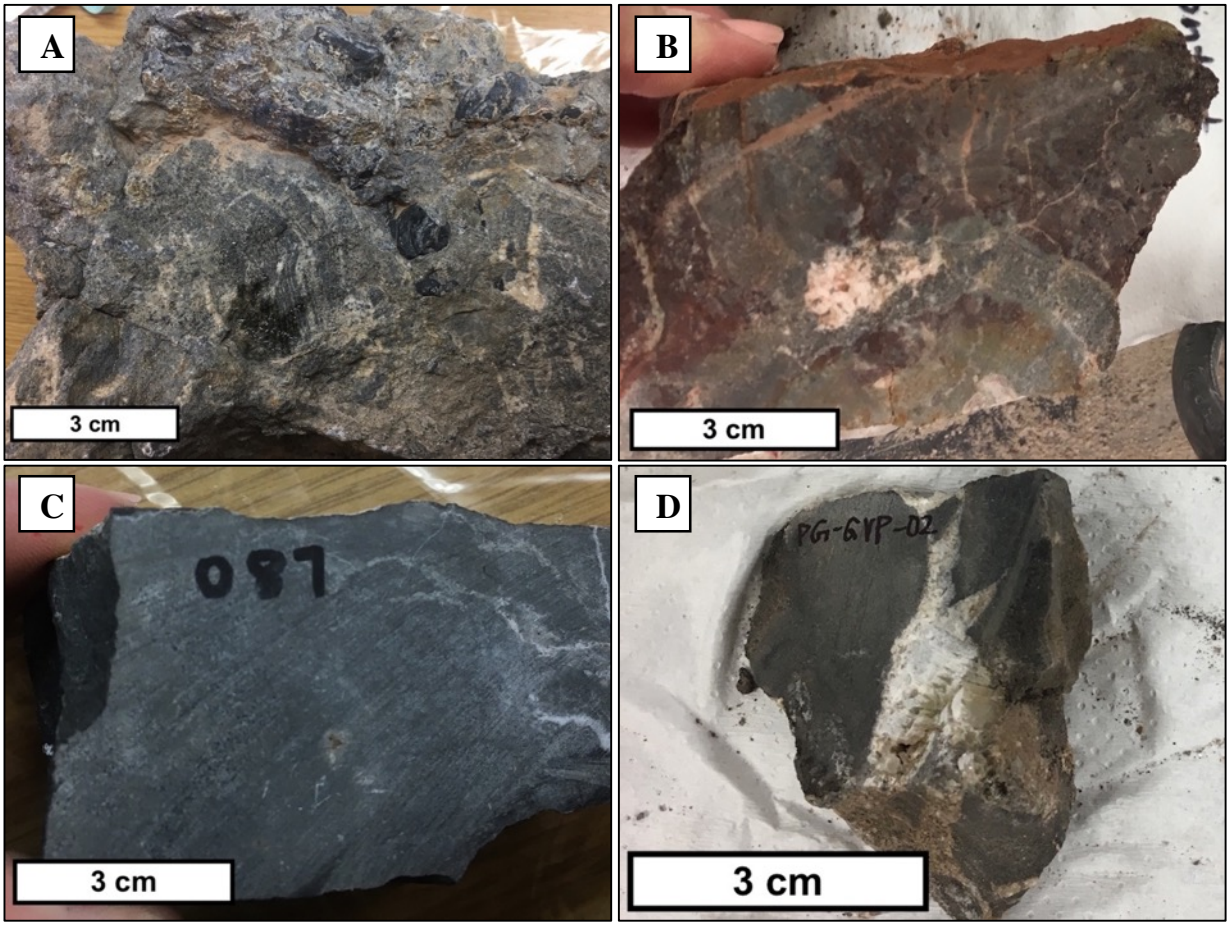

Figure 41. Carbonate capstone samples sent for U-Pb age dating. A. Sample GVP-01, error under 15%; U-Pb age date = 82 ± 20 Ma. Location: Mary Jane Draw, 3m below contact with the Chile Formation. Fabric: Disorganized breccia calcite capstone. B. Sample GVP-03, error under 15%; U-Pb age date = 213 ± 34 Ma. Location: Mary Jane Draw. Fabric: Disorganized breccia calcite capstone. C. Sample GVP087, error under 8%; U-Pb age date = 100 ± 60 Ma. Location: Mary Jane Draw. Fabric: Massive calcite capstone. D. Sample GVP-02, error under 12%; U-Pb age date = 209 ± 36 Ma. Location: Mary Jane Draw. Fabric: Disorganized breccia calcite capstone.

Chapter 5: Discussion

5.1. Interpretation of Capstone Fabrics

5.1.1. Massive Fabrics

The only calcium-sulfate mineral observed at the surface of Gypsum Valley today is gypsum, but abundant anhydrite is undoubtedly present in the subsurface. The massive gypsum fabric is interpreted to originate from the hydration, accumulation, compaction and cementation of anhydrite and/or gypsum during diapiric halite dissolution (Kyle & Posey, 1991). For the carbonate caprock, massive micritic dolomite capstone is the most common massive carbonate fabric. It is interpreted to represent the replacement of the massive gypsum and/or anhydrite capstone with dolomite during carbonate caprock formation (Posey *et al.,* 1987; Kyle & Posey, 1991; Enos and Kyle, 2002).

5.1.2. Porphyritic Fabrics

Unlike the definition for a porphyritic igneous rock, the "phenocrysts" in a porphyritic capstone originate either by neomorphism (e.g. gypsum rosettes in a finely–crystalline gypsum matrix) or by the pseudomorphic replacement of a preexisting mineralogy. The most common "phenocrysts" within the carbonate capstone are silicified nodules within calcitic and dolomitic capstones. The morphology of these silicified nodules most commonly resemble either gypsum lenses or gypsum rosettes. This indicates that larger clusters of gypsum that remained in the carbonate caprock after dolomitization/calcitization of the majority of the gypsum were silicified at a later stage (Warren, 2006). There are several chemical explanations that have been suggested to drive the replacement, which include: a local decrease in pH, caused by either biological

production of CO_2 (Siever, 1962), oxidation of sulfide to sulfate (Clayton, 1986), and mixing of marine and meteoric water (Knauth, 1979).

5.1.3. Layered Fabrics

The orientation of a majority of the layered fabrics, within gypsum and carbonate capstone, parallels that of the adjacent halokinetically drape-folded Chinle Formation. Anhydrite caprock forms in a reverse stratigraphic sequence by salt dissolution and anhydrite residue accumulation as caprock by underplating over a significant period of time. Several authors (Kyle *et al.,* 1987; Kyle & Posey, 1991) have suggested that each layer within the anhydrite zone represents a distinct cycle of salt dissolution, residual anhydrite accumulation, and residue accretion to the base of the overlying anhydrite caprock. It may be further suggested that the enterolithic to wavy nature of some laminae forms in response to stresses generated during the rehydration transformation of anhydrite to gypsum, which corresponds to ~40% volume increase (Warren, 1989). Rehydration typically occurs during periods of erosion of the diapir roof and exposure of previously buried anhydrite, as the sulfate minerals reenter the meteoric realm and are exposed to cooler and fresher water which promote the conversion of anhydrite to gypsum (Warren, 1989).

Banded Fabrics

Banded carbonate capstones contain exceptionally coarse-crystalline internal veins within the finely-crystalline host that resemble zebra stripes. Previous studies of hydrothermal "zebra" dolomites (Diehl *et al.,* 2010; Merino *et. al.,* 2006; Morrow, 2014) describe a fabric very similar to the banded capstone fabric and offers a possible explanation for its genesis. Merino (2006) proposes that the alternating micritic and coarsely-crystalline dolomite bands that constitute this fabric can be attributed to displacive vein growth. Merino (2006) describes the veins to consist of

coarse-crystalline dolomite crystals that grow inward from vein margins and push aside the finely-crystalline (host) dolostone. He suggests that a local stress field, induced by crystal growth, causes the zebra-like, self-organization of dolomite veins. The diagenetically-induced stress field hypothesis can potentially be applied to the banded dolomite and/or calcite capstone fabrics as diagenetic overprint of a precursor microcrystalline carbonate capstone. In addition to Merino's hypothesis for the origin of the coarsely-crystalline dolomite bands, it is also possible that the dolomite bands originated from extensive hydrofracturing of the carbonate capstone (James & Jones, 2016).

5.1.4. Brecciated Fabrics

An essential part of the interpretation of capstone breccias is the compositional analysis of the fragments and matrix to determine the relative timing of formation. To achieve this, the brecciated fragments are compared to the unbrecciated capstone intervals. Dolomitic crackle and mosaic breccias are by far the most common brecciated fabrics within the Gypsum Valley caprock. The brecciated fragments display very similar if not identical features to the unbrecciated massive to microlaminated, microcrystalline dolomite capstone. These characteristics suggest that the dolomitic breccias are made up of intraformational fragments derived from the breaking apart of the massive or microlaminated dolomite primary capstone fabrics. The origin of the mosaic and disorganized calcite breccias are interpreted very similarly, although their genesis requires an additional step, the calcitization of dolomite, either prior to or after brecciation.

There are a variety of mechanisms that could generate fractures in dolostone, causing the abundance of brecciated capstone found at Gypsum Valley. Caprocks associated with salt diapirs are not only subject to substantial diagenetic alteration, but also to mechanical alteration. This

owes to their location at the salt-sediment interface of a mobile salt body as well as deformation caused by volume increase during the conversion of anhydrite to gypsum in caprock that underlies the carbonate caprock. Such mechanical alteration is accommodated by brecciation of the previously formed solid caprock (Kyle & Posey, 1991). Moreover, throughout carbonate caprock formation, dissolution of anhydrite or gypsum zones beneath the carbonate caprock may have created voids that led to collapse brecciation (Kyle and Posey, 1987; Kyle & Posey, 1991). Cracks within these breccias were healed by a later generation of calcite or dolomite cements. This is a suitable hypothesis for the genesis of the disorganized breccias found within the carbonate caprock due to the jumbled nature of the brecciated fragments.

5.2. Paragenesis of Capstone Fabrics

5.2.1. Paragenetic relationships within carbonate caprock

The nature of caprock fabrics is controlled by processes involved in the primary formation of caprock (i.e. underplating of calcium sulfate minerals during halite dissolution) which were followed by multiple stages of subsequent diagenetic alteration of these materials. Therefore, unraveling the paragenetic history and cross-cutting relationships of caprock fabrics has the potential to provide insights into the nature of fluid flow in and around salt diapirs and the kinematics of halokinetic deformation. After detailed petrographic and outcrop analyses of carbonate caprock, the evidence leads to the conclusion that micritic, massive and microlaminated dolomite was the primary carbonate lithology precipitated at Gypsum Valley. Numerous observations corroborate this interpretation: 1) field relationships exhibit the replacement of micritic dolomite by calcite (Figure 42); 2) within brecciated fabrics, veins of coarsely-crystalline calcite and/or dolomite intersect each other, leaving fragments of either massive or microlaminated

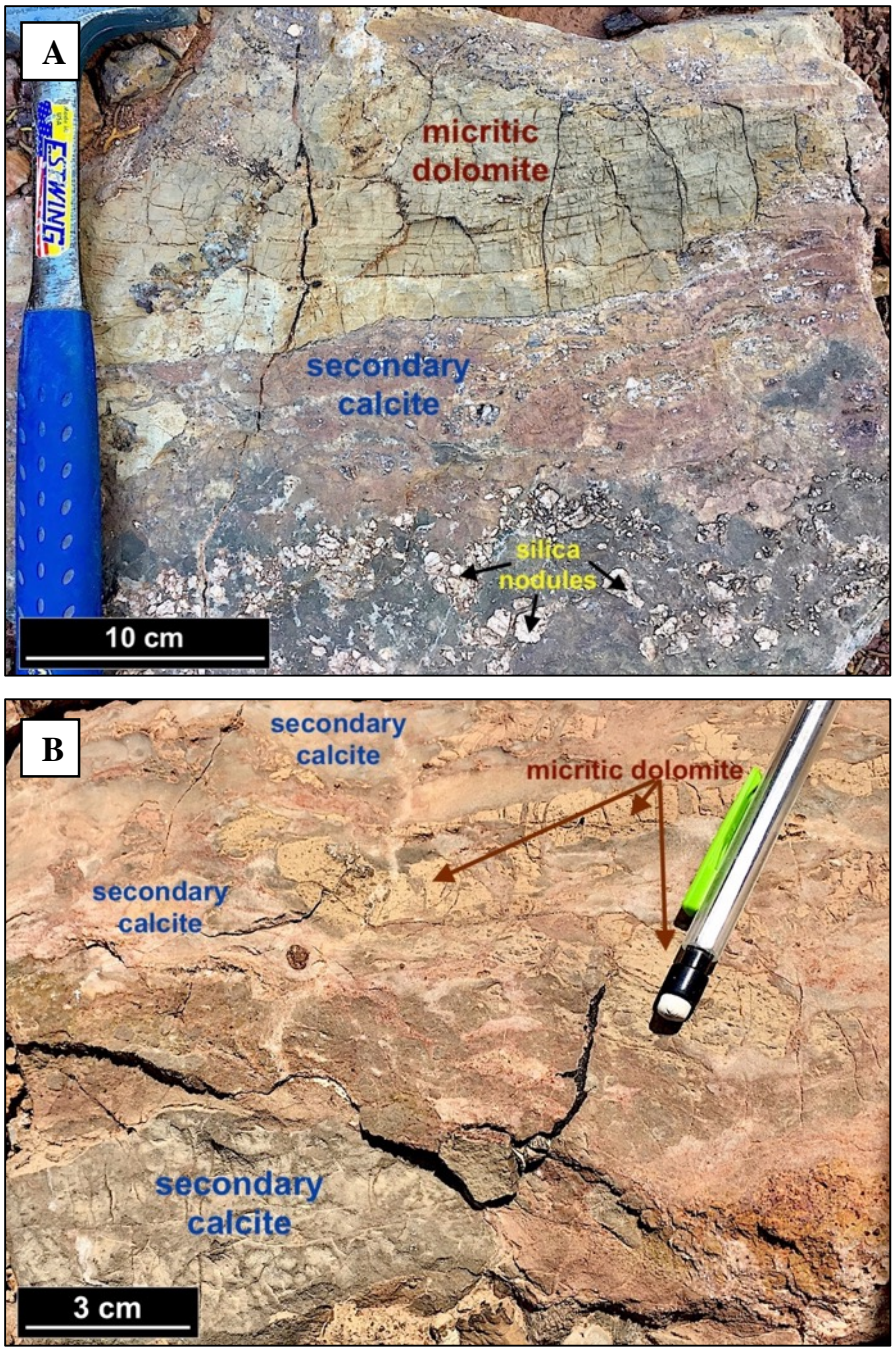

Figure 42. Outcrop examples exhibiting the replacement of micritic dolomite by calcite. A. Outcrop example of a microlaminated dolomite capstone that is being replaced by calcite; white quartz nodules are abundant within the calcite. B. Outcrop example of a small portion of tan, micritic massive dolomite capstone remnants within a secondary pink-gray massive calcite capstone.

micritic dolomite hosts between them; 3) within layered fabrics, coarsely-crystalline dolomite and/or calcite and occasionally silica are seen either replacing, or growing in veins out from massive or microlaminated micritic dolomite hosts; 4) the dolomitic clasts encased within the overlying Chinle Formation, presumably incorporated shortly after the formation of carbonate caprock, are composed entirely of massive or microlaminated microcrystalline dolomite. No other capstone fabrics are preserved as clasts within the Chinle Formation.

5.2.2. Controls on the spatial distribution of capstone fabrics

Mapping the distribution of capstone fabrics along the salt-sediment interface provides additional insight into the evolution of capstone fabrics. If the original carbonate caprock was indeed massive or microlaminated micritic dolomite, other mineralogies and/or fabric types need to be considered as the result of progressive diagenetic alteration of the original dolostone. Alteration of the original micritic massive or microlaminated dolomite capstone is the result of pressure/temperature changes, generations of fluid migration and geochemical environments, and mechanical deformation related to halokinetic deformation. Consequently, it is possible to use the evolution of capstone fabrics as an archive of fluid flow at the salt-sediment interface, which allows for reconstruction of pressure/temperature changes, identification of generations of fluid migration and geochemical environments, and understanding of mechanical deformation related to halokinetic deformation. Moreover, carbonate caprock localities that host the largest variety of capstone fabrics and mineralogies are indicative of important fluid flow conduits during halokinesis.

Based on this concept, the distribution Gypsum Valley capstone fabrics provides ample insight into halokinetic processes. For example, progressive brecciation can be observed from

minimal alteration within crackle breccias, to the maximum alteration in disorganized brecciated fabrics. Locations within the carbonate caprock intervals that are dominantly composed of crackle brecciated dolomite capstones have experienced a smaller degree of alteration than locations that contain abundant disorganized brecciated dolomite capstones and even more so, disorganized brecciated calcite capstones. It follows that there is a trend of increased alteration from the Nubbin and Box Canyon localities, which are dominated by crackle brecciated dolomite capstone to locations than further down the salt wall at Bridge Canyon and Mary Jane Draw, which are dominated by mosaic and disorganized breccias. This suggests that the northern portion of the salt wall experienced less disruption than further down the salt wall. This non-uniform disruption of brecciated fabrics can be attributed to the differential rise of the salt wall through time, where the northern portion of the wall did not rise as extensively as the mid-southern portion of the wall (McFarland, 2016).

Another example of the usefulness of capstone fabrics as indicators for deformation comes from caprocks that are located directly inboard of diapir-parallel, steeply dipping normal faults that are present in the adjacent Chinle Formation and extend up through the Jurassic Navajo Formation (Figure 34 & 35). The fact that the fault planes are shared in the Chinle through Navajo formations indicates a post-depositional timing of movement. This was likely the result of tensional stress caused by the differential rotation of the strata lying on the outboard margin of the salt shoulder, which subsided toward the minibasin to the northeast, whereas the strata on the inboard domain did not (McFarland, 2016). The formation of the drape-fold monocline on the shoulder and subsequent post-depositional gravitational collapse faulting led to the overall antiformal geometry observed today. Although these faults have not been previously thought to have extended down through the caprock (McFarland, 2016), the extensive deformation of the

caprock located inboard of these faults suggests otherwise. Faulting may have mechanically deformed the caprock, but more importantly, it would have provided a conduit for diagenetically altering fluids to migrate through the caprock.

5.3. Geochemical Signature of Carbonate Capstone

5.3.1. Isotopically low carbon signatures of carbonate capstone

To understand the origin of the carbonate found within the caprock at Gypsum Valley, a robust understanding of their geochemistry is required. The geochemical signatures of these rocks provide insights into the environment in which they formed, which cannot be obtained from petrographic analysis alone.

A study of the Texas Gulf Coast salt domes by Feely and Kulp (1957), recognized the extremely light carbon isotope values in calcitic capstones and attributed them to a methane source. This conclusion was based upon the premise that carbon derived from organic matter, such as hydrocarbons, should be depleted in ^{13}C, with values ranging from –20‰ to –50‰ or lower, relative to those derived from inorganic carbon from seawater-precipitated carbonates, which by comparison are enriched in ^{13}C, with values around 0‰ (Feely & Kulp, 1957; Posey *et al.,* 1987; Enos and Kyle, 2002). This observation establishes a genetic link between carbonate caprocks and hydrocarbon because, in order to fuel carbonate caprock formation, hydrocarbons must have been present. Carbonate capstones thus should display ^{13}C–depleted isotope signatures, and values ranging from –5‰ to –60‰ have been reported (Posey *et al.,* 1987; Sassen, 1987; Kyle & Posey, 1991).

Additional evidence for the existence of a process in which anhydrite or gypsum is replaced by carbonate minerals comes from light oxygen isotope signatures of the carbonates. These

signatures reflect waters with ^{18}O–depleted isotope signatures that were involved in the processes that removed salt (NaCl) and subsequently replaced sulfate with carbonate minerals. Meteoric waters have light (^{18}O–depleted) oxygen isotope signatures ($\delta^{18}O_{water}$) because evaporation, which leads to precipitation as rain or snow, discriminates against the heavy oxygen isotope ^{18}O. It is well established that oxygen isotope values of carbonate are a function of $\delta^{18}O_{water}$ and the temperature at which dolomitization/calcitization takes places (e.g. Major *et al.,* 1992). However, the oxygen isotopic signatures of carbonates can be isotopically overprinted by exchange with fluids associated with meteoric and/or burial diagenesis. Increased temperatures typically lower the $\delta^{18}O$ value, so carbonate precipitated in a deep burial diagenetic setting are normally significantly depleted in ^{18}O (Major *et al.,* 1992; James & Jones, 2016). The $\delta^{13}C$ signature of carbonates is less prone to resetting by diagenetic fluids, largely because such fluids typically carry small amounts of carbon (organic or inorganic).

Petrographic observations reveal that almost all samples have undergone some degree of diagenetic alteration, which should be taken into consideration during geochemical interpretations. To address this issue, the isotopic signature of the original capstone carbonate phases, i.e. the primary mineralogies (i.e. micritic dolomite and micritic calcite) were plotted in a $\delta^{18}O$ versus $\delta^{13}C$ cross-plot where the capstone fabrics are identified (Figure 43). Capstone fabrics consisting of micritic dolomite and calcite fall within a narrow range of $\delta^{18}O$ values, between –5.30 ‰ to –0.26 ‰, with four dolomitic outliers that exhibit significantly lighter $\delta^{18}O$ values, around –10 ‰. Interestingly, the four dolomitic outliers depleted in ^{18}O correspond to microlaminated and laminated fabrics. These fabrics also contain hydrothermal dolomite, so it is evident that the micritic dolomite within these samples likely underwent some degree of isotopic overprinting by

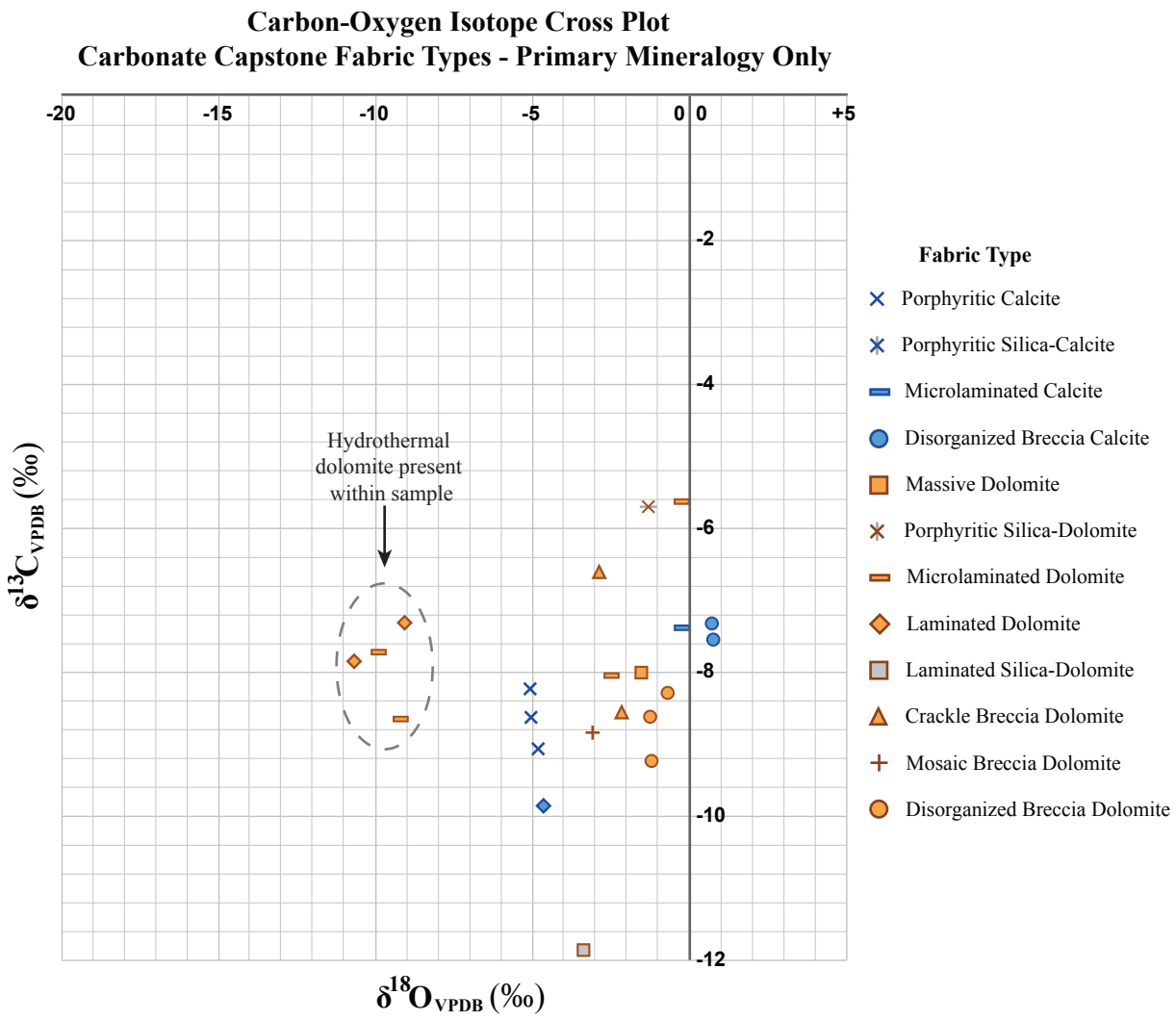

Figure 43. Carbonate isotope cross-plot of $\delta^{18}O$ versus $\delta^{13}C$ comparing the geochemical signatures of the primary mineralogy sampled for all carbonate capstone fabrics. The stable isotope composition of the micritic dolomite capstone fabrics are illustrated in orange, and the micritic calcite capstone fabrics are illustrated in blue.

hydrothermal fluids. Conversely, the micritic carbonate samples that exhibit a narrow range of slightly heavier $\delta^{18}O$ values have experienced a smaller degree of diagenetic alteration. Thus, their $\delta^{18}O$ values are more representative of the environment in which they formed. The micritic dolomite samples with $\delta^{18}O$ values that range from –0.70 to –5.00 ‰ are consistent with carbonate precipitation from meteoric water, where the typical $\delta^{18}O$ composition of meteoric water. The $\delta^{13}C$ values of the micritic carbonate samples range from –11.86 to –5.63 ‰, with a median value of –8.17 ‰. These values are interpreted to reflect the incorporation of light carbon (^{12}C) from the oxidation of hydrocarbons (depleted in ^{13}C) during the formation of carbonate caprock, but are at the upper end of the reported range from –5‰ to –60‰ (Posey *et al.,* 1987; Sassen, 1987; Kyle & Posey, 1991; Enos and Kyle, 2002). This implies that inorganic carbon sources also contributed to the carbonate caprock found at Gypsum Valley, which agrees with the observation that magnesium must have been added to allow for the formation of dolomite (Lerer, 2017). Dewatering of the Paradox Formation shales is the likely source of magnesium.

5.3.2. Diagenetic overprinting on complex carbonate capstone fabrics

Comparing petrographic observations to isotopic data allows for the interpretation of diagenetic processes (Figure 39). Samples that have undergone recrystallization and/or cementation by baroque dolomite have been altered by hydrothermal fluids and tend to exhibit the lightest $\delta^{18}O$ values of the group – an effect caused by high temperatures and light $\delta^{18}O_{water}$ of the circulating fluids. Samples that display recrystallization and or/cementation by a coarsely-crystalline calcite exhibit the widest range of $\delta^{18}O$ values. This pattern can be attributed to multi-generational calcite cementation within different diagenetic environments, reflecting changes in temperature/pressure conditions and a mixture of the percolating fluids. A $\delta^{18}O$ versus $\delta^{13}C$ cross-

plot that compares the geochemical signature of all carbonate capstone fabrics illustrates these same findings (Figure 38). Fabrics that display significant diagenetic alteration and have undergone recrystallization and cementation by baroque dolomite and/or late-stage calcite also display the widest range of geochemical signatures. These include the coarsely layered capstone fabrics such as banded calcite-dolomite capstone and laminated calcite capstone.

5.3.3. Geographic distribution of geochemical signatures along the Gypsum Valley salt wall, starting at the Nubbin

To identify possible trends or patterns in the isotope signatures of carbonate capstone based on geographic location, a plot of $\delta^{18}O$ and $\delta^{13}C$ of samples collected along the Gypsum Valley salt wall was created (Figure 44). The $\delta^{18}O$ profile reveals that the smallest spread in $\delta^{18}O$ values occurs at the Nubbin, and the largest occurs along the Box Canyon to Bridge Canyon transect, although there is a wide data spread at the Mary Jane Draw locality as well. The primary mineralogy at the Nubbin is micritic dolomite, whereas, at the other localities, there is an increase in micritic calcite, baroque dolomite, and coarsely–crystalline calcite. These additional mineralogies found along the salt wall correspond to the increasing variety of carbonate capstone fabrics. A similar trend is observed in the $\delta^{13}C$ data, although there is a narrower range, the widest being at Mary Jane Draw. Seemingly, the wider the spread in the isotopic composition represents a greater degree of diagenetic alteration and isotopic overprinting. The least amount of isotopic variability occurs at the Nubbin location. This suggests that this locality has experienced the least degree of diagenetic alteration, and indicates that micritic dolomite was likely the original carbonate caprock lithology. At the Bridge Canyon and Mary Jane Draw localities, the isotopic range increases, coinciding with ample evidence for diagenetic alteration, such as the abundance

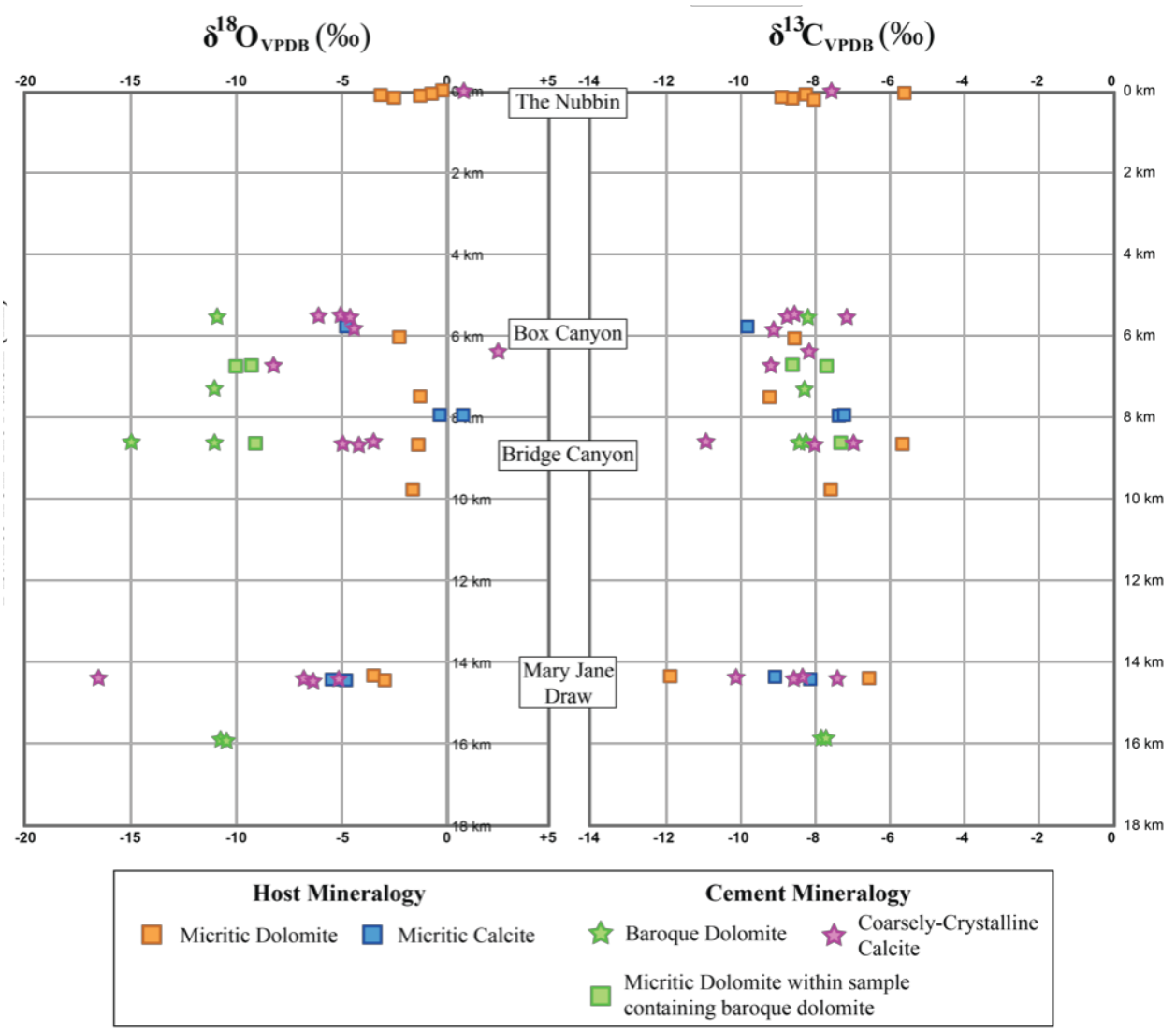

Figure 44. The measured $\delta^{18}O$ (left) and $\delta^{13}C$ (right) values for carbonate capstone host material (micritic dolomite in orange and micritic calcite in blue) and cements (baroque dolomite in green and coarsely-crystalline calcite in purple) have been plotted by each sample's corresponding geographic location along the Gypsum Valley salt wall. This was done to analyze the variation in stable isotope compositions by location.

of later-stage mineralogies (e.g. baroque dolomite and coarsely–crystalline calcite). This increased diagenetic alteration at these localities can be attributed to the extensive alteration and faulting in the outboard stratigraphic units, owing to subsidence of the salt shoulder located along the northeast margin of the Gypsum Valley salt wall (Heness, 2016; McFarland, 2016).

5.3.4. Stable isotope composition of dolomite clasts in Chinle match those of carbonate capstone

To assess if the massive to microlaminated micritic dolomite clasts found within the Triassic Chinle Formation originated from the carbonate caprock body, their isotopic signatures were analyzed and compared. The oxygen and carbon stable isotope composition of the clasts fall within the same range as the *in-situ* carbonate capstones found in Gypsum Valley. Furthermore, the isotopic signature of the clasts is closest to that of the massive micritic dolomite samples that display the least amount of diagenetic alteration. This reveals two interesting points: first, because the fabric of the capstone clasts found within the Triassic Chinle Formation are all massive dolomite or microlaminated micritic dolomite, this must have been the fabric of the exposed carbonate caprock present atop the Gypsum Valley salt wall at the time of Chinle deposition. Second, the isotopic signature of the clasts matches that of the least diagenetically altered dolomite caprock found along the salt wall. This indicates that the isotopic signature of $\delta^{18}O \approx -0.5$ ‰ and $\delta^{13}C \approx -8$ ‰ represent the isotopic signature closest to that of the original carbonate caprock phase, which is micritic dolomite.

5.3.5. U–Pb age dates of carbonate capstones

The preliminary results from the uranium-lead dating provided an age of 211 +/-16Ma. This date is significantly younger than the Paradox Formation (~323 – 310 Ma) and the Honaker Trail Formation (~310 – 298 Ma) and is consistent with the time frame in which the Triassic Chinle Formation (~230 – 201 Ma) was deposited (Cater, 1970). This indicates that the replacement of anhydrite caprock with carbonate must have happened shortly before or during the deposition of the Chinle Formation, allowing for clasts from the caprock to be incorporated into the sediments. This evidence supports the hypothesis that the studied unit is lateral carbonate caprock and rejects the hypothesis that the carbonates were formed either during the deposition of the Paradox Formation or as a unit of the Pennsylvanian Honaker Trail Limestone.

5.4. Hypotheses/Models for Lateral Caprock Emplacement

The following section discusses supporting and detracting evidence for each of the potential genetic models for the origin and emplacement of the gypsum-carbonate unit in this study. Any viable model for the origin for the gypsum-carbonate interval must successfully address the key characteristics of this unit. The model must explain the unique fabrics found within the gypsum-carbonate zone that lack any depositional attributes, such as the lack of fossils, sedimentary structures, sedimentary bedding, and the lack of depositional interfingering with adjacent outboard stratigraphy. The model must also address the orientation of the layering within the gypsum-carbonate unit, which parallels that of the adjacent halokinetically drape-folded Chinle strata. Additionally, the model must address its location at the salt-sediment interface in a semi-lateral position and the lack of an angular unconformity with the overlying Triassic Chinle Formation. Finally, the model must address the light (< –6 ‰) carbon stable isotopic signature of

the carbonate interval and the dolomitic clasts found within fluvial channels of the Chinle Formation. There are four potential hypotheses/models for the origin of the carbonate interval located at the salt-sediment interface: 1) that it represents a highly-rotated section of the Pennsylvanian Honaker Trail Limestone, as it was originally mapped (Stokes & Phoenix, 1948); 2) that it represents non-halite, layered evaporite sequence (LES) from the Pennsylvanian Paradox Formation that has been deformed and plastered against the diapir flank during diapiric rise; 3) that it represents caprock that formed *in–situ* along the flank of the salt wall by unusual NaCl-undersaturated basinal fluids; and 4) that it represents caprock that formed on the crest of the salt wall and was subsequently rotated into a flanking position by halokinetic drape-folding during passive diapiric rise.

5.4.1. Pennsylvanian Honaker Trail Formation Hypothesis

The gypsum-carbonate unit that is the focus of this study was mapped as the Pennsylvanian Honaker Trail Formation by Stokes *et al.* (1948), as it is a marine limestone located stratigraphically above the salt (i.e. Pennsylvanian Paradox Formation). The Honaker Trail Limestone is characterized by interbedded shale or mudstone, arkosic fluvial sandstone, fossiliferous carbonate, organic-rich mudstone, dolostone, halite, and minor amounts of anhydrite (Rasmussen and Rasmussen, 2009). Additionally, it typically displays abundant cross stratified bedforms to massive fossiliferous limestones containing crinoid, brachiopod, fusulinid, and bryozoan faunas (Barbeau, 2003). Although the proposed carbonate caprock has undergone significant diagenetic alteration, this alteration cannot explain the complete lack of fossil material, or interbedded arkosic sandstones and mudstones. Furthermore, if this unit belonged to the Pennsylvanian Honaker Trail Formation, there should be a steeply-dipping angular unconformity

with the overlying Triassic Chinle Formation, which is found at other such contacts along the southwest margin of Gypsum Valley salt wall (Escosa et al., 2018). Finally, the $\delta^{13}C$ values of the Honaker Trail Formation exposed on the southwest margin, range from –3.8 to –1.26 ‰, a range which is consistent with Pennsylvanian marine carbonates (Magaritz & Holser, 1990). Whereas the $\delta^{13}C$ values for the proposed carbonate caprock along the northeast margin are all more negative than roughly –6 ‰ (Figure 45). Due to the vast inconsistencies between the features of the regional Honaker Trail Formation and the unit in question, the Honaker Trail Formation can be eliminated as a potential origin of this gypsum-carbonate unit.

5.4.2. Paradox LES Model

The second possible hypothesis for the origin of the carbonate and gypsum unit is that it represents a rotated carbonate-rich layered evaporite sequence (LES) from the Paradox Formation. The Pennsylvanian Paradox Formation is characterized by 29 depositional cycles consisting of anhydrite, dolomite, shale, and halite (Hite & Buckner, 1981). The rotated LES model, proposed by Schwerdther *et al.* (1978), suggests that a depositional to early post-depositional anhydrite and/or dolomite-dominated evaporite sequence associated with the autochthonous depositional salt strata (i.e. the Paradox Formation) has been rotated upward to a lateral position against the flank of the diapir during diapiric rise. In fact, Mast (2016) concluded that this is the case for a dolomite interval interbedded with black shales from the Paradox Formation along the most southwestern portion of the Gypsum Valley salt wall, where it forms part of a "megaflap" (i.e. a steep stratal panel that extends far up the side of a diapir) (Deatrick, 2015; Rowan *et. al.,* 2016). Although the LES model is present elsewhere in Gypsum Valley, there are numerous inconsistencies between the dolomites from the Paradox Formation and the carbonate-gypsum interval in question. First,

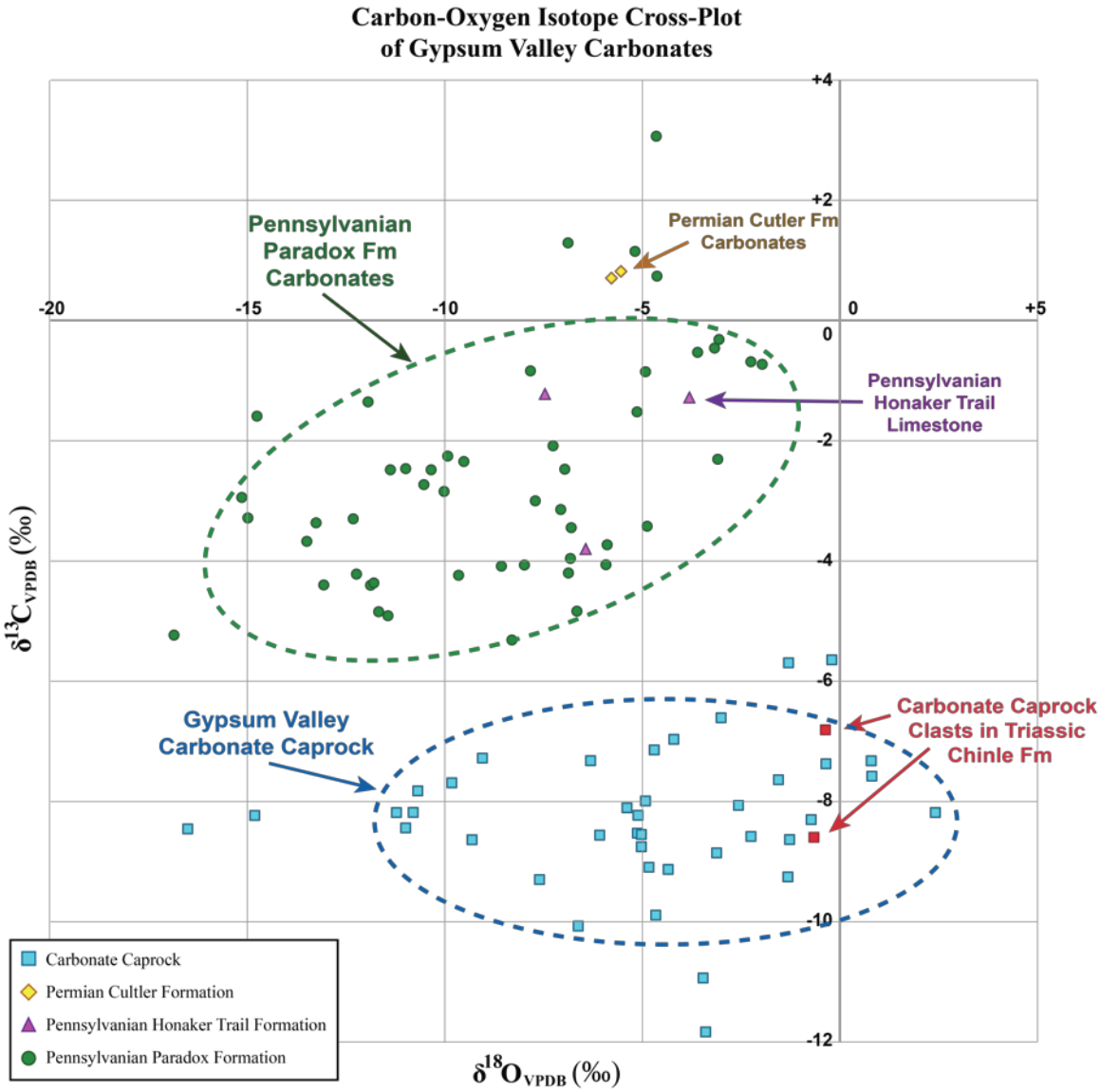

Figure 45. Cross-plot of the $\delta^{18}O$ versus $\delta^{13}C$ values of carbonates exposed at Gypsum Valley. These include: carbonate caprock exposed along the salt-sediment interface (blue); carbonate caprock clasts found within fluvial channels of the overlying Triassic Chinle Formation (red); carbonates form the Permian Cutler Formation (yellow); depositional Honaker Trail Formation marine carbonate samples (purple); and depositional Pennsylvanian Paradox Formation carbonate samples (green).

the proposed caprock interval does not contain interbedded black shales, which are very common within typical Paradox Formation carbonate intervals. Second, the geochemical signature of the proposed carbonate caprock and Paradox Formation dolomites are different (Figure 45). The important difference is in the $\delta^{13}C$ values. The carbon isotopic signature from the proposed carbonate caprock is distinctly lighter than that of the Paradox Formation carbonates, which exhibit heavier values than would be consistent for carbonates precipitated in a marine setting. It is interpreted that the light carbon isotopic signature of the proposed caprock reflects the incorporation of light carbon from the oxidation of hydrocarbons during the formation of carbonate caprock. Third, the carbonates described by Mast (2016) exhibit features, including pisoids, that are not found in the study area. These three major differences between the carbonate interval in question and the Paradox Formation LES model are a strong indication that the latter model is not applicable.

5.4.3. In-situ Model

The *in-situ* model proposed by Jackson et al. (2013) suggests that lateral caprock forms in place along the flank of the diapir. The model proposes that an anhydrite caprock can form in response to the migration of relatively warm, NaCl-undersaturated fluids up the margins of the salt body, causing the dissolution of halite and consequently the accretion of anhydrite along the margin of the diapir. Second, this model proposes that hydrocarbon migration would provide the means to aid in the chemical conversion of $CaSO_4$ minerals to carbonate minerals, driven by sulfate-reducing bacteria. This model does fit numerous characteristics of the proposed caprock at Gypsum Valley. The *in-situ* model is consistent with the observation of carbonate depleted in ^{13}C, owing to the bacterial reduction of organic matter and also provides an explanation for the

precipitation of a carbonate unit that does not contain fossils or interbedded black shales. However, one key piece of evidence, the presence of carbonate caprock clasts within the Chinle Formation, appears to be incompatible with the model. *In-situ* formation of caprock is suggested to take place relatively late in the history of the basin, which excludes a mechanism that places eroded carbonate caprock clasts into the adjacent outboard stratigraphy. Therefore, the *in-situ* model does not adequately address all of the characteristics of the gypsum-carbonate unit at the Gypsum Valley salt wall.

5.4.4. Halokinetic Drape-Fold Model

The halokinetic drape-fold model proposed by Giles et al. (2012) suggests that caprock initially forms in a crestal position on top of the diapir, and is rotated into a lateral position by drape-folding. The model proposes caprock formation occurs by the cross-flow of NaCl-undersaturated waters that dissolve diapiric halite and accrete the less-soluble minerals to the crest of the diapir, forming an anhydrite and gypsum caprock. Next, sulfate-reducing bacteria fueled by hydrocarbons induce the replacement of the calcium sulfate with carbonate caprock. The halokinetic drape-fold model postulates that continued diapiric rise and minibasin subsidence causes drape-folding of the roof strata and competent caprock, which would be rotated off the crest and into a diapir-flanking position. The lateral caprock is therefore associated with a discrete package of roof strata, where the formation age of the caprock should be roughly equivalent to or slightly older than that of the adjacent halokinetically deformed strata (i.e. the Triassic Chinle Formation). Additionally, this model suggests that topographic relief generated by continued diapiric rise results in erosional thinning of the roof and caprock strata, resulting in caprock clasts incorporated into the surrounding sediments. This model is consistent with all outcrop,

petrographic and geochemical characteristics of the gypsum-carbonate interval present at the salt-sediment interface at Gypsum Valley.

5.5. Caprock Formation by the Drape-Fold Model

The halokinetic drape-fold model is the best fit model for all of the data collected on the proposed caprock interval at the Gypsum Valley salt wall. Thus, I conclude that the caprock likely formed syndepositionally with the early Chinle Formation by the dissolution of halite at the crest of the diapir by the abundant amount of flowing NaCl-undersaturated groundwater charged by the Chinle Formation fluvial system. The accretion of anhydrite caprock produced layering within the caprock that paralleled the Chinle Formation during its deposition. After continued burial by the Chile Formation, hydrocarbons, likely sourced by the organic-rich black shales of the Paradox Formation (Trudgill, 2011), entered the system, which would provide energy for sulfate-reducing bacteria to reduce sulfate and produce bicarbonate and permit the precipitation of a carbonate caprock. Abundant Ca^{2+} needed to make calcium carbonate would have been available from the dissociation of $CaSO_4$ during sulfate reduction. The source of Mg^{2+} needed to precipitate dolomite would have likely been derived from the dewatering of shales within the Paradox Formation, or even derived from Mg^{2+}-bearing salts within the dissolving diapir.

After caprock formation, continued diapiric rise would have produced topographic relief that resulted in the erosional thinning of the roof strata. A portion of the dolomitic caprock was also eroded, evident by clasts of dolomite caprock within the halokinetic sequences of the Chinle Formation (Heness et al, 2016) (Figure 46). Finally, continued diapiric rise and minibasin subsidence rotated the caprock and the salt shoulder to a lateral position (Figure 47). Lateral emplacement by drape-folding is evident in the low-angle angular unconformities of the

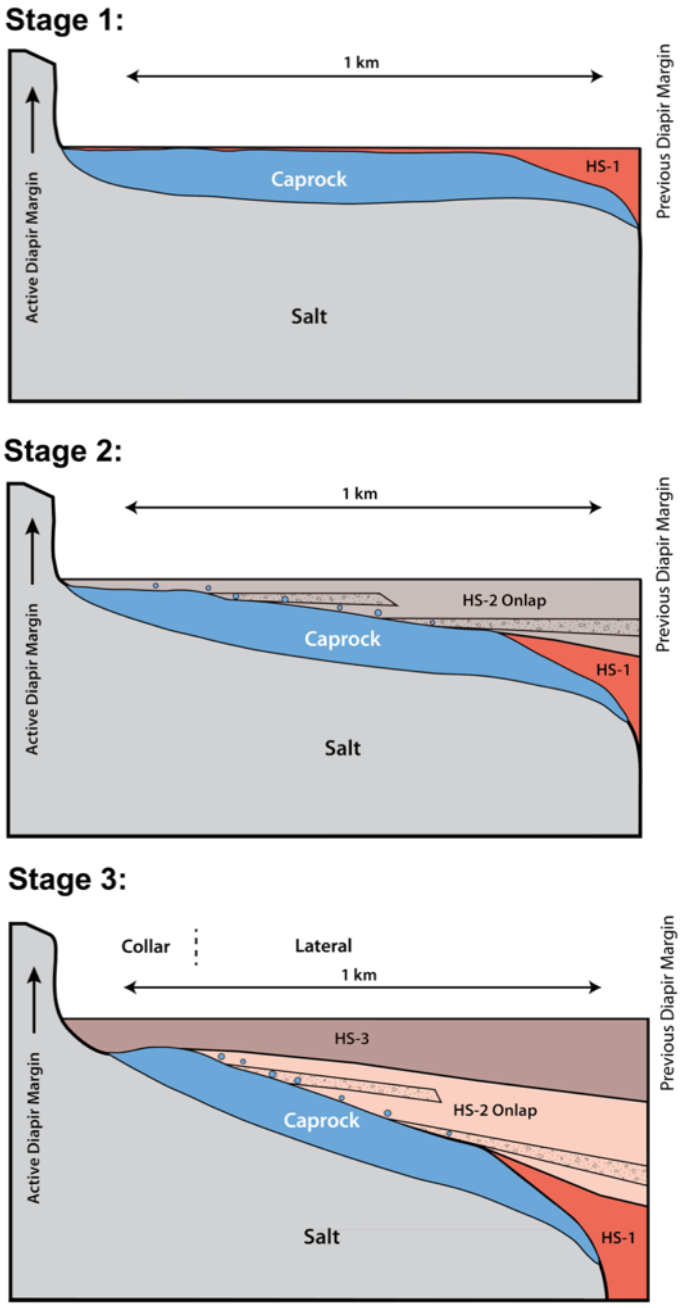

Figure 46. Conceptual illustration of time steps for the development of the Gypsum Valley salt shoulder. Stage 1: Onlap of the first halokinetic sequence (HS-1) of the Chinle Formation onto the previously formed caprock. Stage 2: Continued salt rise and subsidence of HS-1 and progressive onlap of the second halokinetic sequence (HS-2). Stage 3: Continued salt rise and drape-fold subsidence of HS-2 and onlapping of the third halokinetic sequence of the Chinle Formation. Between the deposition of each halokinetic sequence, there is a period of erosion that allows for the incorporation of dolomitic caprock clasts into the following halokinetic sequence of the Chinle Formation. Modified from Langford, 2016.

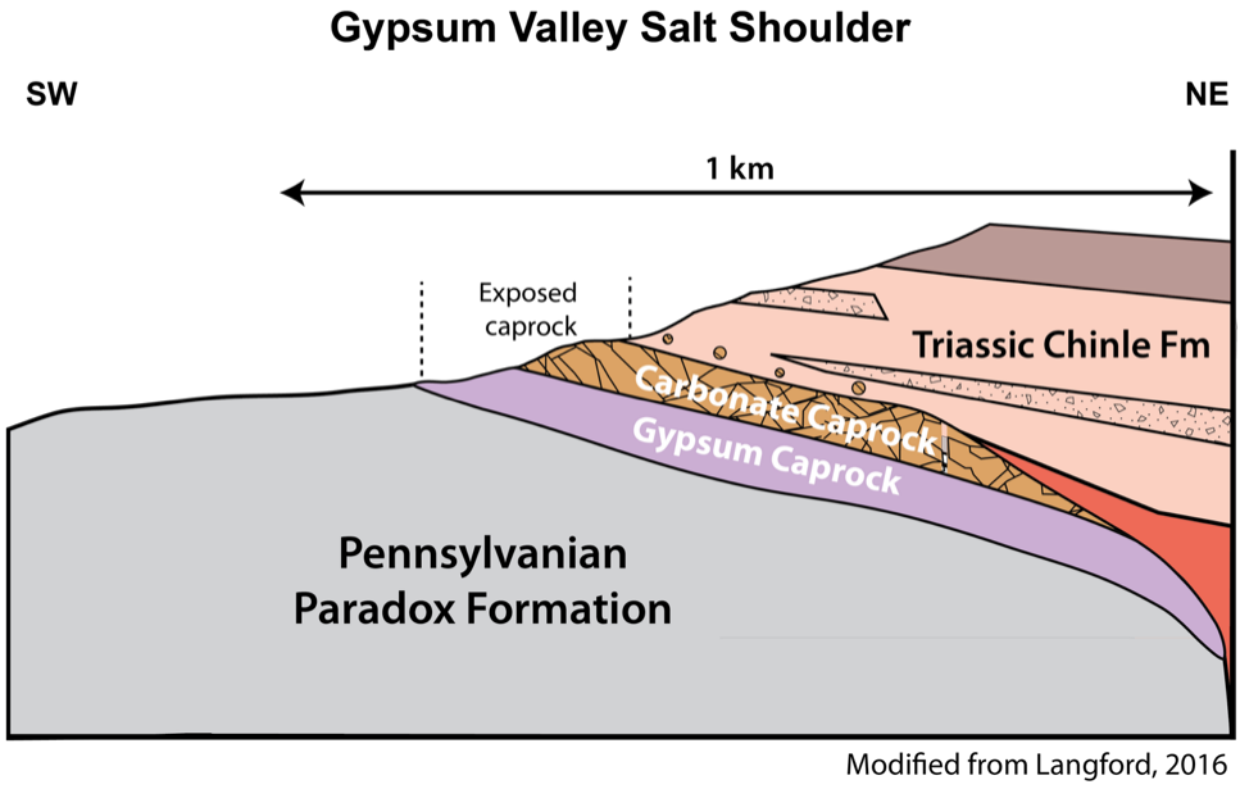

Figure 47. Schematic illustration of the gypsum and carbonate caprock exposed over the modern Gypsum Valley salt shoulder.

halokinetic sequences mapped by McFarland (2016) within the Chinle Formation. The preservation of these unconformities provides evidence that the salt shoulder present along the northwestern margin of the Gypsum Valley salt wall subsided with the outboard minibasin strata.

The presence of dolomitic caprock clasts found within debris flows and fluvial channel sandstones and conglomerates of the Chinle Formation, provides information regarding the relative timing of caprock formation. Clasts of dolomitic caprock are found within the upper Chinle Formation, suggesting that the carbonate caprock had already formed before the deposition and onlapping of the upper members of the Chinle Formation. Therefore, the timing of carbonate caprock formation could have occurred during the early Chinle Formation depositional time, or potentially during the stratigraphically older Moenkopi Formation depositional time. In either case, the Gypsum Valley salt wall must have been at least locally exposed during the late Chinle Formation depositional time, allowing a portion of the carbonate caprock to be eroded off and incorporated into the upper Chinle Formation. Furthermore, because all of the dolomitic clasts found in the Chinle Formation consist of the massive or microlaminated capstone fabrics further leads to the conclusion that the diagenetic alteration that led to the multitude of capstone fabrics present today post-dates the deposition of the upper members of the Chinle Formation, or only took place in locations that remained covered during the thinning of the roof strata.

Chapter 6: Conclusion

Based on new and existing mapping, petrographic and isotopic geochemical analysis, the gypsum-carbonate unit previously mapped as the Honaker Trail Formation located along the northeastern margin of the Gypsum Valley salt wall is reinterpreted in this study to be lateral caprock that formed in the Triassic. The term capstone was introduced to represent a particular caprock lithology, as a distinction from the term caprock, which is generally used in reference to the entire rock body. Four distinct macroscopic capstone fabrics were identified at Gypsum Valley: 1) Massive: homogeneous, with micro-to-coarsely crystalline subdivisions; 2) Porphyritic: comprising two distinct crystal sizes, one significantly larger than the other; 3) Layered: subdivisions based on layer size that includes: microlaminated (1-3mm), laminated (3-10mm), and banded (>10mm); 4) Brecciated: subdivided into crackle, mosaic and disorganized, based on the degree of separation between the brecciated caprock clasts. Paragenetic relationships determined from detailed outcrop and petrographic analyses indicate that the original composition of the carbonate caprock was massive or microlaminated micritic dolomite. This reveals that any other mineralogy and/or fabric type found within the carbonate caprock exposed today is the result of progressive diagenetic alteration of the original dolostone. Due to this finding, it is possible to use the evolution of capstone fabrics as an archive of fluid flow at the salt-sediment interface. Furthermore, this suggests that the localities of carbonate caprock with the largest variety of capstone fabrics and mineralogies are indicative of important fluid flow conduits during halokinesis.

Geochemical analyses of carbonate caprock resulted in carbon stable isotopic signatures ranging from –12 to –6 ‰, which reflects the contribution of isotopically light carbon from the oxidation of hydrocarbons during caprock formation. The oxygen stable isotope signatures range

from –16 to +2 ‰, with the most negative values reflecting hydrothermal conditions. Clasts of microcrystalline dolomite caprock were found within the overlying Triassic Chinle Formation. The stable isotopic composition of the dolomitic clasts exhibits a $\delta^{18}O$ value of roughly –0.5 ‰ and a $\delta^{13}C$ value of roughly –8 ‰, which are consistent with the isotope signature of the *in-situ* carbonate caprock. The presence of dolomitic caprock clasts in the Chinle Formation indicates that the carbonate caprock had formed before the deposition and onlapping of the upper members of the Chinle Formation. The preliminary results from the uranium-lead dating provided an age of 211 +/-16 Ma, which is consistent with the timeframe in which the Triassic Chinle Formation (~230 – 201 Ma) was deposited. This indicates that the replacement of anhydrite caprock with carbonate must have happened shortly before or during the deposition of the Chinle Formation, allowing for clasts from the caprock to be incorporated into the sediments.

Four models were evaluated for the origin of the carbonate strata along the northeast margin of the Gypsum Valley salt wall: 1) that it represents a highly-rotated section of the Pennsylvanian Honaker Trail Limestone, as it was originally mapped; 2) that it represents non-halite, layered evaporite sequence (LES) from the Pennsylvanian Paradox Formation that has been deformed and plastered against the diapir side during diapiric rise; 3) that it represents caprock that formed *in–situ* along the flank of the salt wall by unusual NaCl-undersaturated basinal fluids; and 4) that it represents caprock that formed on the crest of the salt wall and was subsequently rotated into a flanking position by halokinetic drape–folding during passive diapiric rise. The halokinetic drape-fold model is the only proposed model that fits all of the data collected from the studied carbonate unit. The caprock formed likely during the early Chinle Formation depositional time by the dissolution of the crest of the diapir by the abundant amount of flowing NaCl-undersaturated groundwater recharged by the Chinle Formation fluvial system. Next, the

accumulated anhydrite caprock came into contact with hydrocarbons that reached shallow depths above or alongside the salt wall. This allowed for the onset of abundant microbial sulfate reduction coupled with hydrocarbon oxidation, resulting in an environment favorable for dolomite precipitation and the production of biodegraded hydrocarbons. Continued diapiric rise and minibasin subsidence produced topographic relief that resulted in the erosional thinning of roof strata and dolomitic caprock. A portion of the dolomitic caprock was incorporated as clasts into the Upper Chinle Formation. The remaining caprock was then onlapped by the youngest portion of the Chinle Formation. Finally, continued diapiric rise and minibasin subsidence rotated the caprock along with the salt shoulder strata to a diapir-flanking position.

References

Barbeau, D.L. (2003): A flexural model for the Paradox Basin: implications for the tectonics of the Ancestral Rocky Mountains: Basin Research, v. 15, no. 1, p. 97 – 115.

Brunner, B., Arnold G. L., Sandoval A., Mathuri M., Lerer K. and Giles K. (2016): Caprock Geochemistry – the Role of Sulfate Reduction in Carbonate Formation. SSIRC meeting, Cortez, CO.

Cater, F.W. (1970): Geology of the Salt Anticline Region in Southwestern Colorado: Geological Survey Professional Paper, 637.

Diehl, S.F., Hofstra, A.H., Koenig, A.E., Emsbo, P., Christiansen, W., and Johnson, C. (2010): Hydrothermal Zebra Dolomite in the Great Basin, Nevada—Attributes and Relation to Paleozoic Stratigraphy, Tectonics, and Ore Deposits: *Geosphere*: v. 6; no. 5; p. 663–690; doi: 10.1130/GES00530.1.

Doelling, H.H. (1985) Geology of Arches National Park. Accompanied by Map 74, Utah Geological and Mineral Survey, Salt Lake City, 15 pp.

Enos, J.S., and Kyle, J.R. (2002): Diagenesis of the Carrizo Sandstone at Butler Salt Dome, East Texas Basin, U.S.A.: Evidence for Fluid-Sediment Interaction Near Halokinetic Structures: Journal of Sedimentary Research, v. 72, no. 1, p. 68 – 81.

Evans, D.G., Nunn, J.A. & Hanor, J.S. (1991): Mechanisms driving groundwater flow near salt domes: Geophysical Research Letters, v. 18, p. 927 – 930.

Feely, H.W., and Kulp, L.J. (1957): Origin of Gulf Coast Salt Dome Sulphur Deposits: American Association of Petroleum Geologists Bullion, v. 41, p. 1802 – 1853.

Giles, K.A., and Rowan, M.G. (2012): Concepts in halokinetic-sequence deformation and stratigraphy: Geological Society, London, Special Publications, v. 363, no. 1, p. 7 – 31.

Giles, K.A., Lawton, T., Shock, A., Kernen, R., Hearson, T., and Rowan, M.G. (2012): A Halokinetic Drape-Fold Model for Caprock in Diapir-Flanking and Subsalt Positions, *in* Search and Discovery Article #40956 (2012), AAPG©2012, Long Beach, California.

Giles, K.A., Langford, R.P., Hearon, T.E., Brunner, B., Rowan, M.G., Lawton, T.L., Deatrick, K., Escosa, F., Foster, A., Heness, E.A., Lerer, K., Mast, A., McFarland, J.C., and Shock, A.L. (2016): Emerging New Paradigms in the Paradox Salt Basin, Utah and Colorado.

Hallager, W.S., Ulrich, M.R., Kyle, J.R., Price, P.E., and Gose, W.A. (1990): Evidence for episodic basin dewatering in salt-dome cap rocks: *Geology*, v. 18, no. 8, p. 716 – 719.

Hite, R. J. (1960): Stratigraphy of the saline facies of the Paradox Member of the Hermosa Formation of southeastern Utah and southwestern Colorado, Four Corners Geol. Soc. Guidebook 3d Field Conf.: Geology of the Paradox fold and fault belt, 1960, p. 86 – 89.

Hite, R. J., and Buckner, D.H. (1981): Stratigraphic Correlations, Facies Concepts and Cyclicity in Pennsylvanian Rocks of the Paradox Basin: Rocky Mountain Association of Geologists Field Conference, 1981, p. 147 – 159.

Jackson, C.A.-L., and Lewis, M.M. (2012): Origin of an anhydrite sheath encircling a salt diapir and implications for the seismic imaging of steep-sided salt structures, Egersund Basin, Northern North Sea: Journal of the Geological Society, v. 169, no. 5, p. 593 – 599.

Jackson, C. A., Lewis, M. M., and Mannie, A. S. (2013): Characterization and Origin on Anhydrite-Rich 'Lateral Caprock' Adjacent to Halite-Cored Salt Diapirs; Implications for Prospectively in Salt Basins. Oral presentation at AAPG 2013 Annual Convention and Exhibition Pittsburgh, Pennsylvania, May 19 – 22, 2013.

James, N.P., and Jones, B. (2016): *Origin of Carbonate Sedimentary Rocks:* John Wiley & Sons, 2016.

Knauth, L. P. (1979): A Model for the Origin of Chert in Limestone: *Geology*, v. 7, p. 233 – 258.

Kues, B. S., and Giles K. A. (2004): The Late Paleozoic Ancestral Rocky Mountain System in New Mexico: The geology of New Mexico, A Geologic History, New Mexico Geological Society, p. 95 – 136.

Kyle, J. R., and Posey H. H. (1991): Halokinesis, Cap Rock Development, and Salt Dome Mineral Resources. *Evaporites, Petroleum and Mineral Resources*. Ed. J. L. Melvin. N.p.: Elsevier. p. 413 – 474.

Kyle, J. R., Ulrich, M.R., Gose, W.F. (1987): Textural and Paleomagnetic Evidence for the Mechanism and Timing of Anhydrite Cap Rock Formation, Winnfield Salt Dome, Louisiana. *Dynamical Geology of Salt and Related Structures*. Ed. I. Lerche & J. J. O'Brien. N.p.: Academic Press, Inc. p. 497 – 542.

Lerer, K. (2017): The Role of Microbes in the Formation of Caprock, Paradox Basin, Southwestern Colorado, Master's thesis, University of Texas at El Paso.

Mack, G. H., and Rasmussen, K.A. (1984): Alluvial-fan sedimentation of the Cutler Formation (Permo-Pennsylvanian), near Gateway, Colorado: Geological Society of America Bulletin, v. 95, p. 109 – 116.

Magaritz, M., and Holser, W. (1990): Carbon isotope shifts in Pennsylvanian seas: American Journal of Science, v. 290, p. 977 – 994.

Major, R.P., Lloyd, R.M., and Lucida, F.J. (1992): Oxygen Isotope Compositions of Holocene Dolomite formed in Humid Hypersaline Setting: *Geology*, v. 20, p. 586 – 588.

Mast, A. M. (2016): The origin of anomalous carbonate units outcropping at the salt-sediment interface of the southern end of Gypsum Valley salt wall, Paradox Basin, Colorado. Master's thesis, University of Texas at El Paso.

McFarland, J. C. (2016): Structural and stratigraphic development of a salt-diapir shoulder, Gypsum Valley, Colorado. Master's thesis, University of Texas at El Paso.

Merino, E., Canals, A. and Fletcher, R.C. (2006): Genesis of self-organized zebra textures in burial dolomites: displacive veins, induced stress, and dolomitization. *Geol. Acta,* v. 4, p. 383–393.

Murray, G. E. (1966): Salt Structures of the Gulf of Mexico Basin – a review: Am. Assoc. Petroleum Geologists Bulletin, v. 50, p. 439 – 478.

Morrow, D. W. (1982): Descriptive field classification of sedimentary and diagenetic breccia fabrics in carbonate rocks: Bulletin of Canadian Petroleum Geology, v. 30, p. 227 – 229.

Morrow, D.W. (2014): Zebra and boxwork fabrics in hydrothermal dolomites of northern Canada: Indicators for dilational fracturing, dissolution or in situ replacement? *Sedimentology*, v. 61, p. 915–951. doi: 10.1111/sed.12094

Posey, H.H., Price, P.E., Kyle, J. R. (1987): Mixed Carbon Sources for Calcite Cap Rocks of Gulf Coast Salt Domes. *Dynamical Geology of Salt and Related Structures*. Ed. I. Lerche & J. J. O'Brien. N.p.: Academic Press, Inc. p. 593 – 630.

Rasbury E. T., and Cole J. M. (2009): Directly dating geologic events: U-Pb dating of carbonates: Reviews of Geophysics, v. 47, RG3001.

Sassen, R. (1987): Organic Geochemistry of Salt Dome Cap Rocks, Gulf Coast Salt Basin. *Dynamical Geology of Salt and Related Structures*. Ed. I. Lerche & J. J. O'Brien. N.p.: Academic Press, Inc. p. 631 – 649.

Schwerdtner, and Troeng (1978): Strain Distribution Within Arcuate Diapir Ridges of Silicone Putty: *Tectonophysics*, v. 50, p. 13 – 28.

Siever, R. (1962): Silica Solubility, 0º - 200 ºC, and the Diagenesis of Siliceous Sediments: *Journal of Geology*, v. 70, p. 127 – 150.

Stokes, W. L., Phoenix, D. A., & Geological Survey (U.S.). (1948): Geology of the Egnar-Gypsum Valley area, San Miguel and Montrose Counties, Colorado. Washington, D.C.: U.S. Dept. of the Interior, Geological Survey.

Rowan, M. G., Giles, K. A., Hearon, T. E., and Fiduk, J. C. (2016): Megaflaps adjacent to diapirs: Am. Assoc. Petroleum Geologists Bulletin, v. 100, no. 11, p. 1723 – 1747.

Shock, A. L. (2010): Origin and Implications of Permian and Triassic Diagenetic Carbonate Caprock Adjacent to Diapiric Salt Walls, Paradox Basin, Utah. Master's Thesis. New Mexico State University.

Trudgill, B. D. (2011): Evolution of salt structures in the northern Paradox Basin: controls on evaporite deposition, salt wall growth and supra-salt stratigraphic architecture: Basin Research, v. 23, no. 2, p. 208 – 238.

Trudgill, B. D., Banbury, N., and Underhill, J. N. (2004) Salt evolution as a control on structural and stratigraphic systems: Northern Paradox foreland basin, SE Utah, U.S.A., in P. J. Post, D. L. Olson, K. T. Lyons, S. L. Palmes, P. F. Harrison, and N.C. Rosen, eds., Salt-sediment interactions and hydrocarbon prospectively: Proceedings of 24th Annual Gulf Coast Section SEPM Foundation Bob F. Perkins Research Conference, p. 669 – 700.

Vogel, J. D. (1960): Geology and ore deposits of the Klondike Ridge area, Colorado: U. S. Geological Survey, Open-File Report, USGS Numbered Series 60 – 145.

Warren, J. K. (2006): Evaporites: Sediments, Resources and Hydrocarbons: Springer Science & Business Media.

Curriculum Vita

Piper Lee Poe was born in Indianapolis, Indiana on August 13th, 1994 and raised in Oregon, Wisconsin. The first of three children from Chris and Jodie Poe, she graduated from Oregon High School in 2012. Piper acquired her Bachelor of Science degree in geology from the University of Wisconsin-Oshkosh in 2016. When pursuing her degree, Piper was the Treasurer of Sigma Gamma Epsilon and an active member of the Geology Club and the National Society of Leadership and Success. As an undergraduate Piper was very involved in Undergraduate research, completing two research projects that both embodied the theme of understanding diagenetic alteration of carbonate rocks before geochemical data is interpreted. Piper presented her research at the Geological Society of America (GSA) annual meeting in Baltimore, and at numerous campus-wide research colloquiums. Piper received multiple awards and grants as an Undergraduate which include: Undergraduate Small Grant Proposal, Daniel Raaf Scholarship, the Bartlett Award for her dedication to Geology, Outstanding Undergraduate Research Presentation, Karges Award, and the National Association of Geoscience Award. After completing her B.S. Piper began her Master of Science degree at the University of Texas at El Paso (UTEP) with Dr. Kate Giles. At UTEP she was a member of the Association from Women Geoscientists and the President of the American Association of Petroleum Geologists (AAPG) student chapter. As a graduate student, Piper was a field assistant in the Flinders Ranges, South Australia for Ph.D. student studying carbonate caprock on an allochthonous salt body and became the third author on the subsequent publication. Piper presented her graduate research on caprocks at multiple conferences, most notably at the GSA Penrose Conference in the Dead Sea, Israel. She received multiple grants during her graduate studies, which include a grant from the AAPG Southwest Section, AAPG Grants-in-aid, a GSA research grant and travel grant, and the UTEP Dodson Research Grant. As a graduate student Piper worked as a teaching assistant for Historical Geology, held an internship at the National Geospatial Intelligence Agency at White Sands Missile Range in 2018, and an internship at Pioneer Natural Resources in 2018, where she was offered a full-time Geologist position and will start in January 2019.

Contact information: piperlpoe@gmail.com

This thesis was typed by Piper Lee Poe.